Martin Ratschek

Doping Helium Droplets: Development of a High-Temperature Pickup Source

MASTER THESIS

For obtaining the academic degree
Diplom-Ingenieur

Diploma Programme of
Technical Physics

Graz University of Technology

Supervisor: Univ.-Prof. Dipl.-Phys. Dr.rer.nat. Wolfgang E. Ernst
Co-Supervisor: Dr. Markus Koch

Institute of Experimental Physics

Graz, May 2010

Abstract

Superfluid helium nanodroplets (He_N) provide a versatile tool to isolate single atoms and molecules for spectroscopic investigations at 0.37 K. Due to the low temperature also weakly bound, tailored complexes can be analysed. Electron spin resonance (ESR) is a well established method to gain structural, dynamic, and magnetic information of radical atoms and molecules. With the use of spin labels this method is expanded even to ESR-silent species.

Both techniques have been successfully combined for the very first time at the Institute of Experimental Physics, Graz University of Technology, in a unique setup and ESR measurements of single alkali-metal atoms on He_N have been published. The ESR-transitions are recorded indirectly by means of optically detected magnetic resonance, and electron-spin states are selectively prepared and probed by the use of magnetic circular dichroism. The alkali–He_N system has been well characterised with potassium and rubidium atoms, showing highly resolved hyperfine spectra which indicate a shift of the hyperfine constant due to the interaction of the dopant with the droplet. Also, coherent spin transfer could be demonstrated with the measurement of Rabi oscillations. Based on these successful achievements, this thesis aims at an expansion of this method for general applications.

One branch is the use of the surface-located alkali-metal atom as spin label for ESR-silent species inside the droplet. The interaction between the alkali-metal atom and the dopant inside He_N will alter the ESR-spectra and is currently being studied, starting with noble gas atoms as dopants for simplicity. The knowledge of the gas pickup process is therefore of fundamental importance. In this work the pickup of neon, argon, molecular hydrogen, and acetylene is characterised by means of mass spectrometry. A quadrupole mass spectrometer was adapted to the existing setup. Beside the gas pickup also the successful formation of small cluster inside the droplet is shown.

Transition metals like copper (Cu, alkali-like) or chromium (Cr, high-spin septet state) are of technological and fundamental importance and their investigation in He_N is a future goal. For Cr pickup, Cr atoms have to be evaporated requiring temperatures in the range of 1300°C to 1700°C. For this purpose a pickup source based on electron bombardment has been designed, constructed, and implemented into the existing setup. The high temperature pickup source has been well characterised and turned out to work very well. Even multiple pickup of up to four Cr atoms, which form a microcluster inside the He_N, could be demonstrated.

Martin Ratschek

Dotation von Heliumtröpfchen mit schwer verdampfbaren Metallen

DIPLOMARBEIT

zur Erlangung des akademischen Grades
Diplom-Ingenieur

Diplomstudium Technische Physik

Technische Universität Graz

Betreuer: Univ.-Prof. Dipl.-Phys. Dr.rer.nat. Wolfgang E. Ernst
Mitbetreuer: Dr. Markus Koch

Institut für Experimentalphysik

Graz, Mai 2010

Kurzfassung

Superflüssige Helium Nanotröpfchen (He_N) bieten ein ausgezeichnetes Substrat um einzelne Atome und Moleküle zu isolieren und bei 0.37 K spektroskopisch zu untersuchen. Durch die niedrige Temperatur lassen sich sogar schwach gebundene Komplexe gezielt erzeugen und untersuchen. Elektronenspinresonanz (ESR) Experimente bieten die Möglichkeit Struktur, Dynamik und magnetische Eigenschaften von atomaren und molekularen Radikalen zu untersuchen. Selbst ESR inaktive Proben sind inzwischen durch sogenannte Spin Labels untersuchbar.

In einem weltweit einzigartigen Aufbau am Institut für Experimentalphysik an der Technischen Universität Graz, sind nun diese zwei Verfahren erstmals kombiniert worden und es konnten bereits erfolgreich ESR Messungen an einzelnen Alkalimetallatomen auf He_N veröffentlicht werden. Dabei wird der Elektronenspin-Übergang indirekt detektiert durch Ausnutzung der optisch-detektierten magnetischen Resonanz und des zirkularen magnetischen Dichroismus. Nach einer ausführlichen Charakterisierung des He_N-Alkaliatom-Systems mit Kalium und Rubidium, bei denen neben der Verschiebung der Hyperfeinstrukturkonstante durch die Wechselwirkung zwischen He_N und Alkaliatom auch kohärente Elektronenspin Übergänge, durch Messen von Rabi Oszillationen, gezeigt werden konnten, ist nun die Erweiterung des Versuchaufbaus das Ziel dieser Arbeit.

Zum einen sollen die auf der Oberfläche des He_N sitzenden Alkaliatome als Spin Label für ESR inaktive Komplexe im Inneren des He_N verwendet werden. Es wird erwartet, dass die Wechselwirkung zwischen dem Alkaliatom und dem dotierten Teilchen zu einer Änderung des ESR-Spektrums führt. Dies wird zur Zeit, ausgehend von Edelgas-Atomen, wegen ihrer Einfachheit, untersucht. Dafür muss der Pickup-Prozess der Gasatome gut charakterisiert sein. Ein Teil dieser Arbeit beschäftigt sich deswegen mit der massenspektroskopischen Studie der Gase Neon, Argon, molekularem Wasserstoff und Acetylen. Dafür wurde ein Quadrupol-Massenspektrometer an den bestehenden Aufbau angepasst. Es konnte neben erfolgreichem Gas-Pickup auch die Bildung kleiner Cluster im He_N gezeigt werden.

Zum anderen sind Übergangsmetalle wie Kupfer (Cu, alkaliähnlich) und Chrom (Cr, Hoch-Spin Septett Zustand) von technologischer und fundamentaler Bedeutung, weswegen auch deren Untersuchung in He_N ein zukünftiges Ziel ist. Für den Pickup von Cr müssen allerdings Cr Atome verdampft werden, wofür Temperaturen im Bereich von 1300°C bis 1700°C notwendig sind. Eine auf Elektronbombardement basierende Pickupquelle wurde für diesen Zweck entworfen, konstruiert und in den bestehenden Aufbau implementiert. Mit einer ausführlichen Charakterisierung konnte ihre ausgezeichnete Funktion gezeigt werden. Sogar Mehrteilchenpickup von Cr mit bis zu vier Atomen, die zu Mikroclustern im He_N wachsen, ist möglich.

Deutsche Fassung:
Beschluss der Curricula-Kommission für Bachelor-, Master- und Diplomstudien vom 10.11.2008
Genehmigung des Senates am 1.12.2008

EIDESSTATTLICHE ERKLÄRUNG

Ich erkläre an Eides statt, dass ich die vorliegende Arbeit selbstständig verfasst, andere als die angegebenen Quellen/Hilfsmittel nicht benutzt, und die den benutzten Quellen wörtlich und inhaltlich entnommenen Stellen als solche kenntlich gemacht habe.

Graz, am 18.07.2010 ..... Martin Rabsch .....
(Unterschrift)

Englische Fassung:

STATUTORY DECLARATION

I declare that I have authored this thesis independently, that I have not used other than the declared sources / resources, and that I have explicitly marked all material which has been quoted either literally or by content from the used sources.

18.07.2010 ..... Martin Rabsch .....
date (signature)

Contents

List of Tables

List of Figures

Abbreviations, Elements

AD	analog–to–digital
AD/DA converter	analog–to–digital and digital–to–analog converter
BD	beam depletion
DA	digital–to–analog
dB	decibel (here, attenuation)
EC	emission current
ESR	electron spin resonance
GPIB	general purpose interface bus
H_2	molecular hydrogen
He	helium
He_2	helium dimer
He_N	superfluid helium nanodroplet
HT source	high–temperature source
K	potassium
Kr	krypton
LIF	laser induced fluorescence
MCD	magnetic circular dichroism
Ne	neon
ODMR	optically detected magnetic resonance
p_0	nozzle pressure
PID controller	Proportional/Integral/Derivative controller
PV	process variable
QMS	quadrupole mass spectrometer
Rb	rubidium
SEM	secondary electron multiplier (often referred to as SEM voltage)
T_0	nozzle temperature
Ta	tantalum
Xe	xenon

Chapter 1

Introduction

1.1 Motivation

Spectroscopy on superfluid helium nanodroplets (He_N) is a versatile tool to investigate single atoms or molecules at 0.37 K [49, 50]. To expand this branch of research, a second He_N laboratory was established at the Institute of Experimental Physics, Graz University of Technology. It was set up by Markus Koch in his PhD-thesis [27]. A molecular beam apparatus formerly used by John S. Muenter, University of Rochester, was expanded with a He_N beam source, alkali-metal pickup facilities, a microwave cavity, and detection devices like photomultiplier and Langmuir-Taylor detector.

By means of optically detected magnetic resonance measurements, exploiting also the magnetic circular dichroism, the first ESR transitions of doped He_N were detected. The technique provided outstanding results with very high resolutions. A shift of the hyperfine constant of alkali-metal atoms due to the interaction with He_N by about $\sim$400 ppm with an inaccuracy of only $\sim$4 ppm and a droplet size dependency could be demonstrated. However, there is still room for further improvements to increase the resolution. Furthermore, coherent ESR transitions were demonstrated by measuring Rabi oscillations. This further increases the potential of this promising combination of He_N and ESR. The results obtained with potassium and rubidium (Rb) were published in Refs. [28, 30, 29].

After the successful proof of concept one aims at the expansion of the existing setup for further generalisation of ESR measurements. One branch is to use Rb, which is located on the surface of the He_N, as spin labels for ESR-silent species inside He_N. Since the ESR spectra of Rb are shifted due to the interaction with the droplet another species inside the droplet, which will interact with the Rb-atom at least by the van der Waals force, will result in a further shift of the ESR spectra. At first one aims to keep the perturbation as small as possible by using He-like noble gases. Then species with nuclear spin, like one isotope of xenon or ortho-hydrogen, are of interest. In a first step the pickup process of the gaseous species has to be investigated and is one part of this work.

Another branch is the investigation of ESR spectra of transition metals like copper (Cu) or chromium (Cr). Both metals are of high technological and fundamental interest. Cu has a alkali-like shell configuration making the understanding of the ESR spectra more easy. Cr, on the other hand, has a high-spin septet state. Unfortunately both species require a high temperature to reach a sufficient high pickup probability. Therefore a high temperature evaporation source based on electron bombardment is developed in this work.

1.2 Measured Species

In the following chapter the species argon (Ar), neon (Ne), hydrogen (H), acetylene (C_2H_2), and chromium (Cr) are described. Also information on copper (Cu) can be found since it will be used in future experiments. Beside a brief historic overview, especially the abundance of stable isotopes and their magnetic properties are listed. The information is taken from Ref. [35] and the values are given at standard conditions for temperature and pressure if not stated otherwise.

1.2.1 Hydrogen

Hydrogen (H) was discovered in 1766 by Cavendish named after the hydrogen-oxygen reaction where water (hydro) is formed (genes). It is thought that H makes up more than 90% of all the atoms in the universe. On earth H can be found in many molecules like water or hydrocarbons in great numbers. It can be produced easily by electrolysis of water but many other methods are known. Hydrogen is barely found as single atom, hydrogen gas therefore consists of molecular hydrogen (H_2). H_2 is a highly reactive gas if combined with oxidising elements. A mixture in air with a concentration between 4% to 75% (by volume) is explosive and easily ignites by sparks or even the sunlight.
H_2 can be found in two nuclear spin isomeric forms, ortho- and parahydrogen. The spins can be aligned either parallel resulting in spin one, orthohydrogen, or antiparallel without spin, parahydrogen. The spin isomers differ in energy with the orthohydrogen being the "excited" state. The ratio of ortho- to parahydrogen depends on the degeneracy of the states resulting in a ratio of 25% para- and 75% orthohydrogen at standard room temperature and pressure. If cooled the ratio is shifted towards a higher parahydrogen fraction.

Properties:
atomic number: 1
density (gaseous): 0.08988 g/L
melting point: -259.34°C (13.80 K)
boiling point: -252.87°C (20.28 K)
natural abundance: 99.985% ^{1}H protonium; 0.015% ^{2}H deuterium; ^{3}H tritium (unstable: half-life: 12.32 years)
nuclear spin: ^{1}H: +1/2; ^{2}H: +1; ^{3}H: +1/2
ionisation energy (H): 13.59844 eV
ionisation energy (H_2): 15.42589 eV

1.2.2 Neon

Neon (Ne) was discovered in 1898 by Ramsey and Travers. It can be found in the earth's atmosphere to the extent of 1 part in 65000 of air by volume and is produced by fractional distillation of liquid air.

Properties:
atomic number: 10
density (gaseous): 0.89990 g/L
melting point: -248.59°C (24.56 K)
boiling point: -246.08°C (27.07 K)
natural abundance: 90.48% ^{20}Ne; 9.25% ^{22}Ne; 0.27% ^{21}Ne
nuclear spin: ^{20}Ne: 0; ^{22}Ne: 0; ^{21}Ne: +3/2
ionisation energy: 21.56454 eV

1.2.3 Argon

Argon (Ar) was discovered in 1894 by Rayleigh and Ramsay. The concentration in the earth's atmosphere if 0.94% by volume and can be produced by fractional distillation of liquid air.

Properties:
atomic number: 18
density (gaseous): 1.7837 g/L
melting point: -189.35°C (83.80 K)
boiling point: -185.89°C (87.26 K)
natural abundance: 99.60% ^{40}Ar; 0.34% ^{36}Ar; 0.06% ^{38}Ar
nuclear spin: above listed isotopes have a vanishing nuclear spin
ionisation energy: 15.75962 eV

1.2.4 Acetylene

Acetylene is a hydrocarbon gas widely known from its use in welding and is also known by its systematic name ethyne. The the molecular formula of the chemical compound is C_2H_2 and the components are aligned linearly with a triple bond between the two carbons in the centre.

$$H - C \equiv C - H$$

The most abundant isotopic compound has a mass of 26 amu (>98% probability).

Properties:
molar mass: 26.04 g/mol
density (gaseous): 1.097 g/L
boiling point (sublimation): -84.8°C (188.4 K)
ionisation energy: 11.400 eV [35, 43]

1.2.5 Chromium

Chromium (Cr) was discovered in 1797 by Vauquelin and is usually produced from the ore chromite ($FeCr_2O_4$). It is a transition metal with six unpaired electrons, resulting in a high-spin septet state. There is no indication for being a type one superconductor as for most other metals but it was shown for example in Ref. [3] that amorphous Cr layers show superconductivity.

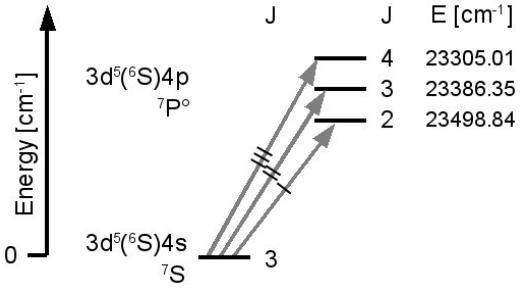

Figure 1.1: Grotrian diagram of chromium.

Cr has a high vapour pressure compared to other metals with a similar melting point (see further down). For pickup an effusive particle flux rate corresponding to a pressure of 35 Pa is needed (see Sec. 3.2.2 and Appendix A.5.3), which requires a temperature of about 1500°C. The vapour pressure can be calculated using the following empirical equation (see Ref. [35]):

$$\log_{10} p = 5.006 + A + BT^{-1} + c\log_{10} T + DT^{-3}. \tag{1.1}$$
$$A = 6.800;\ B = -20733;\ C = 0.4391;\ D = -0.4094;$$
$$[p] = \text{Pa};\ 298\,\text{K} \leq T \leq 2000\,\text{K};\ [T] = \text{K};$$

Note that the equation is not correct concerning the units!

The ground state (^{7}S) has a total angular momentum (J) of 3. The first excited state (^{7}P) shows a fine structure with J=2, 3, and 4. A schematic drawing of the Grotrian diagram can be found in Fig. 1.1. The transitions marked I, II, and III can be excited by laser with the wavelength of 429.0923 nm, 427.5999 nm, and 425.5529 nm. A blueshift of 5 nm to 10 nm can be expected as it was found for silver in helium nanodroplets in Ref. [4]. To selectively address the spin states, the magnetic circular dichroism (MCD) effect, which has been successfully demonstrated for matrix-isolated Cr in Ref. [51], will be used. The investigation of chromium and other metals by means of electron spin resonance (ESR) in conventional atomic beams can be found in Ref. [24] and ESR of Cr in cold matrices is shown in Ref. [53].

Properties:
atomic number: 24
density (solid, at room temperature and 1 atm): 7.18 g/cm^3
melting point (at 1 atm): 1907°C (2180 K)
boiling point (at 1 atm): 2671°C (2944 K)
natural abundance: 83.8% ^{52}Cr; 9.5% ^{53}Cr; 4.3% ^{50}Cr; 2.4% ^{54}Cr
nuclear spin: ^{52}Cr: 0; ^{53}Cr: -3/2; ^{50}Cr: 0; ^{54}Cr: 0
ionisation energy (Cr): 6.76664 eV
binding energy (Cr_2) [47]: 1.42 eV

1.2.6 Copper

Copper (Cu) has been known in prehistoric ages. It is ductile and a good conductor of heat and electricity. With a configuration of ^{2}S ({Ar}3d^{10}4s) it is alkali-like. In its pure form, it does not show superconductivity of type one. For optically detected magnetic resonance a laser wavelength of 327.49 nm = 30 535.302 cm^{-1} for excitation into the $P_{1/2}$ state and 324.85 nm = 30 783.686 cm^{-1} into $P_{3/2}$ is needed. That the MCD scheme works is shown in Ref. [52], where the spin orbit coupling constant of Cu in a noble gas matrix is investigated.

Cu has a low vapour pressure compared to chromium and due to its low melting point Cu will be liquid at the required temperature for doping. To reach the same vapour pressure as chromium of approximately 35 Pa, Cu has to be heated to about 1500°C. The vapour pressure can be calculated with the Eqn. 1.1, and the following parameters:

$$\begin{aligned} \text{solid: } & A = 9.123;\ B = -17748;\ C = -0.7317;\ D = 0;\ 298\,\text{K} \leq T \leq 1357.77\,\text{K} \\ \text{liquid: } & A = 5.849;\ B = -16415;\ C = -0.7317;\ D = 0;\ 1357.77\,\text{K} \leq T \leq 1850\,\text{K} \\ & [p] = \text{Pa};\ [T] = \text{K}; \end{aligned}$$

Properties:
atomic number: 29
density (solid, at room temperature and 1 atm): 8.96 g/cm^3
melting point (at 1 atm): 1084.62°C (1357.77 K)
boiling point (at 1 atm): 2562°C (2835 K)
natural abundance: 69.17% ^{63}Cu; 30.83% ^{65}Cu
nuclear spin: ^{63}Cu: -3/2; ^{65}Cu: -3/2
ionisation energy (Cu): 7.72638 eV

1.3 Superfluid Helium Droplet Beam

One of the goals in spectroscopy is to control external influences on the test species in order to reach a higher resolution. For example, in a gas discharge the spectral lines are broadened basically due to the Doppler broadening which usually renders the detection of the hyper fine structure impossible. One solution to this problem is the reduction of the particle speed in the direction of the detector. This can be achieved in an atomic beam apparatus. The velocity perpendicular to the atomic beam is usually very small, so if the detection methods used are also aligned perpendicular to the beam's propagation direction the Doppler broadening becomes very small.
One is also interested in controlling the energy of the species under investigation. This can be achieved for example by seeded super sonic beams [46] or by isolating the desired species in a cryogenic matrix [54]. In the last decades a new method has come up, spectroscopy in superfluid helium droplets (He_N).

The first report of a successful creation of a He_N beam was published 1961 [5]. Since then a lot of research both experimentally and theoretically has been done. The main aspects necessary for my work, investigating pickup processes, will be summarised in this section.

Spectroscopy on He_N has been reviewed by Toennies and Vilesov [49, 50] and more recently in a book chapter by C. Callegari and W. E. Ernst [11].

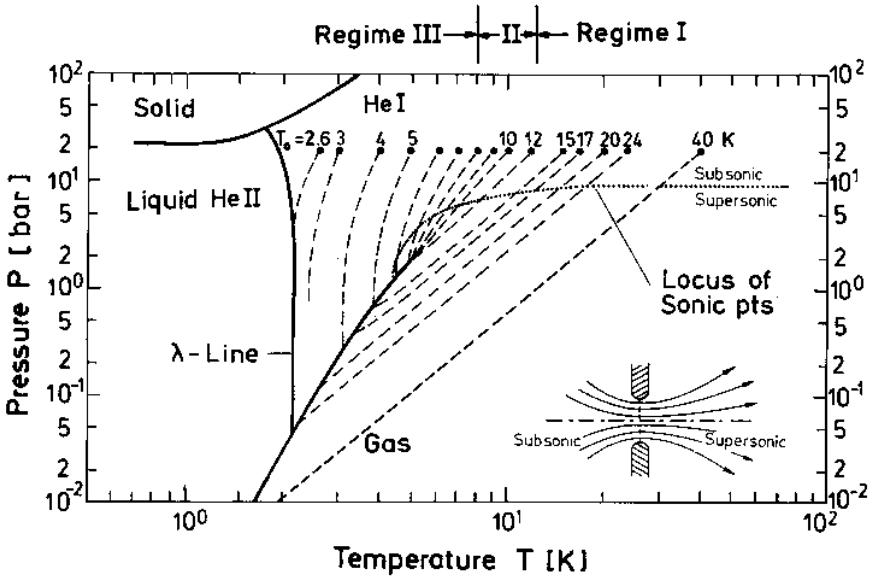

Figure 1.2: He phase diagram; the dashed lines represent the isentropes starting at the He pressure of 20 bar at different nozzle temperatures. A classification is possible into three regimes. (taken from [9])

1.3.1 Production of the Superfluid Helium Droplet Beam

A superfluid He droplet beam (He_N) can be produced in a free jet expansion through a cooled nozzle [50]. After leaving the nozzle the gas is expanding and is therefore cooled adiabatically. In the phase diagram Fig. 1.2 (from Ref. [9]) this process is displayed by an isentrope starting at the nozzle condition, the He pressure and the nozzle temperature. One can see the isentropes, marked as dashed lines, starting at different He pressures and nozzle temperatures. Depending on these initial conditions they can be classified into three regimes.
Regime I, the subcritical region, is indicated by straight isentropes. It can be described as an ideal gas, and condensation occurs due to adiabatically cooling. This is the regime usually used in our experiments with a nozzle temperature of $T_0 = 9.5$ K and a He pressure of $p_0 = 50$ bar resulting in a droplet size in the range of N=1000 to 40000 atoms on the He_N. After the condensation process the droplets are shrinking by evaporative cooling, which stabilises the droplet temperature at about 0.37 K [19].
Regime III, the supercritical region, deviates from the ideal gas behaviour and the gas-liquid transition-line is approached from the liquid side. According to Ref. [10], a bimodal droplet size distribution occurs resulting primarily in large droplets with about N$\approx 10^5$ atoms.
Regime II, the transition region, cannot be described easily since the isentropes all pass near the critical point which can result in density fluctuations Ref. [9].
While a more detailed discussion of He_N beam properties can be found in [33, 17], here only those are mentioned which are of importance for this thesis.

1.3.2 Droplet Size

The droplet size has been measured in scattering experiments [33, 18] and by deflection in an electric field after doping the droplet with electrons [25]. The radial density distribution of the He droplets was also investigated in Ref. [18]. The droplet size can be described by the Knuth model [26, 25] or the power model [27]. The mean number of atoms on the He droplet can be estimated with both models, but due to the simplicity the power model is used in this work. The mean number droplet size ($\bar{N}$) is proportional to the product of the He pressure p_0, the nozzle diameter d, and the nozzle temperature T_0 each risen to a higher power. The factors and exponents where obtained in Ref. [27] by fitting measured data from Ref. [18]. The formula is shown in Eqn. 1.2, with $\bar{N}$ being the mean number of atoms on the droplet, p_0 being the He pressure in bar, T_0 being the nozzle temperature in K, and d being the nozzle diameter in μm.

$$\bar{N} = k_1 p_0^{k_2} T_0^{k_3} d^{k_4} \tag{1.2}$$
$$k_1 = 4(7) \cdot 10^5,\ k_2 = 0.97(9),\ k_3 = -3.88(25),\ k_4 = 2.0(1.1)$$

Typical values used in our experiments are $p_0 = 50$ bar, $T_0 = 11$ K to 28 K, and d= 5 μm. This gives droplet sizes between 1000 and 40000 atoms per He droplet. One has to be careful at larger droplet sizes obtained by lower nozzle temperatures since regime I is left and deviations from the results given by Eqn. 1.2 are increased drastically.

The droplet size distribution has been investigated by Lewerenz [33, 34]. It can be described by a log-normal distribution [18]:

$$P(N) = \frac{1}{\sqrt{2\pi} N \delta} \exp\left[-\frac{(\ln N - \mu)^2}{2\delta^2}\right]. \tag{1.3}$$

The probability to find a droplet with N atoms is given by $P(N)$. The values μ and δ are connected to the mean number of atoms on the He droplet and the full width at half maximum of the distribution respectively. They were measured by scattering the He droplets with Ar and Kr [18]. These values are used in a matlab function "droplet_size_distribution.m" which calculates $P(N)$ with Eqn. 1.3. The values δ and μ have been calculated with the matlab script "droplet_size_distribution_fit.m" where the measured data from Ref. [18] are used in combination with the power law to fit μ by Eqn. 1.4 with a fixed δ.

$$\bar{N} = \exp\left(\mu + \frac{\delta^2}{2}\right) \tag{1.4}$$

The full width at half maximum N_{FWHM} can be obtained by Eqn. 1.5 and its value lies in the same range as $\bar{N}$.

$$N_{\mathrm{FWHM}} = \exp\left(\mu - \delta^2 + \delta\sqrt{2\ln 2}\right) - \exp\left(\mu - \delta^2 - \delta\sqrt{2\ln 2}\right) \tag{1.5}$$

1.3.3 Droplet Velocity

The droplet velocity can be calculated for He droplets in regime I when the droplet generation obeys an adiabatic process. Then, the enthalpy is converted into kinetic energy giving Eqn. 1.6 for an ideal gas [27], with k_{b} being the Boltzmann constant, T being the gas temperature which is set to the nozzle temperature, and m_{He} being the mass of ^{4}He. The factor 5 results from the enthalpy by a factor of two due to the kinetic energy. The enthalpy is the sum of the inner energy $\frac{3}{2}k_{\mathrm{b}}T$ and the so-called flow work pV which equals $k_{\mathrm{b}}T$ for a single particle of the ideal gas.

$$v = \sqrt{\frac{5k_{\mathrm{b}}T}{m_{\mathrm{He}}}} \tag{1.6}$$

For $\mathrm{He_N}$ at low temperatures, due to the crossing of the gas–liquid transition line during the free jet expansion, condensation occurs and therefore the remaining enthalpy at the λ-point H_λ has to be taken into account. The droplet velocity v can then be traced back to the enthalpy at the starting point H_0 and H_λ by Eqn. 1.7 due to the conservation of enthalpy [9].

$$v = \sqrt{2\left(H_0 - H_\lambda\right)} \tag{1.7}$$

In the matlab function "DropVelocity.m", the enthalpy values were taken from the literature [37] and are interpolated to calculate the velocity at a given nozzle temperature for a He pressure of 50 bar. Also, the values for He pressures of 40 bar and 60 bar are included and can be used by uncommenting in the script. Nozzle temperatures in the range of 10 K to 28 K result in droplet velocities between 315 m/s and 550 m/s.

1.3.4 Massflow

For a free jet expansion the equations of conservation of mass, momentum, and energy known from fluid mechanics have to be solved. For a subsonic expansion the total mass flow through the nozzle can be calculated when some simplifications are taken into account. The viscosity has to be ignored, but when high flow rates are considered the viscous region can be neglected, and the exit point of the nozzle has to be at the sonic point. The total mass flow then becomes independent of the background pressure, since downstream of the nozzle the expansion is

supersonic and the isentropes become independent of the background pressure. Then the mass flow can be described by Eqn. 1.8 [27]. An explanation in more detail can be found in Ref. [46, p.19 et seq.] by Miller, or in Ref. [42, p.127 et seq.].

$$\dot{m} = p_0 \frac{d^2\pi}{4} \sqrt{\frac{\kappa m_{\mathrm{He}}}{k_{\mathrm{b}} T_0} \left(\frac{2}{\kappa+1}\right)^{\frac{\kappa+1}{\kappa-1}}} \tag{1.8}$$

p_0 ... He pressure; d ... nozzle diameter; m_{He} ... mass of He; κ ... specific heat ratio ($\kappa = \frac{5}{3}$ for He)

1.3.5 Binding Energy and Ionisation Process

The binding energy of He atoms to the droplet can be approximated by the bulk binding energy of He of 7.2 K, $6.2 \cdot 10^{-4}$ eV, or 5 cm^{-1} [34].

Electron impact ionisation of species inside doped $\mathrm{He_N}$ show an interesting behaviour According to Ref. [10] and Ref. [45] the threshold for electron impact excitation of He droplets has been measured to be (21.0 ± 0.1) eV while the ionisation of He on the droplet lies at (24.6 ± 1.0) eV, forming positive holes. On electron impact either excitons or positive holes (He^+) are formed, depending on the energy. For an ionisation energy of 60 eV the ratio of excitons to positive holes is about 1 : 20 [45]. The excitons create a bubble with a radius of 12 Åfor He at 0 K inside the droplet compared to a 7 Åsized bubble for He^+. Both, the metastable exciton bubble and the positive hole then travels in the droplet by hopping. The average hopping number for excitons lie in the range from $1.9{\cdot}10^3$ to $3.4{\cdot}10^3$ steps and the excitons travel an average distance of 150 Åbefore fragmentation of the droplet occurs. The positive hole hops about $2.7{\cdot}10^4$ times travelling a distance of up to 520 Å. Those numbers are only rough estimations to get an idea about the ionisation processes inside $\mathrm{He_N}$. Nevertheless the travelling distance is usually sufficient to reach the dopant species in droplet and ionisation occurs. The remaining energy of the ionisation process $E_{\mathrm{ion/exciton,He}} - E_{\mathrm{ion,dopant}}$ is then released, can trigger reactions of complexes on the droplet, and usually massive evaporation and fragmentation occurs. One has to imagine that 1 eV of excess energy will result in about 1600 He atoms leaving the droplet.
Due to the movement of the exciton inside the He droplet this process can be referred to as charge hopping.

1.4 Pickup Process

The He droplets can be doped with any gaseous species. One can think of the pickup process as an inelastic collision of two spheres. Since the He droplet is much larger than the dopant species the size of the latter can be neglected. However, due to other effects the collision cross section deviates from the geometrical a little. During the pickup process the added energy due to the inelastic collision will lead to excitation of the droplet and evaporation of He atoms from the droplet. Also multiple pickup is possible and even reactions of several species inside the droplet can be investigated.

1.4.1 Collision Cross Section

The collision cross section can be measured by single–collision scattering experiments like performed in Ref. [33]. This was taken a step further in Ref. [18] by measurements of the He density distribution in the droplets also by scattering experiments. It was shown that the single–collision–capture cross section is a little bit smaller (≈0.5) than the geometrical cross section, according to Ref. [49]. It can be calculated by Eqn. 1.10, with N being the number of particles on the droplet, R the droplet radius for the groundstate (=spherical) in Å, and σ the geometrical cross section:

$$R = 2.22 \cdot N^{1/3} \tag{1.9}$$

$$\sigma = R^2 \cdot \pi \tag{1.10}$$

For the calculations in this work the geometrical cross section is used.

1.4.2 Energy Dissipation on Pickup

Since the pickup process can be described by an inelastic collision the energy added to the He droplet by the scattering partner has to be dissipated. The added energy can be separated into the internal energy of the scattering partner and the kinetic energy of the system. According to Ref. [34] the collisional energy $\langle E_{\mathrm{coll}} \rangle$ can be described by Eqn. 1.11.

$$\langle E_{\mathrm{coll}} \rangle = E_{\mathrm{int}} + \frac{3\ k_{\mathrm{B}} T}{2} + \frac{m_{\mathrm{S}}}{2} v_{\mathrm{cluster}}^2 \tag{1.11}$$

E_{int} ... internal energy of the scattering partner, k_{B} ... Boltzmann constant, T ... temperature in K, m_{S} ... mass of the scattering partner, v_{cluster} ... velocity of the cluster. This approximation can be used when the mass of the scattering partner is a lot smaller than the mass of the He droplet. While the internal energy can be left out on single atom pickup, it has to be taken into account in molecular pickup due to rovibrational energy of the dopant. Single atom pickup therefore leads to roughly 100 to 600 evaporated He atoms and sets a lower limit to the dropletsize.

1.4.3 Controlling the Pickup Process

With the collision cross section given in Eqn. 1.10 the pickup probability can be calculated. In Ref. [34] the multi particle pickup is discussed in detail, and their experimental data is in agreement with Monte Carlo simulations and the theory discussed in the following. A few simplifications have been made. One has to assume a uniform He droplet size, the collision cross section is independent of the number of picked up particles, fragmentation of the dopant

clusters is neglected, and scattering clusters out of the detector area is not taken into account. In a scattering zone with an uniformly distributed collision probability the intensity of the undoped He droplet signal I_{He_N} can be described by Eqn. 1.12, which leads to an exponential decay. I_0 represents the signal of the He droplets, while α, which can be found in Eqn. 1.13, is a parameter composed of the particle density n in the scattering zone, the collision cross section σ, and the velocity averaging correction factor F. For single particle pickup the measured intensity I_1 can be described by Eqn. 1.14. This can be generalised to multi particle pickup I_k where k is the number of particles on the droplet, which leads to a Poisson distribution displayed in Eqn. 1.15. In the Poisson distribution one can also find the the length of the scattering zone L.

$$\frac{dI_{He_N}}{dz} = -\alpha I_0 \tag{1.12}$$

$$\alpha = n\sigma F \tag{1.13}$$

$$\frac{dI_1}{dz} = \alpha\left(I_0 - I_1\right) \tag{1.14}$$

$$I_k = I_{k,0}\frac{(\alpha L)^k}{k!}\exp\left(-\alpha L\right) \tag{1.15}$$

Although σ is kept constant here, it is shown in Ref. [34] that fits of the measured data can be improved by using σ as a function of the dopant atoms on the droplet $\sigma(k)$. This coincides with the fact that He atoms are evaporated on pickup.

On multi particle pickup the species inside the He droplet coagulate within 10^{-8} to 10^{-10} s [34]. With successive multi particle pickup one can see the transition to bulk behaviour for example the delocalised electrons in metal starting with metal clusters [4] or the acid dissociation with successive water pickup [16]. Also reactions can be induced with different species on the droplet [36].

The localisation of the dopant atoms inside the droplet is also of interest. According to Ref. [48] and Ref. [32] due to the flat potential distribution inside the He droplet the dopant atoms are delocalised. There are also species, like alkali-metal atoms, which will stay on the droplets surface [1], [2].

1.5 High Temperature Source

To evaporate species like chromium (Cr) or copper (Cu) temperatures up to 1700°C are required. Those temperatures can be achieved by various ways which will be explained in this section. A brief outline on high temperature sources can be found in Ref. [42, 46]

1.5.1 Source Types

The easiest approach to heat a sample is resistive heating. This can be achieved by using resistively heated **boats** made of high temperature materials like tungsten, molybdenum, or tantalum. They are commercially available and can be used typically up to between 1700°C and 2000°C, depending on the materials and samples. At higher temperatures unwanted alloys between isolating materials or the sample and the material of the boat can be formed. The disadvantage of this method is that the currents, required for heating to such high temperatures, lie in the range of 100 A to 500 A. The stray magnetic field produced by such high currents make this method unusable in combination with high precision magnetic experiments like electron spin resonance.

The same applies to **Knudsen cells**. Usually, a crucible made of an isolating material like aluminium oxide, or boron nitride is heated by contact and radiation. Heater wires made of high temperature materials like tungsten, molybdenum, or tantalum. Several radiation shields are used before the remaining heating power is dissipated into a water cooling. Those sources are also commercially available and usually temperatures up to 1500°C can be reached easily, higher temperatures should also be possible.

Inductive heated ovens can also be used to reach temperatures of up to 2000°C depending on the materials. The temperature limit is set by the crucible containing the sample since unwanted alloys might form at high temperatures. Depending on the sample, it can either be directly heated if the sample is conducting, or the crucible is heated. To obtain sufficient heating powers usually water cooled coils are used at frequencies between 500 kHz and 1 MHz.

Electron bombardment produces, in contrast to the methods mentioned above, a lower stray magnetic field due to the usage of lower currents since the electrons are accelerated in an electric field. A crucible is heated by converting the kinetic energy of impacting electrons into thermal energy. The heating power therefore depends on the number of electrons hitting the sample and their velocity. Typically acceleration voltages up to 5 kV are used. Higher voltages will result in X-Rays generated on impact. The filaments generate the electrons by thermoionic emission which can be described by Richardson's law [7]:

$$j = CT^2 exp\left(-\frac{\varphi}{k_\mathrm{b}T}\right) \tag{1.16}$$
$$C = 4\pi emk_\mathrm{b}^2/h^3 \approx 120\mathrm{A\,cm^{-2}\,K^{-2}}$$

j ... current density, e ... elementary charge, m ... electron mass, k_b ... Boltzmann constant, h ... Planck constant, T ... temperature, φ ... work function of the material.

The efficiency can be increased by using materials with a low work function like thoriated tungsten. In the setup described in this work, typical emission currents are in the range of 300 mA with 1 kV acceleration voltage. The filaments used here are 20 W halogen bulb tungsten filaments which are powered with about 12 V and 1.7 A. This method is due to the use of a crucible also constrained to the formation of unwanted alloys at high temperatures. This also sets a limit for the temperature of about 2000°C.

Electron bombardment sources are often used for surface deposition. For low deposition rates (in the range of 1 nm/s) lower temperatures are required and one can directly heat the sample. The increase in local pressure is then low enough to prevent the occurrence of discharges. Such sources are described in detail in Ref. [23, 22, 40]. Typically, heating powers in the range of 1 W to 10 W are used. To reach higher deposition rates, this method has to be modified. Due to a higher local pressure discharges between the filament and the sample occur. This can be prevented by increasing the distance between the filaments and the sample, with the disadvantage that the heating power will be reduced due to fewer electrons hitting the sample. To effectively use this method a electron beam source has to be used and the electron beam must be focused onto the sample by electron optics. Then a hot spot can be created at the sample surface and the reachable temperature is basically constrained by the applied heating power.

Another method for reaching extreme temperatures is **laser ablation**. A laser is therefore focused on a spot of the sample. Usually the sample is rotated to prevent from burning a hole into the sample. Either continuous or pulsed heating is possible. Due to the high energy in pulsed mode one can even produce small clusters. This method is used in Refs. [12, 38] to dope helium nanodroplets (He_N).

The high temperature source to evaporate chromium (Cr) explained in Sec. 2.4.1 is based on electron bombardment. The required temperature to dope Cr onto He_N was unknown at first so the Knudsen cells were omitted due to the temperature limitation. Boat sources and inductive heated ovens were excluded due to the stray magnetic field which would interfere with the magnetic field required for the electron spin resonance measurements. The expensive equipment required for laser ablation, like a laser with sufficient power, optical feedthroughs and optics designed for such powers, make uneconomical.

1.5.2 Effusive Source

An effusive source creates a beam of particles with thermal velocities. This is achieved by effusion of particles through a small hole of an enclosed box. Effusive sources have been well studied in the last century. The easiest approach is the effusive source with a thin-walled orifice. If the number of particles leaving the source is neglectable to the number of particles inside the source, the effusion rate, the angular distribution, and the velocity distribution can be calculated by means of the kinetic gas theory. The orifice has to be small compared to the mean free path of the particles, the same applies to the thickness of the opening. In other words during the flight through the orifice the particles should not collide. Detailed explanation can be found in Ref. [46, p.83 et seq.]. The number of particles leaving the effusive source can be calculated with:

$$N_0 = 1.125 \cdot 10^{22} \frac{p_0}{\sqrt{MT}} \sigma \tag{1.17}$$

N_0 represents the particles emitted on axis per solid angle of 1 sr and per second. p_0 is the pressure inside the effusive source given in torr, σ is the area of the orifice in square centimetres, M and T are the molecular weight in amu and the absolute temperature of the gas in K, respectively. The unit of the constant factor $1.125 \cdot 10^{22}$ is $\frac{\text{amu}\cdot\text{K}}{\text{Torr}\cdot\text{s}\cdot\text{sr}\cdot\text{cm}^2}$. The intensity distribution depending on the angle of the detector is described by the cosine law, resulting in a low overall intensity if a narrow atomic beam is required. This can be improved by using channels instad of the small hole orifice.

Chapter 2

Experimental Setup

In this chapter the existing setup of the superfluid helium nanodroplet (He_N) beam apparatus is described, more details can be found in Ref. [27, 31]. It is used for spectroscopy in He_N and electron spin resonance (ESR) experiments on He_N in special[28, 30, 29]. The method is now being expanded for more general ESR applications in the course of this work. Therefore, a quadrupole mass spectrometer (QMS), a high temperature (HT) pickup source, and a first implementation of gas pickup have been implemented and characterised. In the following sections a detailed description can be found.

2.1 Existing Setup

In the year 2006 a conventional molecular beam apparatus formerly designed, built, and used by John S. Muenter, University of Rochester, was transferred to the Institute of Experimental Physics, Graz University of Technology. Markus Koch turned the apparatus into a He_N machine and prepared it for electron spin resonance experiments. A detailed description of the apparatus and the laboratory including drawings can be found in Markus Koch's doctoral thesis [27] and in Johannes Lanzersdorfer's diploma thesis [31].

He_N are formed in a free jet expansion under high vacuum conditions. During their flight through the apparatus they pick up particles under investigation and take them to the measurement section. Usually detection methods like beam depletion (BD), laser induced fluorescence (LIF), and mass spectrometers are used on a He_N beam apparatus.

Here, these methods are combined with an electro magnet for magnetic fields from 0 T to 1 T and a microwave cavity along the He_N beam axis. Laser feedthroughs through the pole shoes allow pump and probe experiments in the magnetic field, with the microwave cavity in between the two laser intersections optically detected magnetic resonance (ODMR) experiments are possible. The polarisation of the intersecting lasers can be controlled with Pockels cells to apply the magnetic circular dichroism scheme.

The very first ESR spectra of species on He_N were measured in May 2008 by Markus Koch, starting with potassium (K) but followed soon by rubidium (Rb). The shift of the hyperfine constant due to the interaction of the He_N and the single alkali-metal atom had been studied and Rabi oscillations indicating coherent ESR transitions had been observed. The results were published in Refs. [28, 30, 29].

2.1.1 Vacuum Chambers

The apparatus consists of four chambers mutually separated from each other by valves.

The first chamber is called source chamber since the helium nanodroplet beam is created there. The chamber is pumped by an oil-diffusion pump (Varian diffusion pump 0163) with a pump-speed of 4200 l/s. It's backed with a roots vacuum booster (Leybold-Heraeus WS500) and a rotary vane pump (Alcatel 12100 SD). Depending on the flow of helium through the nozzle different pressures can be reached. With the nozzle at room-temperature (300 K) and a nozzle pressure of 10 bar a final pressure in the lower 10^{-6} mbar can be reached. Under normal flow conditions with the nozzle temperature at about T_0 =15 K and p_0 =50 bar nozzle pressure the final pressure is at about $3 \cdot 10^{-4}$ mbar. The pressure is monitored with a Pirani gauge (Leybold-Heraeus 162 02 Br 2), which is connected to an interlock system for an emergency shutdown of the oil diffusion pump at too high pressures. For the high vacuum range the pressure is measured by a cold cathode vacuum gauge (Leybold Inficon 850-610-G2).

In the second chamber, the pickup chamber, the pickup process takes place. It is pumped by a turbomolecular pump (Leybold Turbovac 361) backed with a rotary vane pump (Varian CD 0700). Typically after about a week of pumping a final pressure of about $3 \cdot 10^{-7}$ mbar is possible. Usually a pressure of between $3 \cdot 10^{-6}$ mbar and $7 \cdot 10^{-6}$ mbar is reached within a day, depending on the level of contamination after opening the vacuum chamber. If the high temperature evaporation source is used the pressure will rise due to heating the inner surface of the vacuum chamber. The chance of discharges inside the high temperature evaporation source is increased at higher pressures, therefore it should only be used at pressures below $2 \cdot 10^{-5}$ mbar. The vacuum is measured by two instruments, a Pirani gauge (Leybold-Heraeus 162 02 B3) which is connected to the interlock system to stop the turbomolecular pump in case of emergency, and a full range vacuum gauge, a combination of a Pirani and a cold cathode ionisation gauge (balzers PKR 250).

The third chamber contains the measurement section. It is also pumped by a turbo molecular pump (Pfeiffer TMU521P) which is backed by the same rotary vane pump (Varian CD 0700) as the pickup chamber. The final pressure reached in this chamber is approximately $3 \cdot 10^{-7}$ mbar. The pressure is measured with a Pirani gauge (Leybold-Heraeus 162 02 B3) for the interlock system, and a full range vacuum gauge, a Pirani and Penning gauge combination (Pfeiffer Vacuum PKR 251).

The last chamber contains a quadrupole mass spectrometer which has been added to the apparatus in the course of this thesis. It's pumped by a small turbomolecular pump (balzers TMU065) with a membrane pump (Vacuubrand 18331909 04) as backing pump with a final pressure in the upper 10^{-8} mbar range. The pressure is measured with a Bayard-Alpert gauge (Granville-Phillips 274002).

2.1.2 Existing Detection Methods

The superfluid helium nanodroplets are produced by a free jet expansion through a 5 μm nozzle. The nozzle is cooled by a two stage coldhead (Leybold RGD 1245) with the first stage at about 35 K and the second stage at approximately 9.5 K. The nozzle temperature is stabilised by a PID controller, a silicon diode, and a conventional heater and can be varied between 9.5 K and approximately 29 K. Usually, He at a pressure of $p_0 = 50$ bar is used, resulting in a mean number droplet size of 10^4, see Sec. 1.3. The helium beam is then skimmed by a skimmer

with an opening of 300 μm. This gives a divergent beam with a virtual source located 61 mm upstream of the skimmer and a divergence of $4.95 \cdot 10^{-3}$ rad [27].

Downstream the skimmer the droplets flies into the pickup chamber, where they can be doped with different atoms or molecules. After a chopper, which is used for differential measurements, up to two pickup cells can be used for the doping process. A gas feedthrough into the pickup chamber designed for a gas pickup cell was used to flood the whole pickup chamber with different gases. The pickup process is described in more detail in the next section (Sec. 2.2.1), and results can be found in Sec. 3.2.1. To dope the droplets with rubidium and potassium pickup cells were used which can be heated resistively to about 500°C. A high temperature evaporation source was developed which can be heated to approximately 1700°C and was used to dope chromium into the droplets. The experimental setup with the high temperature (HT) source can be found in Sec. 2.2.2.

After the pickup chamber the droplet beam reaches the measurement chamber. Optically detected magnetic resonance (ODMR) measurements are done there. A large electromagnet is used to produce a magnetic field perpendicular to the direction of flight. Two holes are drilled into the pole shoes to intercept the droplet beam, which lies between the pole shoes, with lasers. Between those interaction regions the droplet beam passes through a microwave cavity. At the second laser interaction area a combination of a spherical and an ellipsoidal mirror focuses the fluorescence light into a glass rod which leads to a photo multiplier. In this way, laser induced fluorescence (LIF) experiments can be performed based on single photon counting. A Ti:Sa (titan sapphire) laser with up to 3 W and a diode laser with up to 500 mW can be used for the experiments. With pockels cells for each of the two laser feedthroughs the laser light can be polarised circularly to exploit magnetic circular dichroism (MCD). There is also the possibility to use a Langmuir–Taylor detector for depletion experiments. More details can be found in Ref. [27].

At the end the droplets can be measured with a quadrupole mass spectrometer (balzers PPM 422). Ions are formed by electron impact ionisation with an emission current of typically 0.5 mA and an ionisation energy of typically 60 eV. Single charged particles with a mass up to 512 amu can be detected. The ions are measured with a secondary electron multiplier (SEM) with an acceleration voltage typically between 2.2 kV and 2.5 kV. For differential measurements the chopper modulates the droplet beam and triggers a counter, which counts the signals from the SEM. The difference between the chopper open signal and the chopper closed signal gives the signal for species on the He droplet. The counter is usually used with counting periods of 20 ms which has to be adjusted to the chopper trigger signal by an tuneable delay, usually 5.4 ms. A schematic of the counting process can be found in Fig. 2.5 in Sec. 2.4.2.

2.2 Expanded Setup

In this section the changes of the existing setup for the experiments performed in this thesis are described. The gas and high temperature pickup experiments required changes of the pickup chamber, Sec. 2.2.1 and Sec. 2.2.2. The pickup process is monitored by a quadrupole mass spectrometer, which had to be adapted to the existing setup, Sec. 2.2.3. For the high temperature pickup experiments temperature measurements are necessary and the measurement instruments had to be calibrated, Sec. 2.2.4. Detailed assembly instructions for the high temperature (HT) source can be found in Sec. 2.5. The HT source is controlled by a PID controller which is connected to the necessary electronics, Sec. 2.4. The measurements are recorded by a computer via self-written LabVIEW programs and the results are processed typically with MATLAB scripts, Sec. 2.3.

2.2.1 Gas Pickup

The gas pickup was obtained by flooding the whole pickup chamber with the dopant gas. For later experiments a gas pickup cell with a length of 32 mm will be used. The first approach is used because of the possibility to measure the dopant gas pressure, which allows a more exact investigation of the pickup statistics. The pickup process can take place along the whole pickup chamber, therefore increasing the pickup probability compared to a short gas pickup cell at the same particle number density. The pickup chamber is approximately 30 cm long and with the used nozzle parameters the droplets have a velocity between approximately 300 m/s and 550 m/s. So the He droplet's flight time through the pickup chamber is between 1 ms and 0.5 ms. If the source conditions remain unchanged, the only parameter having an impact on the pickup probability is the particle number density of the dopant atom, that is, the pressure. The pressure was varied between about $2 \cdot 10^{-6}$ mbar and $8 \cdot 10^{-5}$ mbar indicated on the cold cathode ionisation gauge. This pressure has to be scaled to the effective pressure due to the gas type dependent detection probability. The vacuum gauge used, a "balzers PKR 250", has the same cold cathode ionisation unit as the "Pfeiffer IKR 251", for which the gas type correction factors can be found in the manual[1]. This makes the pressure of the different gas types, and therefore the pickup statistics, compareable. The pickup process was monitored with the quadrupole mass spectrometer mentioned before.

2.2.2 Chromium Pickup

In contrast to the gas pickup, different considerations have to be taken into account with the Cr source. No pressure can be defined in the interaction volume since the particles move along straight lines until they adsorb on the cooled surrounding. The pickup process can therefore better be described by a particle beam crossing the He droplet beam. Concerning the Cr source, the parameter influencing the pickup probability is the particle flux rate, which depends on the temperature.

The HT source is mounted in the pickup chamber with the opening slit being adjustable to the He droplet beam. The interaction area above the slit has a length of approximately 5 cm. The distance between the slit of the thermal protection shield around the HT source and the He droplet beam should be as small as possible. A distance of about 7 mm to 10 mm can be achieved, giving an overall distance to the Cr source between 15 mm and 20 mm. The Cr is

[1] Compact cold cathode gauge IKR 251, Pfeiffer Vacuum, BG 805 101 BD/C

located inside a Ta crucible which is heated by electron bombardment. The heating power is defined by the emission current (EC) times the acceleration voltage. Both can be varied to control the heating power, but in the experiments described here, the acceleration voltage was fixed at 1 kV while the emission current was varied by changing the filament voltage. The temperatures reached at certain heating powers can be found in the next section (Sec. 2.2.4). The heating process is controlled by a PID-controller (Eurotherm 3204) stabilising the heating power. More details on the electronic can be found in Sec. 2.4 while the Cr source itself is described in Sec. 2.5.

2.2.3 Quadrupole Mass Spectrometer

A quadrupole mass spectrometer (QMS), from balzers Instruments (PPM 422), was installed at the beam exit of the measurement chamber, and aligned to the helium nanodroplet beam axis to directly monitor the droplet beam. After electron beam ionisation the ions are selected by their mass-to-charge ratio in the quadrupole. They are then deflected by 90° and detected by a secondary electron multiplier (SEM). The mass spectrometer is, furthermore, fitted with ion optics, and the self-made mount, which is explained in detail in the following, is prepared for laser induced ionisation. The QMS is contained in a separated vacuum chamber pumped by a small turbomolecular pump (balzers TMU 065) which is backed by a membrane pump (Vacuubrand 18331904 94). The pressure is measured by a Bayard-Alpert gauge (Granville-Phillips 274002) and lies typically within the range of $8 \cdot 10^{-8}$ Pa. The QMS is mounted on a plate (Fig. B.1, Fig. B.2), which is secured to the frame of the apparatus by three M20 threaded rods, allowing translational adjustment and tilting. The QMS chamber is connected to the measurement chamber by a metal bellow and a flange (Fig. B.3) which is prepared to be expanded for laser induced ionisation in addition to electron beam ionisation. A small hole between the measurement and the QMS chamber allows differential pumping and can be sealed if desired.

2.2.4 Temperature Measurement and Calibration

The temperature of the high-temperature evaporative source and the prototype has to be measured. Since the source is designed to evaporate chromium with a correspondingly high melting point, one should be able to measure temperatures up to 1700°C. Two ways were chosen, a Type-R thermocouple, and a pyrometric approach, which will be explained in detail in the following sections.

Type-R thermocouple

The Type-R thermocouple consists of 2 wires, one platinum wire and one platinum-rhodium alloy wire with 13% rhodium. Those thermocouples can be used up to approximately 1750°C. On one side the two wires are spot welded to eachother and preferably also to the object under measurement. If the thermocouple just touches the object under measurement, experiments showed a significant increase in measurement inaccuracy (50% and more) if the object is kept under vacuum conditions and at temperatures above $>$ 800°C. The other side of the thermocouple is connected to a multimeter which was kept at room temperature to measure the voltage. [2] Depending on the temperature difference between the hot and the cold end of

[2] This is the well known thermoelectric or Seebeck effect.

the thermocouple voltages up to 21 mV are generated. One has to be very careful since due to the fact that the object under investigation is connected to a high voltage source, also the multimeter used to measure the thermocouple voltage is at the same potential. In the case of my prototype setup this was 1 kV which will lead to electrocution on contact.

A reference table from the "NIST ITS-90 Thermocouple Database" [41] was used in the program "temp_typ_r.m" which calculates the temperature difference at a given voltage. The program can be found on the enclosed CD.

For the prototype setup a multimeter with a 0.01 mV resolution was used. Unfortunately no information about the measurement inaccuracy could be found so it is assumed to be about 0.05 mV. Compared to the ITS-90 Table [41] this leads to a measurement inaccuracy of about $\Delta T_{\mathrm{NIST}} = \pm 5°\mathrm{C}$. Adding the room temperature uncertainty of $\Delta T_{\mathrm{room}} = \pm 2°\mathrm{C}$ leads to $\Delta T = \pm 7°\mathrm{C}$. But the comparison of different measurements indicate that the over all measurement inaccuracy can be estimated with $\Delta T = \pm 30°\mathrm{C}$.

Pyrometer

The one and two channel pyrometer, Raytek MRS1, was used to measure the temperature. Two main problems arose from using a pyrometer.

First of all the object under measurement is small compared to theacceptance angle of the detector. This basically affects the one channel measurement and the pyrometer will show a lower temperature than the actual temperature of the object.

Second, since the object is inside a vacuum chamber a window has to be used, a 15 mm thick acrylic glass for the prototype setup and a 6 mm thick acrylic glass window for the main setup. This influences both modes of the pyrometer because the window shows adsorption depending on the wavelength. The two different wavelengths used in the 2 channel mode will be affected differently, leading to a too high temperature measurement. The one channel mode is influenced due to the adsorption of the window. In this case the pyrometer indicates a lower temperature.

Furthermore, the one channel mode is affected by the emission coefficient of the object under measurement. Depending on whether pointing at the tantalum crucible or the chromium itself, different emission coefficients have to be taken into account. According to Ref. [35, p.10-261] the emission coefficient of tantalum at 1500°C is 0.21 and for chromium at 500°C to 1000°C it is between 0.28 to 0.38. The different emission coefficients do not affect the two channel mode of the pyrometer as long as the sample obeys Planck's law of radiation.

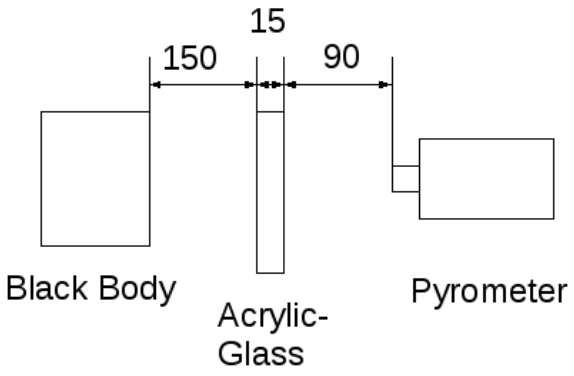

Figure 2.1: Setup of the temperature calibration

The pyrometer was calibrated with a black body between 1000°C and 1300°C including the 15 mm acrylic window (Fig. 2.2.4). Both the two channel mode and the one channel mode where calibrated. The different thickness of the acrylic window used for the main setup influences the results shown in one channel mode due to the reduced adsorption. The pyrometer's parameter for the one channel mode is the emission coefficient, called EPS,

and for the two channel mode it is the slope of the line connecting two intensities at different wavelengths. This is conform to the differential quotient of the Planck's law of radiation. Three measurements where taken at each temperature step and for each mode of the pyrometer and are shown in Tab. 2.1 and Fig. 2.2. At first the emission coefficient was set to 1 (EPS=1), referred to as T_{11}, to see the adsorption of the window. Also the slope was set to a standard value of slope=1, referred to as T_{21}. Then, the parameters were optimised for 1300°C with EPS=0.82 (T_{12}) and slope=1.056 (T_{22}), which means that at a black body temperature of 1300°C EPS and slope were altered so that the pyrometer showed the black body temperature within ±1°C. To see the temperature dependence of the parameters they were also altered at each temperature step taken, referred to EPS and slope.

Since the object under measurement was small only the two channel mode of the pyrometer can be trusted. The one channel mode, however, sets a lower limit to the temperature since the emission coefficient of the object's material was not taken into account.

For the two channel mode the measurement inaccuracy is $\Delta T = \pm 20$°C in the temperature range between 1000°C and 1300°C. Unfortunately it was not possible to calibrate to higher temperatures due to the limits of the black body, so the parameters and the measurement inaccuracy had to be scaled up to reach the measured of up to 1700°C. Taking the extrapolation and the different thicknesses of the acrylic windows into account, leads to an measurement inaccuracy of about $\Delta T = \pm 50$°C.

Table 2.1: Pyrometer temperature calibration using a black body (see Fig. 2.2)

T_{ref} ... black body temperature ($\Delta T_{\text{ref}} < 1$°C)
T_{11} ... one channel mode with EPS=1
T_{12} ... one channel mode with EPS=0.82
EPS ... one channel mode with EPS adapted ($\Delta T = \pm 1$°C)
T_{21} ... two channel mode with slope=1
T_{21} ... two channel mode with slope=1.056
slope ... two channel mode with slope adapted ($\Delta T = \pm 1$°C)

T_{ref} [°C]	T_{11} [°C]	T_{12} [°C]	EPS	T_{21} [°C]	T_{22} [°C]	slope
1300	1268	1300	0,82	1410	1301	1,056
1250	1221	1250	0,82	1352	1251	1,056
1225	1197	1226	0,83	1326	1227	1,058
1200	1173	1201	0,83	1300	1203	1,058
1175	1149	1177	0,83	1273	1180	1,060
1150	1126	1153	0,83	1248	1157	1,061
1125	1102	1127	0,83	1222	1134	1,062
1100	1078	1103	0,84	1197	1111	1,063
1050	1030	1053	0,84	1148	1064	1,066
1000	982	1003	0,84	1096	1017	1,069

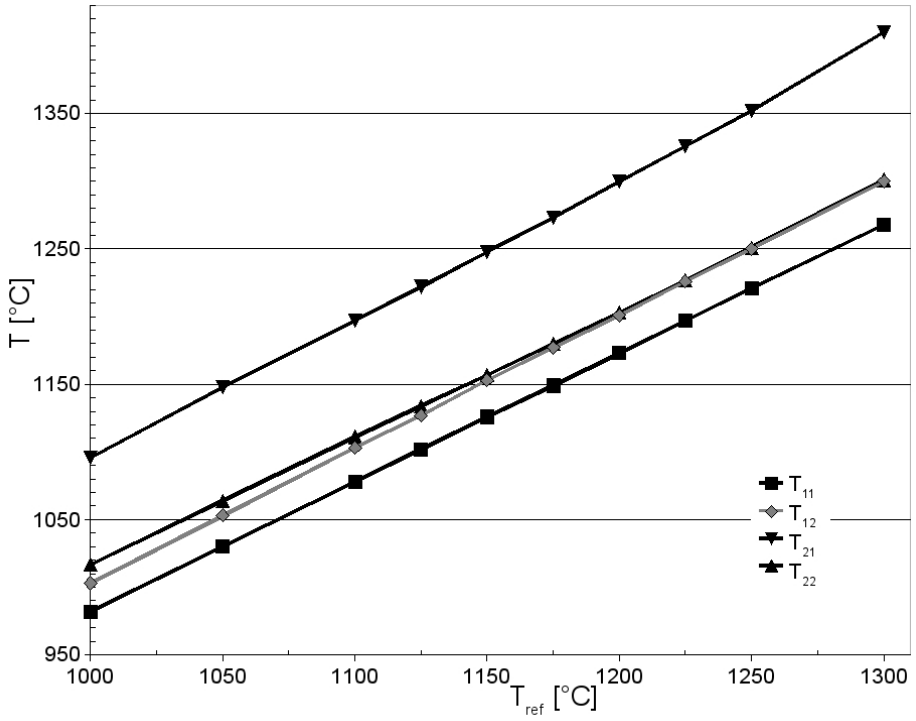

Figure 2.2: Temperature calibration of the pyrometer under different conditions (values see Tab. 2.1)

2.3 Software

In this section the LabVIEW programs used for measurements are described briefly. Also, the measured data was analysed with Origin after it was preprocessed by Matlab/Octave scripts. The pickup process itself was evaluated in another Matlab/Octave program.

2.3.1 Measurement Programs

For pickup statistics the dopant species is monitored with a quadrupole mass spectrometer (QMS). In combination with the high temperature (HT) source a PID-controller "Eurotherm 3204" is used to stabilise the heating power. During measurements both devices are connected to the computer by RS232 interface and can therefore be controlled and read by computer programs written in LabVIEW (8.5.1).

Eurotherm Programs

The programs named with "Eurotherm" in the beginning are used to controll the HT source. The software can be found in [CD:\Software\HT_Source\].

"Eurotherm_read.vi" reads the process value of the PID-controller. It is direct proportional to the heating power by a factor of about 10.

"Eurotherm_Setpoint.vi" allows to set a new setpoint for stabilising the heating power. The controller has to be set to automatic mode.

With "Eurotherm_Write.vi" the heating process can either be automatically or manually controlled. The program sets the PID-controller to manual mode, sets the manual output value and the setpoint, and the user can choose wether the PID-controller should stay in manual mode, using the manual output value, or should change to automatic mode, stabilising to the setpoint value. The manual output value represents a percentage of the maximum filament voltage. It is limited to a maximum of 16V by hardware, representing 100% of the manual output value. The PID-controller is restricted to a value of 80% of the manual output value, resulting in a filament voltage of maximal 12.8 V.

"Temperature_measurement.vi" can be used to measure the temperature characteristics of the HT source. The program sends the manual output value to the PID-controller, which has to be set to manual mode before. Then, the temperature, measured with a pyrometer, is entered by hand and the data is appended to a file by clicking on "write to file". The chart displays the process value, which is also written to the file.

Quadrupole Mass Spectrometer Programs

The programs starting with "QMS" are used to control the QMS. The token "diff" at the end of the name indicate differential measurement using a chopper modulated counter signal. In all the programs the voltages V1 to V7 and the resolution of the QMS can be set, see the manual[3] for more information on the voltages. Also, the filament emission current (I_{EC}) for the electron impact ionisation and the acceleration voltage (U_{SEM}) of the secondary electron multiplier can be controlled and switched on or off. Usually, the following values were used during experiments: V1 = 120 V; V2 = 60 V (represents an ionisation energy of 60 eV); V3 = 9 V; V4 = 5 V; V5 = 20 V; V6 = 324 V; V7 = 110 V; I_{EC} = 0.5 mA; U_{SEM} = 2.2 kV to 2.5 kV; resolution = 20. A switch labelled "integration time" scales the measured signal to

[3] PPM 422 Documentation (Order No 515 431); balzers Instruments

counts per second. The counter can be used with an integration time of either 0.2 s or 1 s and the switch will scale the value up by a factor of five when 0.2 s are selected. All the programs should be stopped by using the stop button on the front panel since the communication with the QMS requires a termination of the communication via RS232.

"QMS_sample.vi" is used to monitor one specific mass selected by the mass input field. The signal is shown in the chart, with the actual counts on the lower righthand side. Also, the mean over the last seven measurements is calculated and displayed.

"QMS_sample_diff.vi" is analog to the program explained above but instead of showing the counts directly the difference between open and closed chopper channels is displayed. No average value is shown but the open and closed counts are displayed.

"QMS_SampleMulti_diff.vi" is used to monitor the difference signal of up to five different masses. They can be switched on and off separately. Also, the charts can be cleared either alltogether or separately. The program reads both the process variable of the PID-controller as well as the output value, which corresponds to the filament voltage like the manual output value. This program is used for the measurements of the chromium pickup characteristics.

"QMS_samplearray_diff.vi" is used for the gas pickup characteristics. Analog to the program above one can specify several different masses in an array and the masses will be measured consecutively. With cycles per mass the number of counting periods for each mass can be controlled. A value larger than one must be chosen since due to mixing of the signal of different masses, the first measurement cycle of each mass must be rejected. One can enter the current pressure of the pickup chamber since this was one of the parameters relevant in the gas pickup process.

"QMS_scan_diff.vi" is used to record a mass spectrum. A start and stop pointfor the mass spectrum must be entered and the increment, usually about 0.25 amu, must be specified.

2.3.2 Data Analysis

Many different scripts have been written to prepare the data for analysis. In the following the scripts of general use are explained briefly and the scripts used for data preparation are listed. Also, a program was written to compare the measured data with a model. They are commented and explained within the files. The scripts can be found in [CD:\Scripts\]. They are organised in different subdirectories depending on their use.

Generic:
Here, independent scripts can be found. The two scripts "vapour_pressure_Cr/Cu.m" can be used to calculate the vapour pressure for chromium and copper given by the vapour pressure curve of Ref. [35]. The temperature must be entered in K and the pressure is then calculated in Pa.
"temp_type_r.m" calculates the temperature difference in K when the thermocouple voltage of a type R thermocouple is given in mV. The thermocouple voltages given by Ref. [41] are interpolated.

Pickup:
In this directory the scripts for modelling the pickup process can be found.
"Acetylene/Ar/Cr/H2/Ne_Pickup.m" are used to prepare the measured data for further analysis. "droplet_size_distribution.m" can be used to calculate the probability to find a helium nanodroplet of a certain size for a given mean number droplet size, which can be calculated

by the power model for example. For this script some parameters have to be obtained by measured data from Ref. [18]. The data was fitted in "droplet_size_distribution_fit.m" but the results are hardcoded in the script named above. "DropVelocity.m" can be used to calculate the velocity of the droplets for a given nozzle temperature, in K. This script was formerly written by Markus Koch [27] and has been adapted slightly.

Processing:
Since some of the matlab scripts, like "Cr_Pickup.m", produce "eps" files, they can be converted on linux systems by using the shell script "convert_ps_to_jpg.sh" which relies on Ghostscript.

Modelling the High Temperature Pickup Process

The pickup process with the use of the HT source is modeled in "Cr_Pickup.m". An effusive source is used for the HT source. The particle flux from the effusive source can be calculated by the script "effusive_source.m" which already is trimmed to the dimensions of the used HT source. This script requires "vapour_pressure_Cr.m" to work properly, since the pressure inside the effusive source has to be calculated. These scripts give the number of chromium atoms in the interaction area with the helium droplet beam. At the beginning of "Cr_Pickup.m" one can control the output by several variables, which will also result in different calculation processes. The easiest approach to model the pickup characteristics is by the use of a mean number droplet size given by the power model ("show_pickupP=1"). This results in the pickup probability of a single particle. The droplet size distribution can be taken into account ("show_pickupD=1"). Since the geometrical cross section of the droplet is dependend on the droplet size distribution, the droplet size dependency can be taken into account by a convolution. The above described methods focus only on single droplets. The massflow through the nozzle has also be taken into account ("show_pickupM=1"). The nozzle temperature also affects the massflow through the nozzle. But the droplet size might have a bigger impact on the number of droplets produced. Larger droplets require more He atoms resulting in fewer large droplets.

The model can be used to see rough trends of the measured data. There is still some discrepancy between the model and the measurements which arise due to the fact that the complex process of electron impact ionisation leads to unpredictable fragmentation. This will be improved by laser induced fluorescence measurement where one can directly address different Cr oligomers selectively. Also, the destruction and deflection of smaller droplets on pickup has not been considered in the model above. A quick approach would be to use a cutoff droplet size in the He_N size distribution.

2.4 Electronics

2.4.1 High Temperature Source

For a high temperature (HT) pickup source based on electron bombardment two power supplies (one for the filaments and one for the acceleration voltage) and a controller is required. The power supply for the acceleration voltage should be dimensioned to fit the required heating power. The two parameters are the acceleration voltage, which is limited to approximately 5 kV due to generating X-rays with higher voltages, and the emission current of the filaments, which is limited to roughly 200 mA per filament in our case. In this case the power supply, a KSI Series 5000, can supply 1 kV with up to 1 A. It is set to its maximum voltage (1 kV) and the emission current is controlled by changing the filament voltage.

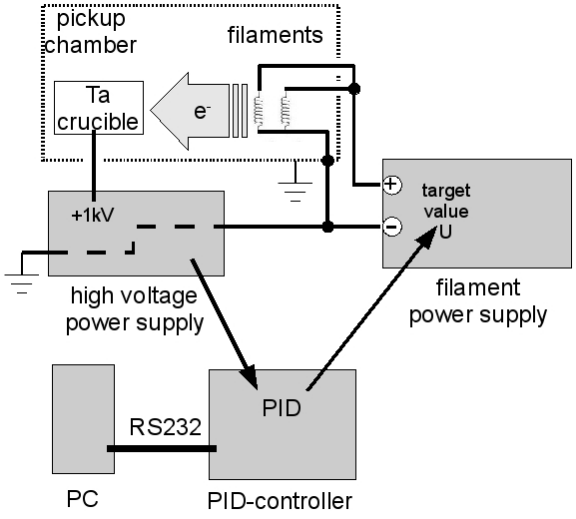

Figure 2.3: Schematic of the electronics of the HT source.

The power supply for the filaments should be dimensioned to supply a power of about 150% of the total specified powers of the filaments. A laboratory power supply "EA-PS 3032-10B" from "Elektro - Automatik" is used which can supply up to 10 A at 32 V. The filaments used are 20 W halogen bulbs (standard G4 types) with 12 V rated voltage, resulting in 1.7 A current at the rated power. Two filaments are used at the same time which are connected parallel, resulting in up to 5 A required current. A schematic setup is shown in Fig. 2.3.

A fundamental item of the electronics is the PID-controller, Eurotherm 3204, which stabilises the HT source to a given emission current, which corresponds to the heating power. It is connected to the computer via a RS232 interface, so that the parameters can be adjusted with a software. A stand alone operation is also possible, however. The controller receives the value of the emission current from the acceleration voltage power supply, and varies the filament voltage at the filament's power supply in order to stabilise the emission current to a given value. The acceleration voltage supply is connected to the controller with a 25 pin Sub-D connector, which is used to clear the interlock, indicate the high voltage output status by a LED next to the PID controller, and to monitor the current with the controller. Detailed information can be found in the manual[4]. The interlock is disabled by connecting the pins eleven and 23, since eleven is an internal power source at +15 V, pin 23 is then at the same voltage. The LED next to the PID controller is also powered by the power supply. Therefore, pins ten, the internal ground, and nine, one side of the high voltage indicator, are connected with eachother. The LED is then connected to pins four, the other side of the

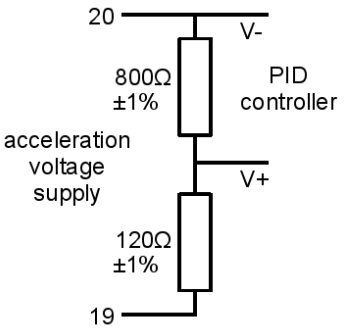

Figure 2.4: Voltage divider to scale 10 V down to 1.3 V.

[4]Series 5000, High Voltage Power Supply, Kaiser Systems Inc.

high voltage connector, and pin eleven, the +15 V power supply. The voltage (0 V to 10 V) between pins 19 and 20 is proportional to the emission current. The voltage is scaled down to an adequate value by a voltage divider shown in Fig. 2.4 before it is monitored by the PID controller.

The outputs 3A and 3B of the PID controller are used to control the voltage of the power supply used for the filaments. The output delivers a current of up to 20 mA which is converted to a voltage by a 250 Ω resistor. The voltage signal between 0 V and 5 V corresponds to an output voltage between 0 V and 16 V. The power supply is capable of 32 V output power but 16 V were chosen to prevent unwanted overloading of the filaments. The PID controller is connected to line power via a fused line filter by the connectors N and L. Also, to provide a RS232 interface, the connectors HD, HE, and HF, being common, rx, and tx[5], are connected to pins five, three, and two of a 9 pin Sub-D socket, respectively.

The filament power supply is connected to the PID controller via a 15 pin Sub-D connector as described above. A description of the pins can be found in the manual[6]. The voltage of the power supply is controlled by pins one and eleven, with one being the signal and eleven the ground. The current control must be set to maximum by connecting pins two, the target current value, and three, a 10 V reference voltage. A LED next to the PID controller is used to display the status, on or off, of the power supply. The LED is therefore connected to pins twelve, a supply voltage with up to 15 V, and pin four, the ground. To enable the external mode pin five is connected to pin four.

2.4.2 Quadrupole Mass Spectrometer

A PPM 422 quadrupole mass spectrometer from balzers Instruments is used to determine the species in the He_N. After electron impact ionisation the ions are filtered according to their charge-to-mass ratio in the quadrupole section. Then, they are deflected by 90° into a secondary electron multiplier (SEM). A schematic drawing of electronics following the SEM is shown in Fig. 2.5. The SEM signal is amplified by a preamplifier by a factor of 200 and dampened by an 10 dB attenuator before the discriminator. The discriminator is connected to a counter which which is capable of four channel counting. The counter is triggered by the modulation signal of a chopper which is connected to the counter via a signal delayer. The chopper signal must be delayed by about 5.4 ms for the optimum signal. The counter is then read by the computer.

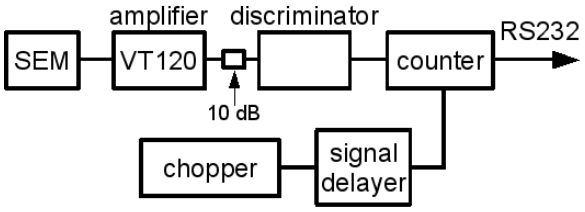

Figure 2.5: Schematic drawing of the quadrupole mass spectrometer electronics.

The controller of the QMS is also connected to the computer via RS232 and is controlled by LabVIEW programs described in Sec. 2.3.1. Also the standard parameters used for the measurements can be found there. Eight voltage parameter allow the adjustment of acceleration, focussing, and deflection elements in the quadrupole system. More details on each parameter can be found in the manual[7].

[5] common, rx, tx are used for ground, receive data, and transmit data, respectively
[6] Laboratory Power Supply EA-PS 3032-10 B (Nr.: 35320174) Elektro-Automatik
[7] PPM 422 Documentation (Order No 515 431); balzers Instruments

2.5 Construction of the High Temperature Pickup Source

In this section the assembly instructions of the high temperature (HT) pickup source can be found. A schematic drawing is shown in Fig. 2.6 and can be compared to a photo in Fig. 2.7. This design is based on the experience obtained from preliminary tests with a prototype HT source set up in an external vacuum chamber (see Appendix A)

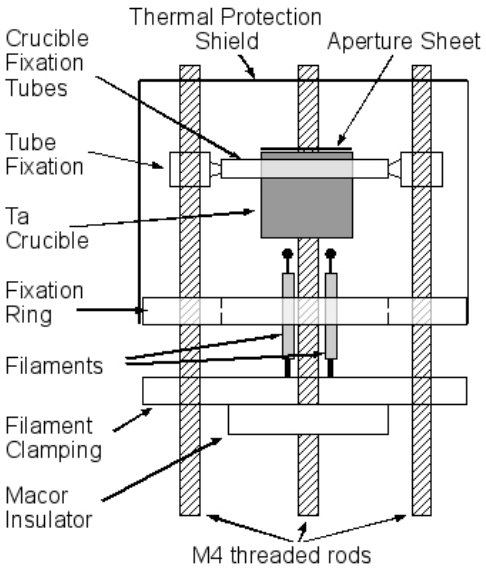

Figure 2.6: Schematic drawing of the high temperature pickup source. no to-scale drawing!

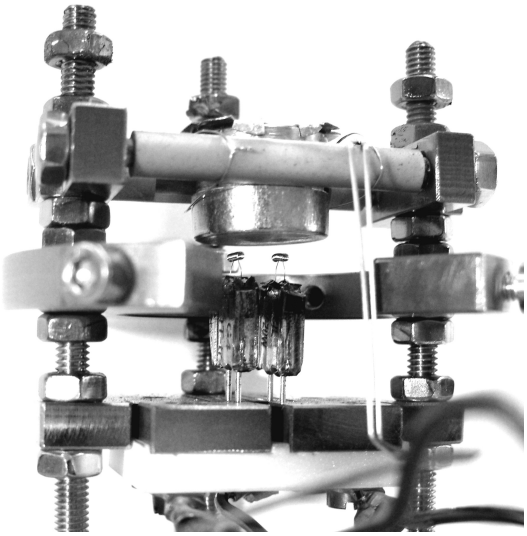

Figure 2.7: Photo of the high temperature pickup source without thermal protection shield.

To build the HT source one needs the following materials: stainless steel M4 threaded rods, about 30 stainless steel M4 nuts, a few M3 screws preferably stainless steel, stainless steel plates with 5 mm and 6 mm to 8 mm thickness, a Macor plate with approximately 5 mm thickness, a copper or brass tube with about 58 mm inner diameter, a copper or brass sheet with up to 5 mm thickness, a tantalum sheet approximately 0.2 mm thickness, a tantalum rod with 16 mm diameter, tungsten or other high temperature material wires, high temperature ceramic tubes with 5 mm outer diameter, and a copper tube with 4 mm outer diameter. The listed materials should give a rough overview of the required materials, but they can be varied depending on availability.

Baseplate

For mechanical stability it is best to start with a baseplate where the pickup source can be mounted on. For this purpose a baseplate made of a 10 mm thick aluminium plate is prepared to carry two separate pickup sources. This allows a combination of Cr pickup with the pickup of eg. gaseous or low melting species. The dimensions are shown in Fig. B.4. Two holes to fit M4 threaded rods were added on one side to mount a shield above the HT source to prevent contamination of the pickup chamber with Cr.

Three M4 threaded rods of about 110 mm length are put through three adjacent holes with 4.1 mm diameter in the baseplate. They should stick out for about 20 mm on the lower side and are kept in place by a nut on each side of the baseplate for each rod.

To each rod three nuts are added on the upper side of the baseplate. Two of them will be used for positioning the filaments and the uppermost one is used as lower fixation point of the fixation ring. It should be placed about 35 mm off the rods end. The fixation ring can be found in Fig. B.5. It is secured by another nut on each of the rods. The fixation ring has four holes drilled radial towards the centre for fixating the thermal protection shield later on. This contact is needed for cooling due to heat conduction.

Mounting the Crucible

Now the tantalum (Ta) crucible is added (Fig. B.6). The crucible must be electrically isolated to the rest so it is supported by two ceramic tubes. The tubes are prepared as shown in Fig. B.7. The tubes are hold by the tube fixation shown in Fig. B.8 and are secured by four M4 threaded rods formed as shown in Fig. B.9. The crucible is covered by an aperture sheet, Fig. B.10, made of a 0.2 mm tantalum sheet. The sheet is cut radially inwards for about 2 mm several times to create small sectors that can be bend downwards to secure the aperture sheet on the crucible. To find the correct position of the crucible one starts by adding one nut to each of the two rods along the long axis of the baseplate. The third rod, which lies off axis, is not used for the crucible fixation. Those nuts should touch the nuts securing the fixation ring. Then, the T-shaped tube fixations are added in a way that the top of the T is pointing outwards. After they are secured by nuts the conical shaped M4 rods are screwed inwards so that the cones pertrude on the inside a little.

The crucible has to be prepared with an electric contact. Therefore, a 0.2 mm (or more) tungsten wire with a length of about 200 mm is used. The wire must be able to support currents of up to 1 A. The wire is wound once around the notch of the Ta crucible and twisted, to hold in this position. It is bend upwards pointing in the direction of the opening of the crucible. The two ceramic tubes are then placed with the flat side towards the crucible in the notch. The wire wound around the crucible should be located inside the tubes. The most difficult part is to position these parts with the tube fixation. The ceramic tubes with the crucible inbetween is positioned between the tube fixations by screwing the cone shaped rods inwards carefully. The cones must fit into the tubes but the tubes should still be loose enough to prevent them from breaking by thermal tensions. The crucible should now be centred between the tube fixations and secured by high temperature wires (0.1 mm tungsten is used in my case) by clamping the tubes together. The wires must not touch any parts on ground potential, like the rods, the tube fixations or the cone shaped rods. Now the cones can be countered by nuts on the outside. A screwdriver must be used to make sure that the cones itself are not moved. Now the contact wire, still pointing upwards, is U shaped downwards through the open area of the fixation ring. Also, it must not touch anything on ground potential and it is best placed in a distance of at least 5 mm to everything on ground potential. One has to be careful after heating the HT source, as the tungsten wires will get brittle after exposition to high temperatures.

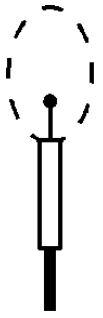

Figure 2.8: Preparation of the filaments, the dashed part is crushed in a vice.

Filaments

Now the filaments are added. The filaments used are pin halogen light bulbs (standard G4 types) with 20 W. There are two different designs available, with the filaments parallel or perpendicular to the pins. The latter ones are needed for this design. The glass bulb has to be crushed in a vice, so that only the filaments connected to the pins remain, Fig. 2.5. For mounting the filaments the following parts are used: the filament clamping Fig. B.11, the Macor insulator Fig. B.12, and the filament connectors Fig. B.13. The Macor insulator is connected to the filament clamping by two M3 screws in a way that the protrusion points towards the clamping. One of the screws is used to bring the filament clamping in contact with a wire, by the use of an eye-crimplet. Notice that the insulator should have direct contact to the clamping, so the wire contact is not in between. Then, the filament connectors are placed in the pockets of the Macor insulator protrusions that the small holes are close to eachother and to the clamping. Before these connectors are secured, also by M3 screws, they have to be connected to wires by eye-crimplets. Now the filaments are placed by prying the 0.5 mm slits open and inserting one of the two pins of the filament. The other pin should be bend slightly before to fit into the 0.8 mm hole of the filament contact stiffly. One has to be careful not to break the Macor insulator in this process. The two filaments should be placed parallel to each other and at the same height. Then the filament clamping is added to the existing construction. With the overall six unused nuts the filament clamping can be positioned underneath the crucible in a way that the filaments are in a distance of 1 mm to 2 mm, and that they are centred relative to the bottom of the crucible.

Thermal Protection Shield

To assemble the water-cooled thermal protection shield a brass tube with 58 mm inner diameter and a height of 30 mm is used, Fig. B.14. To establish a good thermal contact between the the fixation ring and the shield, it is fastened by four screws to the fixation ring. Therefore four slits are cut into the tube as shown. A cover (Fig. B.15) is hard-soldered onto the tube on the opposite side of the four slits. The holes and the slit of the cover are relative oriented in respect to the four slits of the tube in order to be mounted on the fixation ring and the three M4 rods. A copper tube with 4 mm outer and 3.75 mm inner diameter is wound around the tube of the thermal protection shield four or five times and also soft-soldered or hard-soldered to the shield. One should have at least 100 mm to 150 mm tube extended on both ends for connection to the water feedthroughs. The thermal protection shield is placed on the existing HT source as high as possible, since the He_N beam will pass over the shield and the two M4 rods. It is secured by three nuts and is connected to the fixation ring by four screws. The rods should protrude the nuts, securing the shield, only slightly if at all. The slits of the aperture sheet must be aligned to the slit in the shield. One should have about 10 mm distance between the aperture sheet and the shield since due to the particle flux in this area the local pressure is increased drastically facilitating discharges.

Electric and Water Feedthroughs

For the supply of the HT source a flange with three electric and two water feedthroughs has been prepared, Fig. B.16. Two 900 mm long stainless steel tubes with 4 mm outer and 3 mm inner diameter are welded into the 4.2 mm holes so that they protrude about 100 mm on the outside of the flange. On the inside of the flange they are connected to the copper tubes of the thermal protection shield with Swagelok connections. Two of the three electrical feedthroughs are used for contacting the filaments with 1 mm enamelled copper wires, the third electrical feedthrough is connected to the tungsten wire of the HT source by a clean copper wire. The ground potential of the filaments is connected to the flange itself by securing an enamelled copper wire with a M3 screw to the inside of the flange. The copper wires are connected with luster terminals. Since the contact of the HT source will reach high temperatures, the plastic parts of the luster terminals have to be removed.

As mentioned before an aluminium shield was mounted above the HT source to prevent contamination of the pickup chamber.

Chapter 3

Results

In this chapter the results of the high temperature source and gas pickup experiments are shown. A high temperature (HT) pickup source is designed to evaporate chromium (Cr) to dope a helium nanodroplet (He_N) beam. The details on the experimental setup and the construction is shown in Chap. 2. The temperature characteristics of the HT source, which reaches up to ∼1650°C at a heating power of ∼200 W can be found in the following section. Detailed pickup statistics for Cr at different heating powers and at different He_N sizes can be found in Sec. 3.2.2, demonstrating the outstanding performance of the HT source by the formation of Cr microclusters with up to four Cr atoms on the He_N. For future experiments the knowledge of the pickup process of some gaseous species is of importance, and therefore, pickup characteristics of molecular hydrogen (H_2), neon (Ne), argon (Ar), and acetylene (C_2H_2) are investigated in particular in Sec. 3.2.1.

3.1 Temperature of the High Temperature Pickup Source

The temperature of the HT source was measured with the two channel pyrometer Raytek MR1S. The direct measurement of the Cr temperature was not possible since it is enclosed inside a Ta crucible. So the crucible's temperature was measured instead. To provide the direct line of sight a acrylic window with 6 mm thickness was installed and the HT source was used without the thermal protection shield.The fact that the window replaces the electrical feedthroughs of the chopper, prevents the determination of the temperature and of the pickup statistics at the same time. Also, a stable operation of the HT source is only possible with the use of the thermal protection shield. Without it the vacuum chamber is heated by radiation which increases the pressure and discharges at the HT source occur. To prevent excessive heating of the vacuum chamber several heating experiments were performed well separated in time and the data were merged.

The heating power can be controlled either with the setpoint of the PID controller (Eurotherm 3204) or one can directly control the voltage applied to the filaments and therefore the emission current. The PID controller needs some time, in the range of a few minutes, to stabilise at the desired heating power so this method is unfavourable since the vacuum chamber heats up and discharges occur. The slow reaction of the PID controller is set on purpose to prevent overshooting when a discharge occurs. On the other hand the filaments can be controlled directly. It takes about 20 s to 30 s for the heating power to stabilise. This makes the heating process faster and therefore the chance of discharges is reduced. The self-written

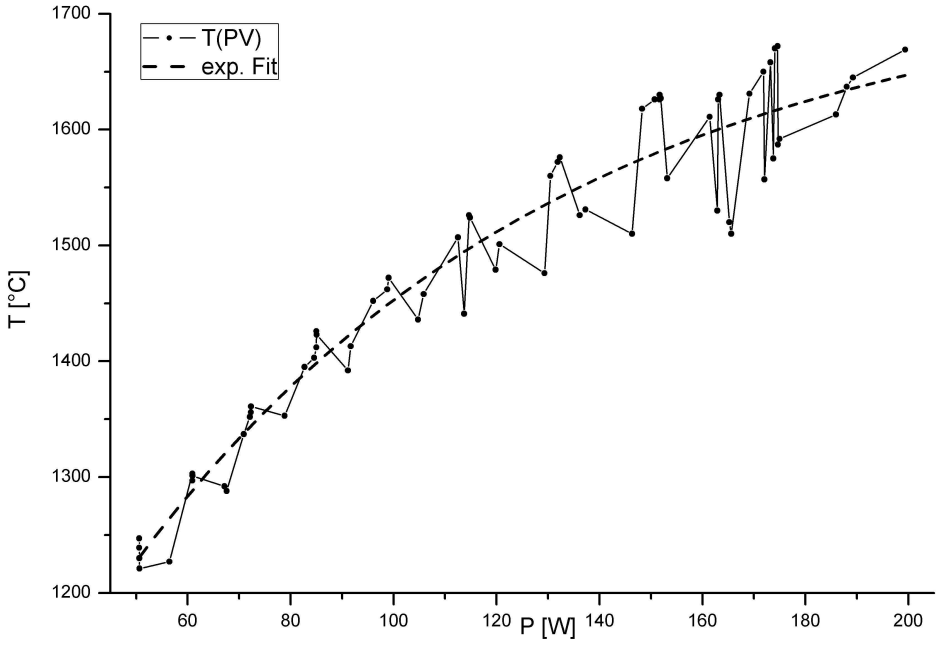

Figure 3.1: Temperature measurements (T) at different heating powers (P) of the HT source

LabVIEW program "Temp_Measurement.vi" was used to record the temperature depending on the filaments voltage. More details on the program can be found in Sec. 2.3.

The heating cycles usually were started at 50 W heating power and then the manual output value of the PID controller, which is proportional to the filament's voltage, is increased. The measurements were stopped when discharges occurred, which usually happened at 200 W heating power. A few cycles were started at higher heating powers in order to reach 200 W faster. This might lead to an increase in measurement inaccuracy. According to Sec. 2.2.4 the inaccuracy can be estimated to about $\Delta T = \pm 50°\mathrm{C}$. For the pickup process the exact knowledge of the temperature is not of prime importance as long as the source is stable.

The results are shown in Fig. 3.1 and one can see that temperatures above 1200°C are already reached with 50 W heating power. At 200 W heating power about 1650°C were achieved. The measured data was fitted with an exponential function.

3.2 Pickup Statistics

For experiments on doped He nanodroplets a profound knowledge of the pickup process is essential. In this section the pickup process of atomic and molecular gases will be discussed. Furthermore, the pickup of Cr with the self–built HT source is investigated. The pickup parameters for single and multiple particle doping and the problem of contamination with unwanted species are obtained as result. The pickup statistics is monitored by a quadrupole mass spectrometer and the signal is modulated by a chopper to distinguish between the dopant and the effusive signal. A detailed explanation can be found in Sec. 2.2.

3.2.1 Gas Pickup

The gas pickup is established by flooding the pickup chamber with the desired gas through a feedthrough. The flow is controlled by a leak valve. A stable pressure is reached within about one minute after changing the flow rate, and a equilibrium between influx and pumping speed will be established. The pressure is measured with a Penning gauge (balzers PKR 250) but the displayed value must be corrected due to the different sensitivity of the gauge depending on the gas type. A description of the pickup chamber in more detail can be found in Sec. 2.1.1. For the calculation of the corrected pressure, data from the manual[1] of an identical cold cathode ionisation gauge "Pfeiffer IKR 251" was used.

The analysed gases are argon (Ar), neon (Ne), molecular hydrogen (H_2), and acetylene (C_2H_2). The first two were chosen because in future studies the interaction of single alkali-metal atoms on the surface and other species inside the He droplets will be investigated. Molecular hydrogen has two spin isomers – para- and orthohydrogen, with anti-parallel and parallel spin orientation, respectively. Especially the latter one with a spin of one is of interest for future experiments. Since the spin does not affect the pickup process gaseous H_2 in its natural ortho/para mixture at room temperature was used.
Acetylene was chosen when testing the quadrupole mass spectrometer (QMS) since it was available and it has a mass which can easily be distinguished from other contaminations like water and from He cluster fragments itself.

As mentioned above the pressure measured has to be multiplied by a correction factor given in Tab. 3.1 to get the corrected pressure. $p_{eff} = K \times$ indicated pressure The values were taken from the manual of the Penning gauge[1]. The gauge is calibrated for air. The factors are valid for a corrected pressure of up to 10^{-4} mbar except for xenon (Xe) and krypton (Kr) where this linear relationship is broken at $p_{eff} \approx 10^{-5}$ mbar. No correction factor was found for acetylene so the indicated pressure is used.

For all pickup studies with the QMS the He dimer, mass eight, was also monitored. This is an indicator for the number of He clusters reaching the mass spectrometer. With no pickup present, the droplet beam conditions are compareable between the experiments. The reduction of the He dimer signal during pickup

Table 3.1: Gas type dependence correction factors for cold cathode gauges[1]

g . . . gas type
K . . . correction factor

g	K
air	1.0
Xe	0.4
Kr	0.5
Ar	0.8
H_2	2.4
Ne	4.1
He	5.9

[1] Compact cold cathode gauge IKR 251, Pfeiffer Vacuum, BG 805 101 BD/C

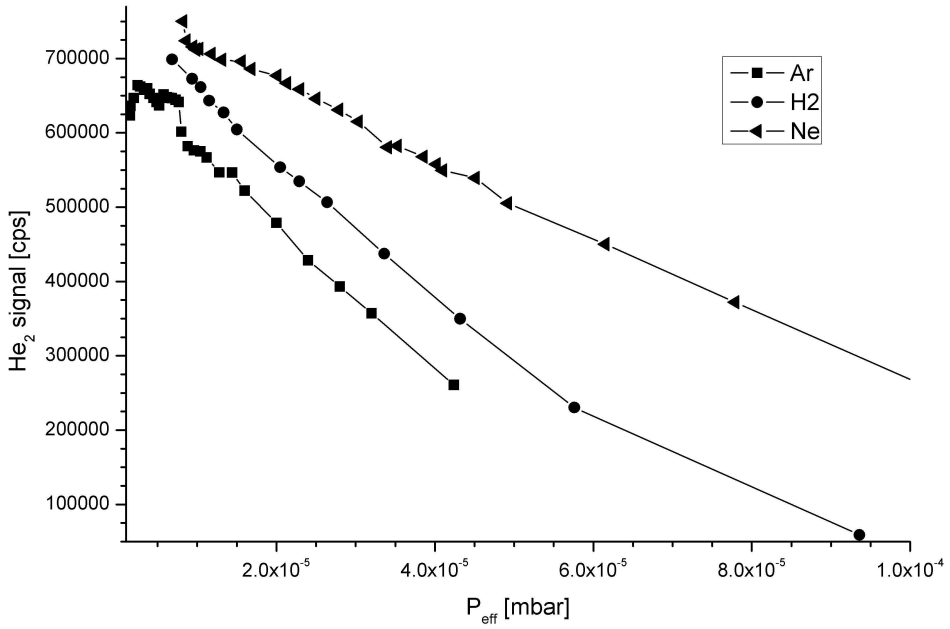

Figure 3.2: The He dimer signal for Ne, Ar, and H_2 in dependence of the corrected pressure (p_{eff}); SEM: 2.3 kV; EC: 0.5 mA; T_0 = 15 K; p_0 = 50 bar
[CD:\Analysis\Pickup\100311_Gas_Pickup.opj]

can be explained by the complete evaporation of the He droplet upon multi particle pickup, and additionally the deflection of smaller droplets [34]. The He dimer signal over the corrected pressure can be found in Fig. 3.2 for Ne, Ar, and H_2. Acetylene was not included due to the missing corrected pressure relation and the missing comparability to the other gases. As expected, the same number of doped atoms leads to more evaporation of He in the case of Ar pickup as compared to the pickup of lighter Ne atoms. H_2 lies in between, presumable due to activated internal degrees of freedom (vibration and rotation). The measurement was done with 2.5 kV SEM voltage, an emission current (EC) of 0.5 mA, and a count rate of 1 s using the program "QMS_samplearray_diff.vi", which is explained in Sec. 2.3. The nozzle parameters were T_0 = 15 K, and p_0 = 50 bar, resulting in approximately 12000 He atoms per droplet, calculated with the power model (Sec. 1.3.2, Eqn. 1.2). This gives a droplet cross section of about 8200 Å^2 [50], see Sec. 1.3.

Ne Pickup

The pickup process of neon shows an untypical characteristic. The monomer, trimer and tetramer signals have well defined maxima. This is in contrast to the dimer signal, which just decreases with increasing corrected pressure. Since trimers and tetramers are obviously existing also dimers must be a valid constellation inside the droplet. A direct pickup of Ne clusters is not possible because no clusters are formed in the gasphase. A possible explanation is the destruction of the dimers during the charge hopping process upon electron impact ionisation in the mass spectrometer.

The maximum of the monomer peak is reached at about $p_{eff} = 4 \cdot 10^{-5}$ mbar, the trimer and tetramer maxima are found at approximately $p_{eff} = 6 \cdot 10^{-5}$ mbar (Fig. 3.3). Note that the He_2 signal is reduced to ∼70% at $p_{eff} = 4 \cdot 10^{-5}$ mbar, which indicates a massive destruction

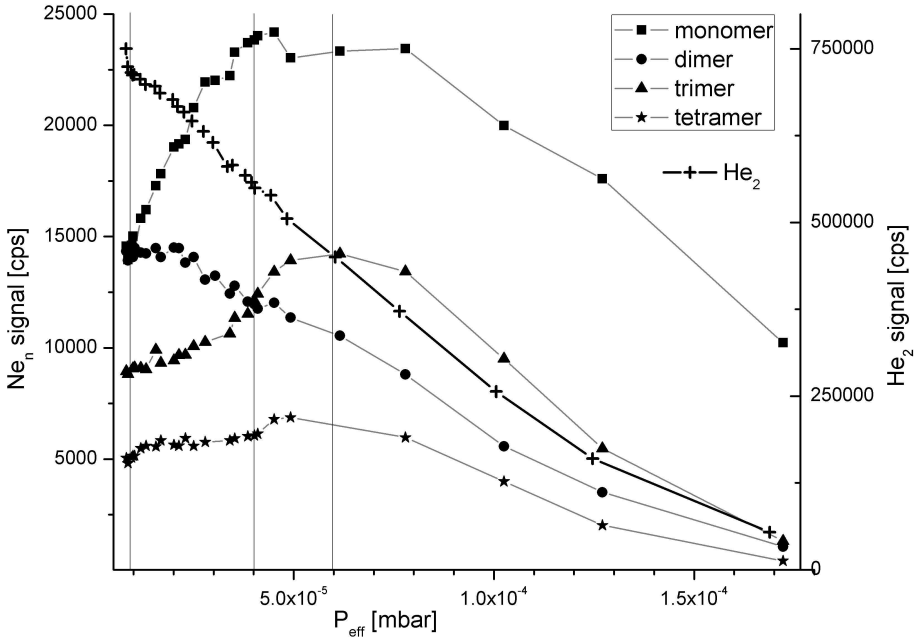

Figure 3.3: Pickup characteristics of Ne depending on the corrected pressure (p_{eff}). The vertical lines show the pressures where mass spectra have been recorded. Chosen values are shown in Tab. 3.2. SEM: 2.5 kV; EC: 0.5 mA; T_0 = 15 K; p_0 = 50 bar
[CD:\Analysis\Pickup\100311_Gas_Pickup.opj]

of the He droplets. This implies that the tetramer maximum would occur at higher pickup pressures if the droplets would not have been destroyed.

For comparability with data of Ar, H_2, and acetylene (see following sections) it is informative to have a look at the masses four, eight, 18 and 19 beside the Ne oligomer masses 20 and 40. The first two are indicators for the condition of the He droplet beam, whereas the masses 18 amu and 19 amu are related to the contamination of the He droplet beam with water. Water easily dissociates on ionisation leading to protonised signals, which means that the mass of the former signal is increased by one. So a signal at 19 amu indicates not only the pickup of water but even the formation of water clusters inside the He droplet [14]. The count rates are shown in Tab. 3.2.

Table 3.2: Count rates for different masses for Ne; The SEM voltage was reduced for the scans.
SEM: 2.3 kV; EC: 0.5 mA; T_0 = 15 K; p_0 = 50 bar

m ... mass (He, He_2, H_2O, H_2O + H, Ne, Ne_2)
$ct_{no\ Ne}$ ... counts at $p_{eff} = 0.9 \cdot 10^{-5}$
ct_{Ne} ... counts at $p_{eff} = 4 \cdot 10^{-5}$
ct_{Ne_3} ... counts at $p_{eff} = 6 \cdot 10^{-5}$

m [amu]	$ct_{no\ Ne}$ [kcps]	ct_{Ne} [kcps]	ct_{Ne_3} [kcps]
4	545±2	492±2	408±2
8	114.8±0.4	99.3±0.4	74.5±0.6
18	85±2	41±2	51±2
19	72.5±0.3	43.5±0.3	24.9±0.2
20	1.6±0.1	2.7±0.3	4.4±0.4
40	0.7±0.1	0.9±0.1	0.7±0.1

Ar Pickup

The Ar pickup process, which is shown in Fig. 3.4, also has an unconventional behaviour. While the oligomer signals, dimer, trimer, and tetramer, have a distinctive peak, the monomer signal is highly broadened. Like with Ne, a possible explanation is the fragmentation of Ar clusters inside the He droplet during the charge hopping ionisation. Single Ar ions leave the Ar cluster and are detected as monomers. While this reduces the detected signal of the oligomers, it increases the measured numbers of monomers. Also the monomer peak is shifted considerably towards higher corrected pressure values. One can find a similar behaviour in Ref. [34] where several mass spectra were taken for different Ar pressures in the pickup chamber. Tab. 3.3 shows the count rates for He_2, as indicator for the droplet beam, H_2O, H_2O + H, to see the water contamination, the Ar monomer, and the Ar dimer. One data set was taken from the maximum of the Ar dimer peak at a corrected pressure of $p_{eff} = 6 \cdot 10^{-6}$ and the other one was taken with no Ar present.

Table 3.3: Count rates for different masses for Ar; The values are taken from mass spectra recorded at pressures marked by the vertical lines in Fig. 3.4. SEM: 2.35 kV; EC: 0.5 mA; T_0 = 15 K; p_0 = 50 bar

m ... masses (He_2, H_2O, H_2O + H, Ar, Ar_2)
$ct_{no\ Ar}$ ... counts at $p_{eff} = 2 \cdot 10^{-6}$
ct_{Ar_2} ... counts at $p_{eff} = 6 \cdot 10^{-6}$

m [amu]	$ct_{no\ Ar}$ [kcps]	ct_{Ar_2} [kcps]
8	664±1	671±1
18	276±4	202±4
19	623±1	542±1
40	12.3±0.5	27±1
80	4.6±0.2	29.4±0.3

In the mass spectrum in Fig. 3.5 one can see the Ar monomer and the Ar dimer. Also He_n clusters attached to the dimer can be found [8]. The same result can be found in Ref. [34]. The trimer and the tetramer are not marked in the figure since they are indistinguishable from the surrounding peaks. The noticeable peak at 149 amu can be assigned to phthalic ester, a softening agent. It is found in most of our mass spectra and can be traced back to the seals used in the vacuum chambers.

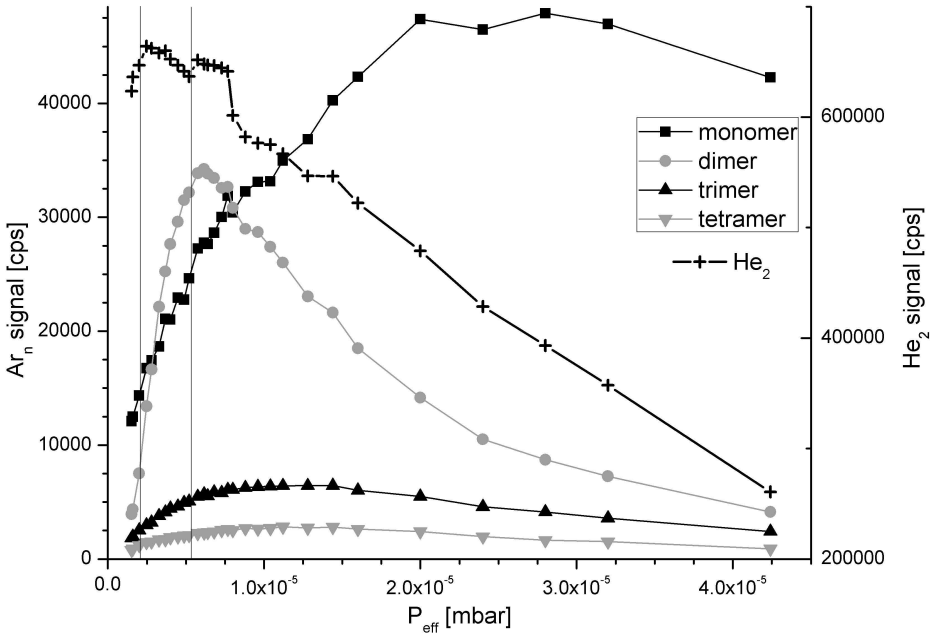

Figure 3.4: Pickup characteristics of Ar depending on the corrected pressure (p_{eff}). The vertical lines show the pressures where mass spectra have been recorded. Chosen values are shown in Tab. 3.3. SEM: 2.5 kV; EC: 0.5 mA; T_0 = 15 K; p_0 = 50 bar;
[CD:\Analysis\Pickup\100311_Gas_Pickup.opj]

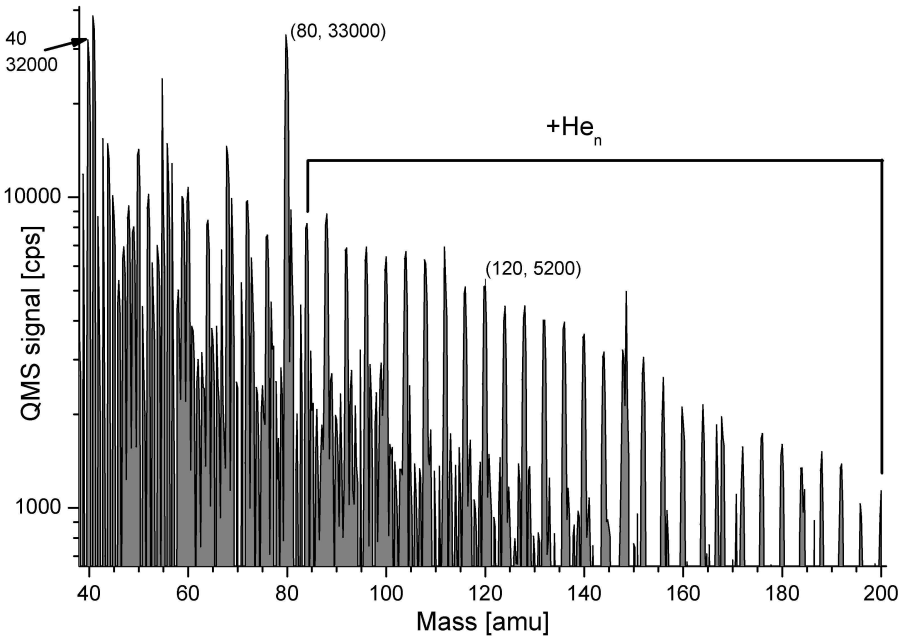

Figure 3.5: Mass spectrum to see Ar based complexes at a corrected pressure of $p_{eff} = 6 \cdot 10^{-6}$
SEM: 2.35 kV; EC: 0.5 mA; T_0 = 15 K; p_0 = 50 bar;
[CD:\Analysis\Pickup\100311_Gas_Pickup.opj]

H_2 Pickup

The hydrogen pickup is difficult to detect due to several reasons. First since hydrogen has a mass of one, one would expect that each peak in the mass spectrum is altered in its height. Then, the oligomers of H all occur at low mass numbers where contaminations like carbon, and H_2O can also be found. The monomer could not be detected at all due to very low count rates namely about 100 cps at 1 amu compared to a signal of over 200 kcps at 3 amu under the same conditions.

Table 3.4: Count rates of different masses for H_2; SEM: 2.3 kV; EC: 0.5 mA; T_0 = 15 K; p_0 = 50 bar

m ... mass (He, He_2, H_2O, H_2O + H, H_2 + H, 2 H_2 + H, He + H_2 + H, He_2 + H_2 + H)
$ct_{no\ H_2}$ ... counts at $p_{eff} = 4 \cdot 10^{-6}$
ct_{H_2+H} ... counts at $p_{eff} = 17 \cdot 10^{-6}$

m [amu]	$ct_{no\ H_2}$ [kcps]	ct_{H_2+H} [kcps]
4	473±2	507±2
8	93.5±0.3	98.7±0.3
18	48±2	28±2
19	74.0±0.3	72.8±0.3
2	2.2±0.4	15±1
3	8.2±0.1	14.6±0.1
5	1.04±0.03	1.84±0.04
7	0.52±0.02	1.30±0.04
11	0.41±0.02	0.96±0.03

The pickup process can be found in Fig. 3.6 and a magnification of the lower signals is pictured in Fig. 3.7. The pickup characteristics was measured with a SEM voltage of 2.5 kV and an EC of 0.5 mA. The masses three, five, seven, eight, nine, eleven, and 21 were investigated. Mass eight again is the reference for the condition of the He droplet beam, but all the other masses can be seen as oligomers of hydrogen. No mass spectrum is shown since not much information can be gained from it in the case of hydrogen. It is noticeable though that the even numbered oligomers of hydrogen all seem to have negligibly small signals, if no contamination interferes with the peak. Especially the masses six, ten, 14, and 20 are good examples, with a signal in the range of ∼100 cps if one substracts the difference signals between no H_2 and a H_2 pressure of the maximum of the trimer signal in the pickup chamber. This process has also been investigated in Ref. [21]. It can be explained by an exothermic reaction that takes place on ionisation of an even numbered H_n^+ cluster, which will then form an odd numbered H_{n-1}^+. Their results also show that the signal of odd numbered oligomers surpass the even numbered oligomer signal by orders of magnitude. The formation of the He_2H_2 complex was studied in detail in Ref. [20].

In Fig. 3.7 one can not only see the oligomers of hydrogen but also the combination of an hydrogen oligomer with an He cluster fragment. At the masses seven and eleven a bump at about $p_{eff} = 1.2 \cdot 10^{-5}$ is indicating the combination of the hydrogen trimer, which also reaches its maximum at the same corrected pressure, and one or two He atoms. It is unclear, though why the signal of the two masses stays low. For comparability reasons the count rates close to the maximum of the trimer peak are shown in Tab. 3.4.

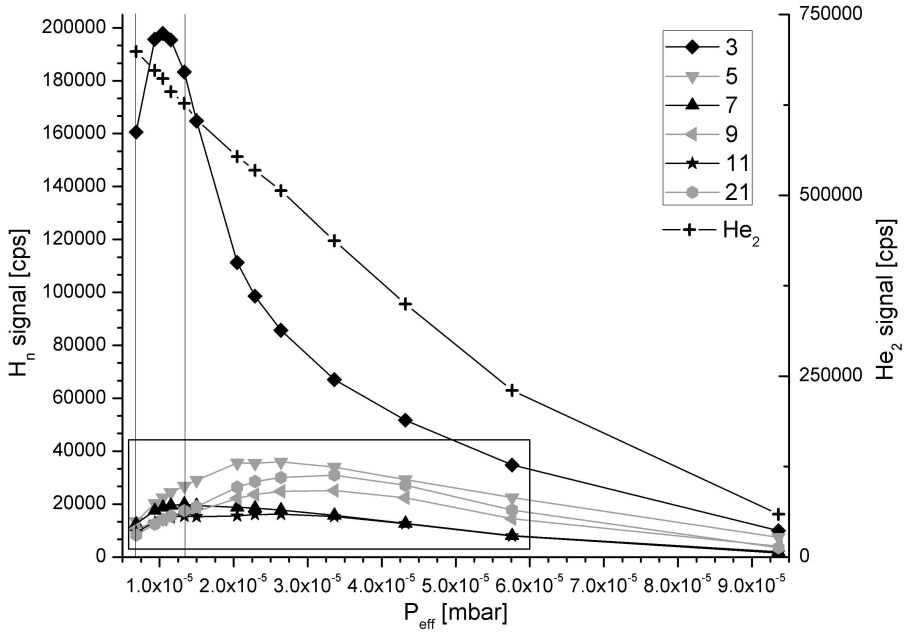

Figure 3.6: Pickup characteristics of H_2 depending on the corrected pressure (p_{eff}), see also Fig. 3.7. The vertical lines show the pressures where mass spectra have been recorded. Chosen values are shown in Tab. 3.4. SEM: 2.5 kV; EC: 0.5 mA; T_0 = 15 K; p_0 = 50 bar; [CD:\Analysis\Pickup\100311_Gas_Pickup.opj]

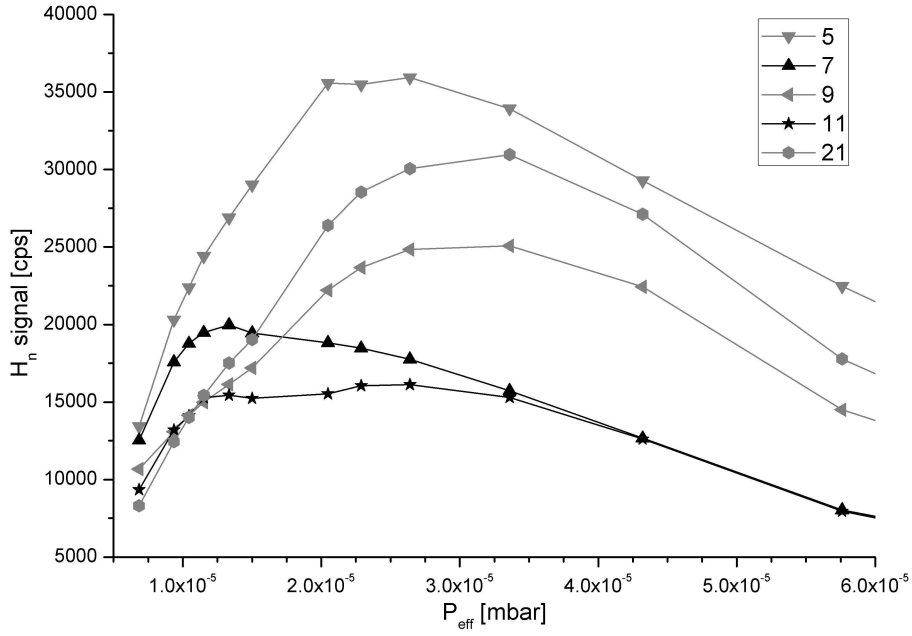

Figure 3.7: Pickup characteristics of H_2; magnification of the box in Fig. 3.6
SEM: 2.5 kV; EC: 0.5 mA; T_0 = 15 K; p_0 = 50 bar;
[CD:\Analysis\Pickup\100311_Gas_Pickup.opj]

Acetylene Pickup

Acetylene (C_2H_2) has been chosen additionally because of its well resolved pickup statistics (Fig. 3.8). The monomer, dimer, and trimer peaks are easily distinguishable and even the tetramer peak can be found. The maxima are located at pressures of $0.3 \cdot 10^{-5}$ mbar for the monomer, $1 \cdot 10^{-5}$ mbar for the dimer, $2.2 \cdot 10^{-5}$ mbar for the trimer, and approximately $3 \cdot 10^{-5}$ mbar for the tetramer. The pressure given for acetylene is as indicated by the Penning gauge, no conversion to a corrected pressure was possible due to missing correction factors.

Table 3.5: Count rates of different masses for Acetylene; SEM: 2.3 kV; EC: 0.5 mA; T_0 = 15 K; p_0 = 50 bar

m ... masses (He, He_2, H_2O, H_2O + H, acetylene, $acetylene_2$)
$ct_{no\ C_2H_2}$ ... counts at p= $2.4 \cdot 10^{-6}$
$ct_{C_2H_2}$ ... counts at p= $7 \cdot 10^{-6}$
$ct_{(C_2H_2)_2}$ ... counts at p= $15 \cdot 10^{-6}$

m [amu]	$ct_{no\ C_2H_2}$ [kcps]	$ct_{C_2H_2}$ [kcps]	$ct_{C_2H_2}$ [kcps]
4	530±2	764±2	737±2
8	115.0±0.3	240.8±0.5	200.3±0.5
18	59±2	77±2	41±2
19	57.3±0.3	23.1±0.2	2.7±0.1
26	16.5±0.2	53.8±0.6	21.1±0.8
52	1.3±0.1	56.6±0.3	57.0±0.3

Compared to the pickup characteristics of the three other gases shown above, acetylene shows the highest signal. The reason for that is probably the contamination of the He droplets with water. In Fig. 3.9 the monomer (26 amu) plus and minus one hydrogen atom is shown and also mass 19 (H_2O + H) can be found. One can see the fragmentation of acetylene on ionisation. It is unlikely that a hydrogen atom leaves the acetylene molecule on ionisation, indicated by mass 25. Acetylene plus an additional hydrogen atom gives a mass of 27 amu. This can either happen due to fragmentation of an acetylene cluster, but that is contrary to the low peak at mass 25, or the hydrogen can be split from H_2O. This process most likely happens, indicated by the peak at mass 19 compared to the peak at 18 amu. One can also see that with an increase of the acetylene signal the protonised water signal (19 amu) is reduced drastically. This can probably be explained by different ionisation energies of water and acetylene. Since there is no direct ionisation of the species inside the He droplet with electron impact ionisation, a charge hopping process takes place. The dopant is ionised indirectly and the excess energy is released resulting in evaporation of the He droplet. When the droplet contains different species at the same time, one can imagine that the species with the lower ionisation energy has a higher chance for the charge transfer. Since acetylene has an ionisation energy of 11.4 eV [43] and water of 12.62 eV [44], the high countrate of acetylene can be explained. This is in contrast to the ionisation of the rare gases shown above and will be discussed in Sec. 3.2.3.

A mass spectrum was taken at a pressure of $2 \cdot 10^{-5}$ mbar and is shown in Fig. 3.10. The acetylene oligomer peaks are marked and there also appear significant peaks at a fixed distance of ten amu and 18 amu to the acetylene peak. The latter one might be the combination with water but the first one is unclear. One can also see the side peaks of the acetylene oligomers with plus and minus 1 amu.

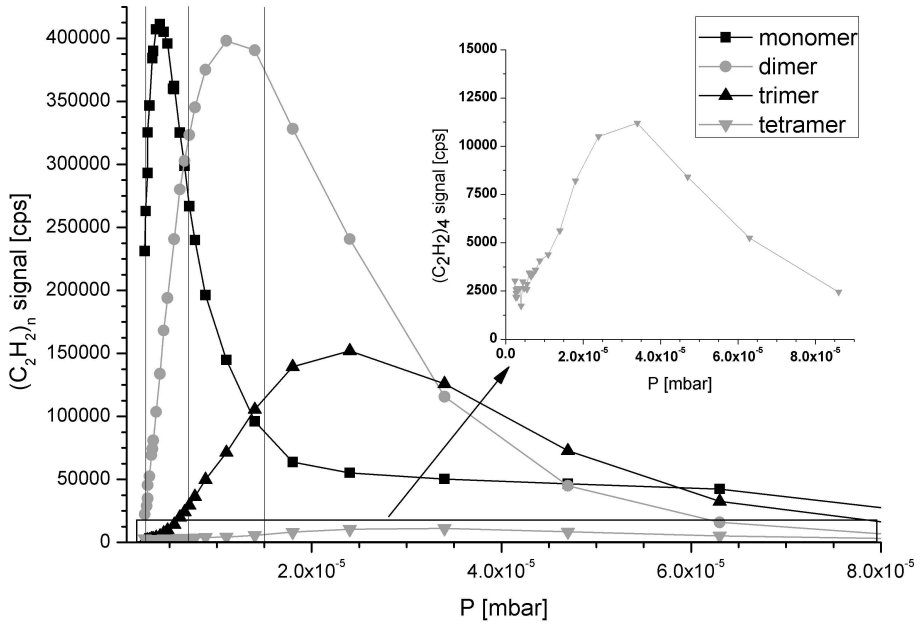

Figure 3.8: Pickup characteristics of acetylene depending on the pressure. The vertical lines show the pressures where mass spectra have been recorded. Chosen values are shown in Tab. 3.5. The tetramer signal is shown in the box. SEM: 2.5 kV; EC: 0.5 mA; T_0 = 15 K; p_0 = 50 bar; [CD:\Analysis\Pickup\100311_Gas_Pickup.opj]

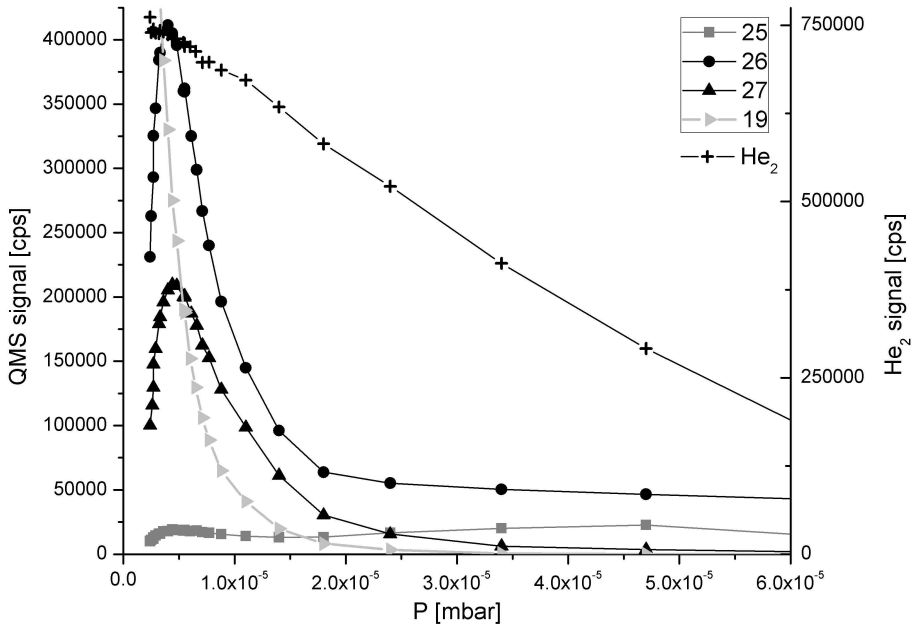

Figure 3.9: Acetylene's monomer with depending on the pressure
SEM: 2.5 kV; EC: 0.5 mA; T_0 = 15 K; p_0 = 50 bar;
[CD:\Analysis\Pickup\100311_Gas_Pickup.opj]

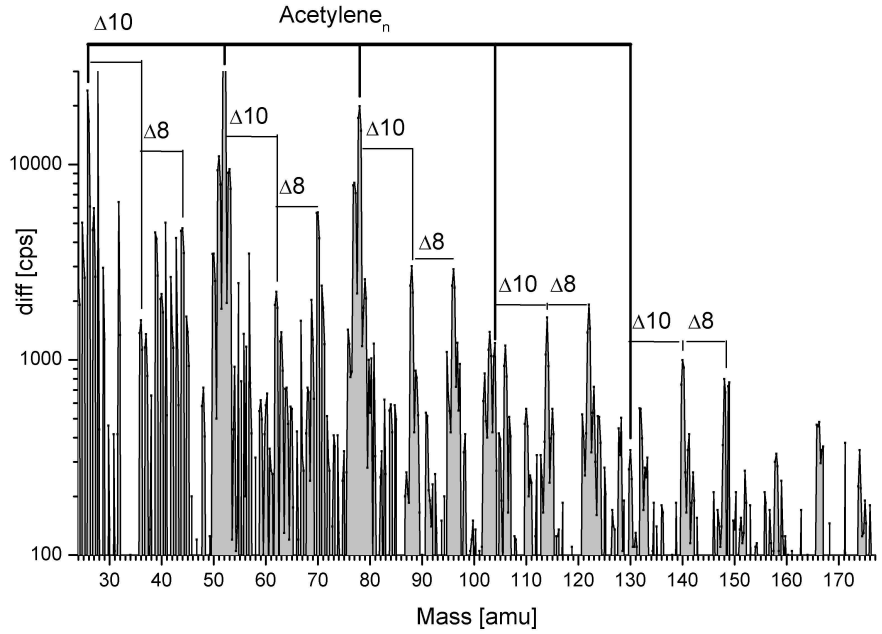

Figure 3.10: Mass spectrum to see acetylene based complexes at a pressure of $p = 2{\cdot}10^{-5}$ mbar. It is noticeable that the oligomer peaks of acetylene are accompanied by peaks at ± 1 amu, $+10$ amu, and $+18$ amu. SEM: 2.3 kV; EC: 0.5 mA; $T_0 = 15$ K; $p_0 = 50$ bar; [CD:\Analysis\Pickup\100311_Gas_Pickup.opj]

3.2.2 Chromium Pickup

The following results show the successful pickup of chromium (Cr) atoms on He nanodroplets (He_N) for the first time. One to four atoms can be selectively doped to He_N by choosing the temperature of the Cr source. This pickup statistic has been investigated.

Cr can be brought into gasphase by different ways described as in Sec. 1.5.1. Here, Cr is heated inside a crucible by electron bombardment (see Sec. 2.5 for more details) to reach a certain particle flux which is crossed with the He_N beam. The heater can be thought of as an effusive source producing a Cr particle beam, and the Cr particle flux rate depends on the source temperature, see Sec. 1.5.2. On the other hand the pickup probability for each single droplet depends on the dropletsize. The droplet size can be controlled by the nozzle parameters, like the nozzle temperature and the pressure, see Sec. 1.3. With these parameters one can find the highest pickup probability experimentally and therefore the maximum signal for single and multi particle pickup.

The nozzle temperature was varied from 11 K to 23 K in 1 K steps and additionally the temperatures 25 K and 28 K were used, resulting in droplets with a mean number of 40000 to 1000 He atoms per droplet. The He droplet crosssection therefore lies between 18000 Å^2 and 1500 Å^2 , see Sec. 1.4 for further details.

As described before, the other parameter is the Cr particle flux which can be varied by changing the heating power between 50 W and 200 W. Temperatures up to 1650°C were reached, but for a detailed dependence of the heating power and the temperature see Sec. 3.1. Although there is a high absolute measurement inaccuracy of the temperature, the heating power is sufficiently stable. Apart from statistical fluctuations there is no drift during a pickup experiment at a stabilised heating power as long as no discharges occur. Discharges are likely to occur above

180 W heating power, which means approximately every 5 min to 10 min. On a discharge the acceleration voltage breaks down and takes about 3 s to 5 s to be return to 1 kV, so that the sample cooles down a little. Measuring the temperature on cool down indicates that the sample's temperature decreases in the range of 100°C. In the meantime the PID controller tries to compensate by increasing the emission current which leads to overshooting when the acceleration voltage is back on. It will then slowly, within about 10 s to 20 s, stabilise at the original heating power. Due to the highly non linear correlation between the particle flux rate and the temperature, these small temperature bursts have a noticeable impact on the pickup process. So it is best to avoid discharges by either using a lower heating power or increasing the filament to crucible distance (see Sec. 1.5.1 and Sec. A.5.2).

The pickup probability is a function of the nozzle temperature T_0 and the heating power P (the nozzle pressure p_0 is kept fixed at 50 bar). In the following Fig. 3.12 and Fig. 3.13 the Cr mono- and dimer signal, as measured with the QMS, is shown over this two dimensional parameter space.

The He dimer (He_2) signal is a good indicator for the total amount of He reaching the QMS in form of droplets. This is shown in Fig. 3.11. One can see that with an increase in heating power, the number of detected He droplets is reduced. This can be explained by the same effects as in the gas pickup: increased heating powers result in a higher pickup probability, and subsequently stronger He evaporation. Furthermore, smaller droplets will either be evaporated or deflected and are therefore not detected. A more detailed description of the evaporation process can be found in Sec. 1.3.

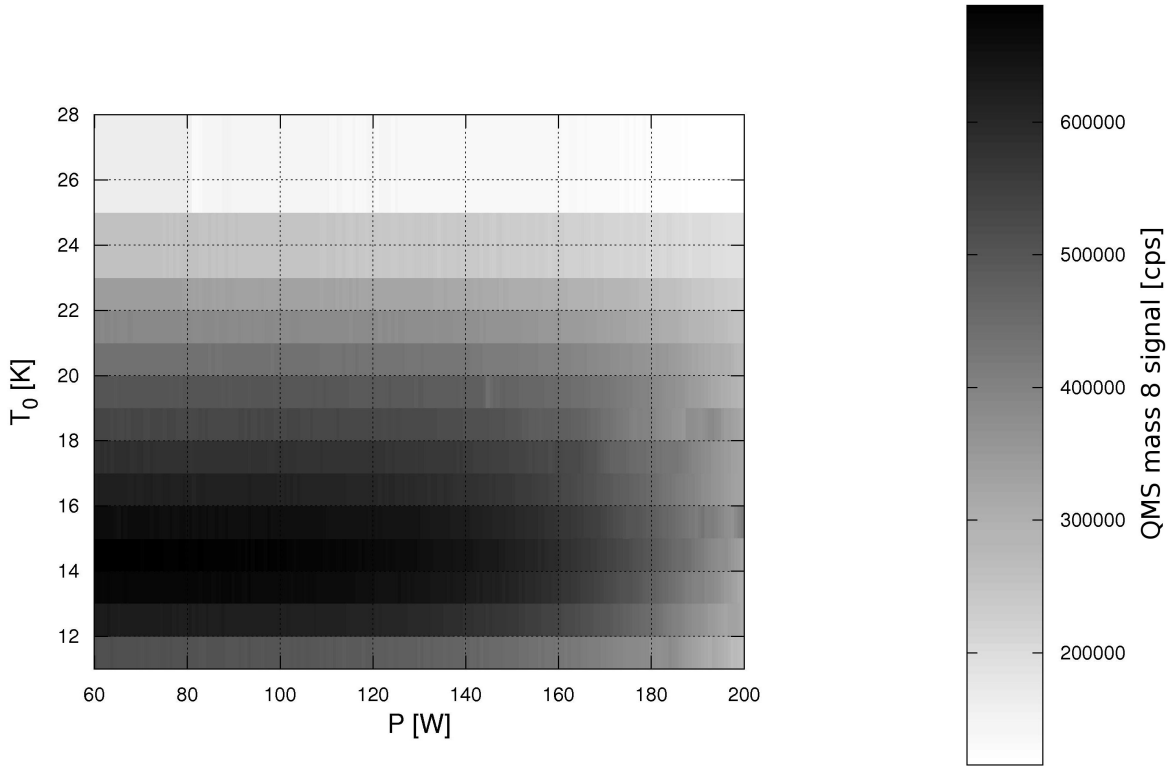

Figure 3.11: Characteristics of the He dimer signal with Cr pickup. (in colour on CD [CD:\Results\Pickup\100426_Cr\Cr_mass_8_stat_color.jpg])
SEM: 2.5 kV; EC: 0.5 mA; T_0 from 11 K to 28 K; p_0 = 50 bar; heating power from 50 W to 200 W; [CD:\Scripts\Pickup\Cr_Pickup.m]

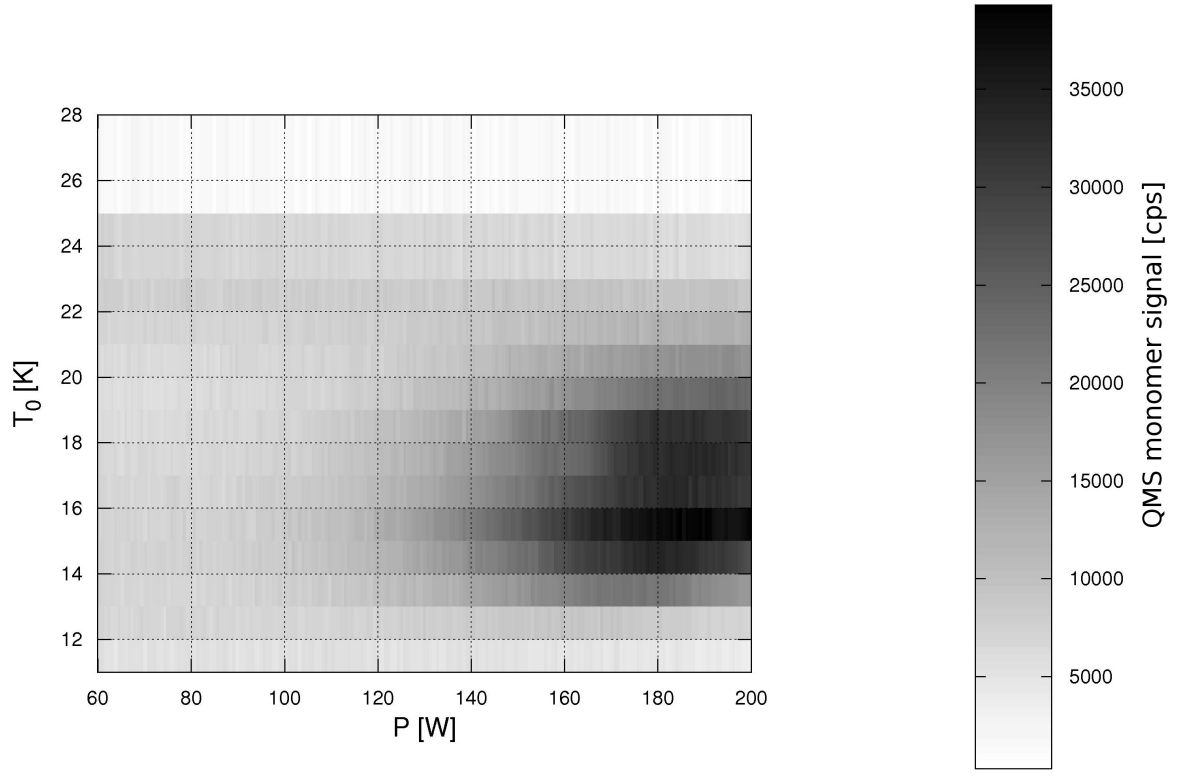

Figure 3.12: Pickup characteristics for Cr monomer: QMS monomer signal shown as function of the nozzle temperature T_0 and the heating power P. (in colour on CD [CD:\Results\Pickup\100426_Cr\Cr_monomer_stat_color.jpg])
SEM: 2.5 kV; EC: 0.5 mA; T_0 from 11 K to 28 K; p_0 = 50 bar; heating power from 50 W to 200 W; [CD:\Scripts\Pickup\Cr_Pickup.m]

The dependence of the Cr pickup (QMS monomer and dimer signal, Fig. 3.12 - 3.13) on T_0 and P can be understood qualitatively as follows: The pickup probability for each single He droplet with a mean number of atoms per droplet increases with an increase in heating power of the HT source and decreases with the nozzle temperature. Taking the distribution of the number of atoms on the He droplet into account shifts the distribution from lower nozzle temperatures to higher nozzle temperatures but does not fit the measured data. Calculating the pickup probability for the He beam and not only for one droplet by the use of the mass flow through the nozzle broadens the distribution along the nozzle temperature. The influence of the nozzle temperature is then hardly noticeable and again does not fit the measurements.

Because of being of importance for the following spectroscopic and ESR experiments, the Cr monomer and dimer pickup have been investigated in more detail. The measurements shown in Fig. 3.12 and Fig. 3.13 were fitted with Gaussian distributions. Actually, they should be Poisson distributed [34] but their asymmetry is not evident due to the increasing He evaporation at higher heating powers. The Gaussian fits are shown in Fig. 3.16 and Fig. 3.17 but the parameters of interest are the amplitude and the centre of the Gaussian fits, which are shown in Fig. 3.14 and Fig. 3.15. The amplitudes increase at first with the nozzle temperature due to an increase in the number of He_N produced. At about 15 K and higher temperatures the signal decreases due to an decrease of the He_2 signal. This can be explained by the evaporation and deflection of the smaller He_N. The centre of the Gaussian fits tend towards higher heating powers when the nozzle temperature is increased. This can easily be understood since the

droplet size decreases with higher nozzle temperatures and therefore the pickup probability also decreases.

One can find an interesting effect when looking at the amplitude of the Gaussian fits. The dimer peak rises earlier than the monomer peak and there is a crossover between 13 K and 14 K nozzle temperature. This can be explained by a change in the He droplet beam. At lower nozzle temperatures a bimodal droplet size distribution can be found [10]. This is an effect which can be understood by investigating the He phase diagram. It is explained in more detail in Sec. 1.3.1. One can leave regime I and enter the transition region regime II where the isentropes pass close to the critical point. This drastically affects the droplet production.

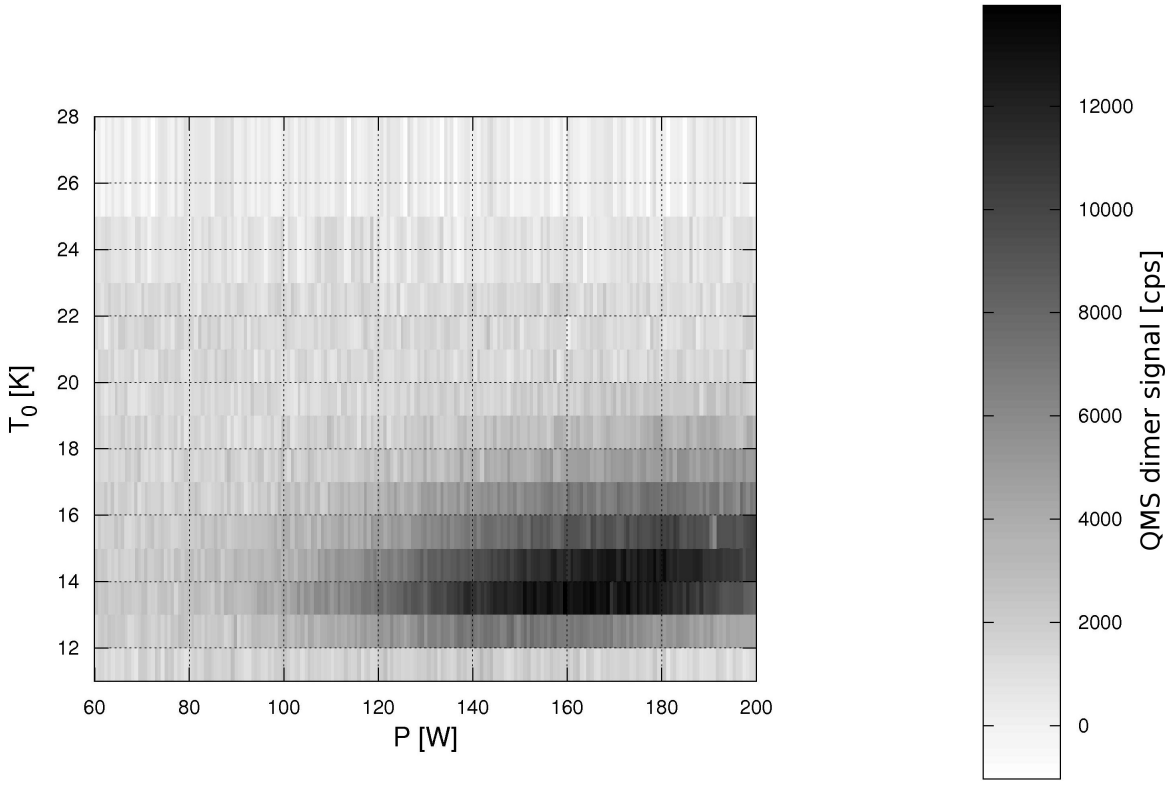

Figure 3.13: Pickup characteristics for Cr dimer: QMS dimer signal shown as function of the nozzle temperature T_0 and the heating power P. (in colour on CD [CD:\Results\Pickup\100426_Cr\Cr_dimer_stat_color.jpg])
SEM: 2.5 kV; EC: 0.5 mA; T_0 from 11 K to 28 K; p_0 = 50 bar; heating power from 50 W to 200 W; [CD:\Scripts\Pickup\Cr_Pickup.m]

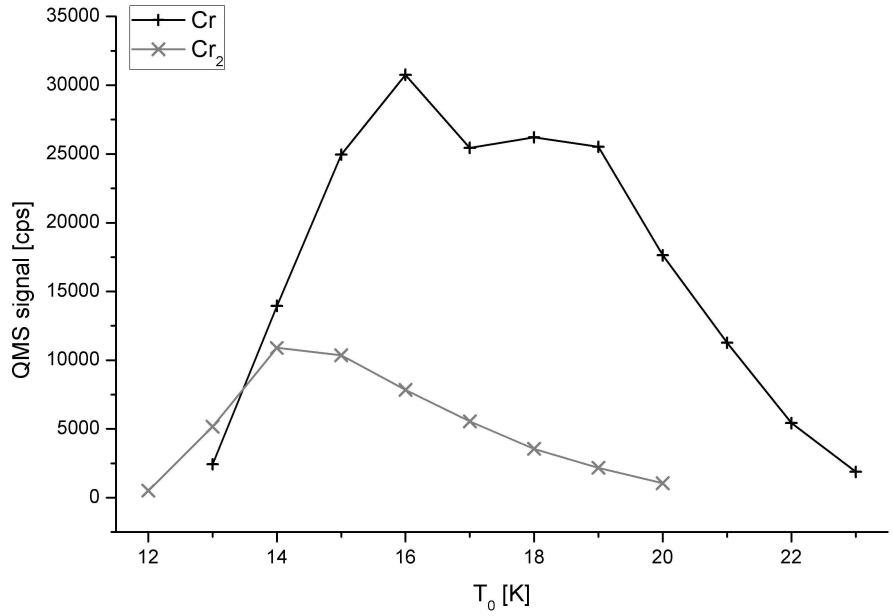

Figure 3.14: Amplitude of the Gaussian fits for the Cr monomer and dimer; measurement inaccuracy is $< \pm 150$ cps; SEM: 2.5 kV; EC: 0.5 mA; T_0 from 11 K to 28 K; $p_0 = 50$ bar; [CD:\Analysis\Pickup\100426_Cr_on_He_Nozzle_Temperature_cleaned.opj]

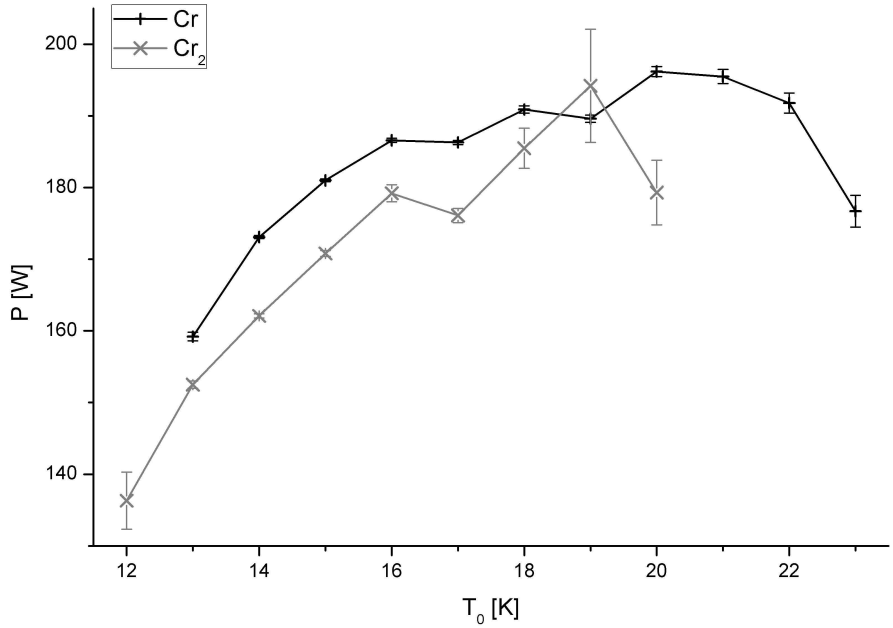

Figure 3.15: Centre of the Gaussian fits for the Cr monomer and dimer SEM: 2.5 kV; EC: 0.5 mA; T_0 from 11 K to 28 K; $p_0 = 50$ bar; [CD:\Analysis\Pickup\100426_Cr_on_He_Nozzle_Temperature_cleaned.opj]

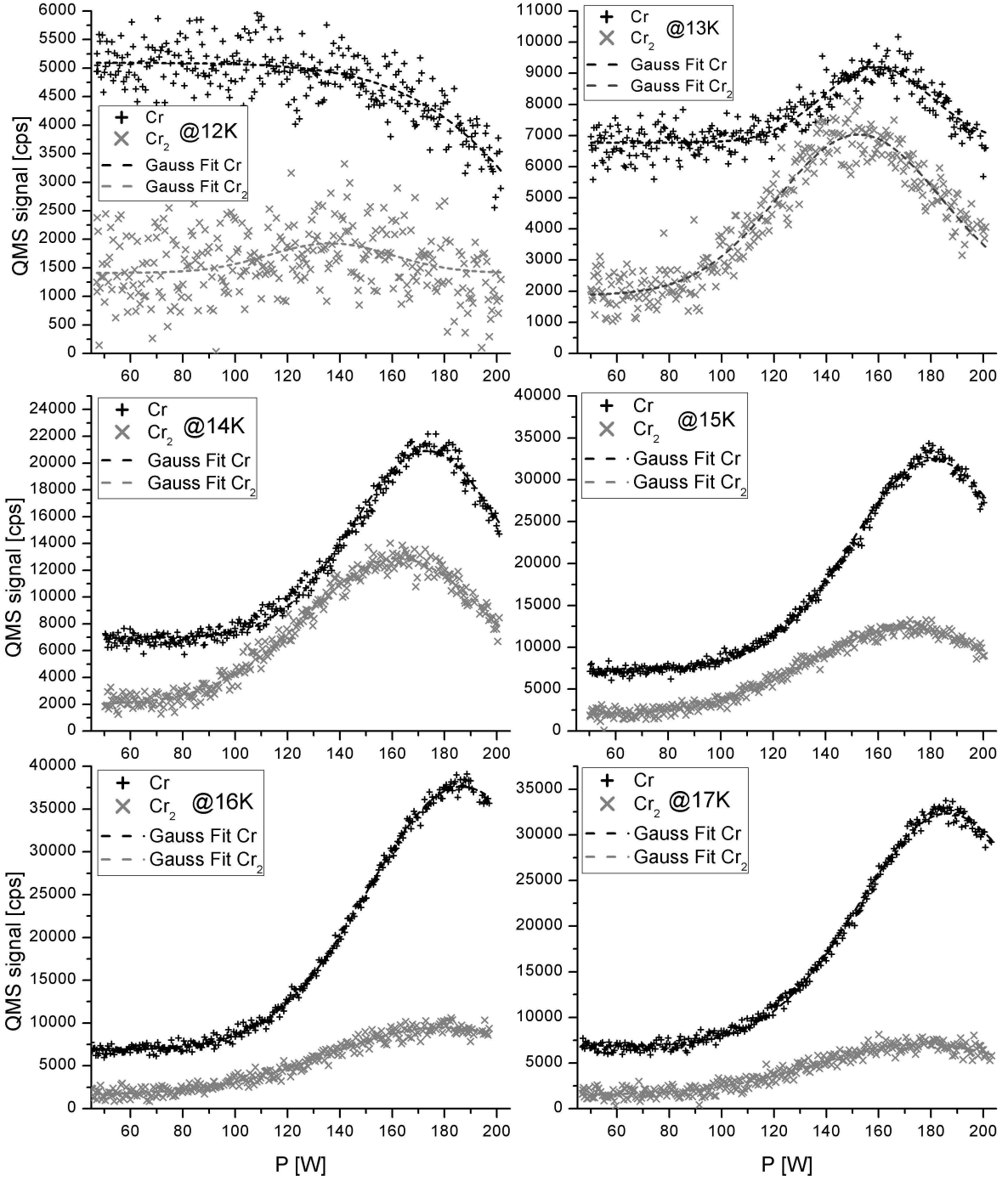

Figure 3.16: Gaussian fits of the Cr monomer and dimer pickup; 12 K to 17 K
SEM: 2.5 kV; EC: 0.5 mA; T_0 from 12 K to 17 K; p_0 = 50 bar; heating power from 50 W to 200 W; [CD:\Analysis\Pickup\100426_Cr_on_He_Nozzle_Temperature_cleaned.opj]

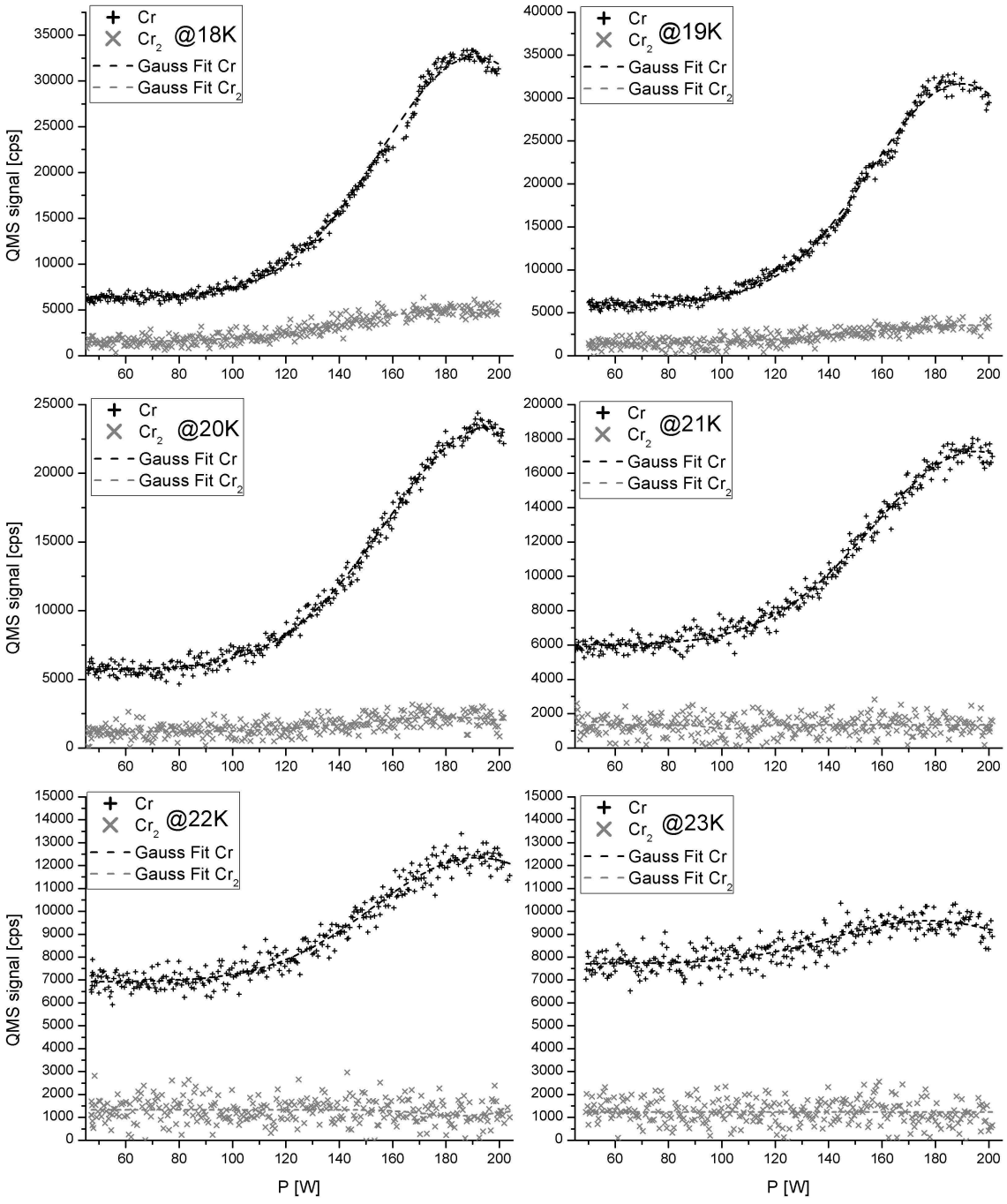

Figure 3.17: Gaussian fits of the Cr monomer and dimer pickup; 18 K to 23 K
SEM: 2.5 kV; EC: 0.5 mA; T_0 from 18 K to 23 K; p_0 = 50 bar; heating power from 50 W to 200 W; [CD:\Analysis\Pickup\100426_Cr_on_He_Nozzle_Temperature_cleaned.opj]

For experiments in the distant future, the creation of Cr oligomers is of interest. This could be proven to be possible with the detection of the tetramer. The pickup process at a nozzle temperature of 15 K and a He pressure of 50 bar was investigated with different heating powers of the HT source. The apparatus was differently adjusted for these measurements, than in the measurements shown above. The heating powers required for the maxima of the peaks are therefore located at different heating powers. The listed nozzle parameters result in droplets with about 12000 atoms and a crosssection of approximately 8200 $Å^2$.

The results are shown in Fig. 3.18 and the tetramer peak is clearly visible. There is a limit for the Cr pickup on the He droplet though. The kinetic energy of the Cr atom is transfered to the droplet upon impact and will result in evaporation of He [34], which also reduces the droplet's crosssection. The energy released on collision is approximately 0.42 eV, which will evaporate about ∼700 atoms [49]. Adding another Cr atom even reduces the droplet size a lot more. At first there is the collision which leads to an evaporation of again ∼700 atoms, but then usually within 10^{-8} s to 10^{-10} s the two Cr atoms will form a dimer [34] and the binding energy of about 1.42 eV is released [47]. This leads to further evaporation of ∼2300 atoms. So a dimer on the droplet means that the droplet has lost about ∼3700 atoms, setting a lower limit to the droplet size.

As expected one can see the decrease of the He_2 signal with an increase in heating power due to the destruction and deflection of the smaller He_N. Also, the maxima of the Gaussian fits appear at higher heating powers with higher numbered Cr oligomers. They are might be shifted to the left due to the decreasing He_2 signal though. The bump at 198 W was caused by a discharge which lead to overshooting of the PID controller and therefore a instability of the heating power (see Sec. 3.1).

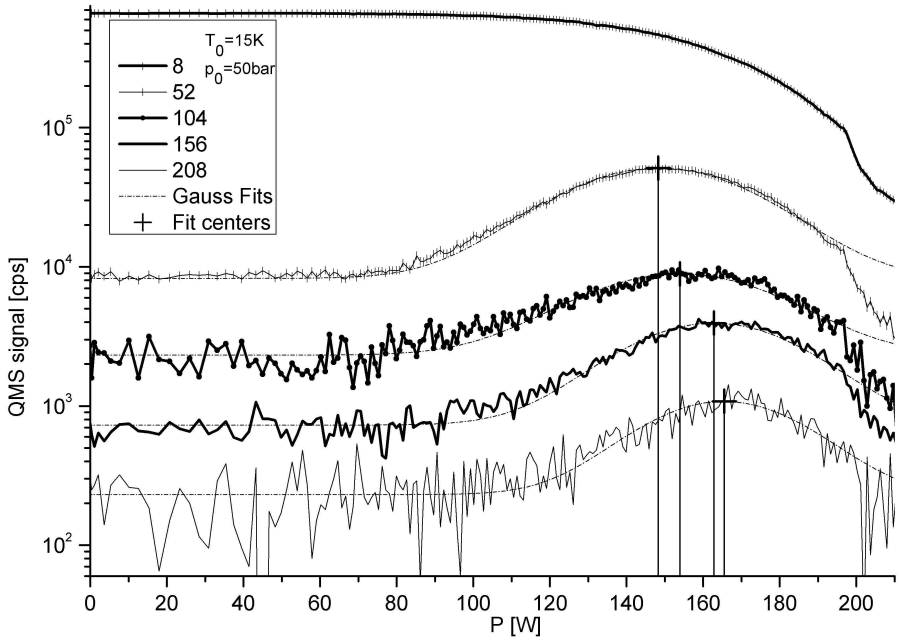

Figure 3.18: Cr oligomer peaks and their gauss fits with marked centres; the process variable (PV) is used on the abscissa, but it is directly proportional to the heating power by a factor of ten; SEM: 2.5 kV; EC: 0.5 mA; T_0 = 15 K; p_0 = 50 bar; heating power from 0 W to 200 W; [CD:\Analysis\Pickup\100426_Cr_on_He_Nozzle_Temperature_cleaned.opj]

3.2.3 Conclusion

The Cr pickup was shown successfully and oligomers up to tetramers have been detected in the droplet. With bigger He droplets one can form even bigger Cr clusters. Open, however, remains the question how the oligomers are composed in terms of spin multiplicity. Can the dimers be found in the singlet state? Also, the structure of the other oligomers is undetermined, wether clusters are formed or chains due to the dipole-dipole interaction. In Ref. [39], the polar molecule hydrogen cyanide (HCN) was investigated on He_N, and the formation of chains with up to seven molecules was detected by spectroscopic investigation of the H-C stretch vibration in a strong ($\sim$ 30 kV/cm) electric field.

Table 3.6: Ionisation energies for Ne, Ar, H_2, acetylene, Cr, and H_2O

spec ... species (Ne, Ar, H_2, acetylene, Cr, H_2O)
I ... ionisation energy

spec	I [eV]
Ne[35]	21.6
Ar[35]	15.8
H_2[35]	15.4
H_2O[44, 35]	12.6
acetylene[43, 35]	11.4
Cr[35]	6.8

The gas pickup showed a strong contamination with water on the He droplet. The water peak (18 amu) or the protonised water peak (19 amu). As stated in Ref. [14] on multiple water pickup, the protonised water peak exceeds the water peak itself, which suggests that even water oligomers are formed inside the He droplet. Comparing the ionisation energy of the measured species, one can see that only acetylene and Cr have a lower ionisation energy than water, see Tab. 3.6. The results might imply that if a heterocomplex is formed on the droplet, the dopant with the lowest ionisation energy has a higher ionisation probability. This would explain the only slightly change in count rates for the water and protonised water peak during Ar, Ne, and H_2 pickup, which is in contrast to the drastically reduced countrate of the protonised water on acetylene pickup. Nevertheless, it seems to be important to focus on a reduced water contamination for future experiments.

Chapter 4

Summary and Outlook

Based on the demonstrated feasibility of ESR in alkali-metal doped He_N this work is aimed at the generalisation of ESR in He_N. The use of the He_N beam apparatus leads to two paths for future experiments. On the one hand, the information gathered on alkali-metal atoms is used to utilise for example rubidium atoms located at the surface of He_N as spin labels for ESR-silent species inside He_N. For this purpose gaseous species are used. In this work a quadrupole mass spectrometer was added to the existing setup to investigate the pickup statistics of the noble gases neon (Ne) and argon (Ar) and of molecular gases like hydrogen (H_2) or acetylene (C_2H_2). Also, cluster formation of these species on He_N have been demonstrated successfully. The results showed a contamination of He_N with water molecules in the vacuum chamber. Since water has a strong dipole moment it is crucial to reduce the amount of water in the vacuum chamber to prevent unwanted interaction when spin label experiments are done. Krypton and xenon are already under investigation right now.

The other part of this thesis aim at experiments on atoms with high spin states like chromium (Cr). Since high temperatures are required for Cr pickup, the major part of this work focused on the development of a high temperature (HT) evaporation source based on electron bombardment. The source has been designed, constructed and implemented in this work. This advanced method was chosen due to the lower magnetic stray fields produced compared to other heating methods. This is crucial for ESR experiments, which highly rely on homogeneous magnetic fields. The very first pickup of single Cr atoms and the formation of microclusters with up to four Cr atoms in He_N, demonstrate the outstanding performance of the HT source. Heating powers up to 300 W can be reached and a high particle flux in the range of 100 $\frac{\mathrm{mg}}{\mathrm{h \cdot sr}}$ for Cr can be obtained. The maximum temperature can still be increased with optimising the existing setup for example with radiation shields or additional filaments. The setup is designed to allow the use of a second pickup source, either the existing gas or low temperature pickup sources or another HT source.

In future measurements Cr will be investigated spectroscopically on He_N for the first time. The existing setup will require adaption since due to the high temperature of the source stray light is produced which might lead to high background signals. This will require the installation of additional baffles to reduce the stray light from the pickup chamber into the measurement chamber. Then also the magnetic circular dichroism effect of Cr on He_N will be investigated making later ESR measurements possible. Therefore a second adaptation step is required. With the alkali-metals also an effusive beam of free atoms could be measured by means of ESR, which was used for high accuracy the magnetic field measurements. The different pickup geometry for Cr, where the He_N beam is crossed with the Cr particle beam,

makes this approach impossible. The magnetic field has to be measured precisely by other means, for example by using nuclear magnetic resonance detectors close to the ESR cavity. The technique is not only restricted to Cr, other metals requiring similar temperatures for the pickup process can be used. One example is copper (Cu), which is alkali-like and therefore easier to model.

Appendix A

Prototype

A.1 Introduction

The development of a new machine, like the HT source described in this work, is an iterative process and takes time.For this reason the testing of the HT source took place in a separate test setup - a stand-alone vacuum chamber. In the following sections the vacuum chamber and the prototype will be explained. Since there was no possibility to test the pickup of chromium on He-nanodroplets in this chamber, I focused on the evaporation rate depending on the chromium temperature or the heating power. Despite a long planning phase one had to modify the HT source several times so that in the end the design was not appropriate for the final setup anymore and a new smaller HT source was developed in the end. Nevertheless building the prototype was a good way to learn about electron bombardment, testing ideas, and improving the technique for a final setup.

A.2 Test Vacuum Chamber

The test vacuum chamber is explained in detail in the following, since after testing the prototype, it can be used for other purposes. It consists of a plus shaped recipient with four openings. Three of them can be used for mounting and feedthroughs while one is connected to the pumps via a valve. Since the recipient is placed vertically a metal mesh with approximately 1 mm lattice spacing was inserted above the valve to prevent parts from falling into the pumping section. The test vacuum chamber is pumped with a water cooled 700 W diffusion pump backed by a rotary vane pump (Leybold-Haraeus D6).

The pressure is measured by a Pirani gauge (Leybold-Haraeus 16216Br2, 4485) and a cold-cathode ionisation (Edwards Penning 505 CP25-K) gauge. The pressure reached after one hour of pumping is approximately $5 \cdot 10^{-6}$ Torr $\approx 7 \cdot 10^{-6}$ mbar. At pressures higher than $2 \cdot 10^{-5}$ mbar the high temperature evaporation source should not be used since the higher pressure facilitates discharges when the HT source is in use.

Several feedthroughs into the vacuum chamber exists: three high-voltage feedthroughs, 15 electrical feedthroughs, and two water feedthroughs. One high-voltage feedthrough is used for the heating process itself, the other two are platinum and platinum-rhodium wires (Ø 0.1 mm) used as Type-R thermocouple inside the chamber. Eight of the 15 other electrical feedthroughs are used as follows, the remaining seven are left blank: three are connected inside and used as ground for the filaments, three are used for powering each of the 3 filaments separately, one feedthrough was used for a Faraday cup, and one for a repulsion shield behind the filaments.

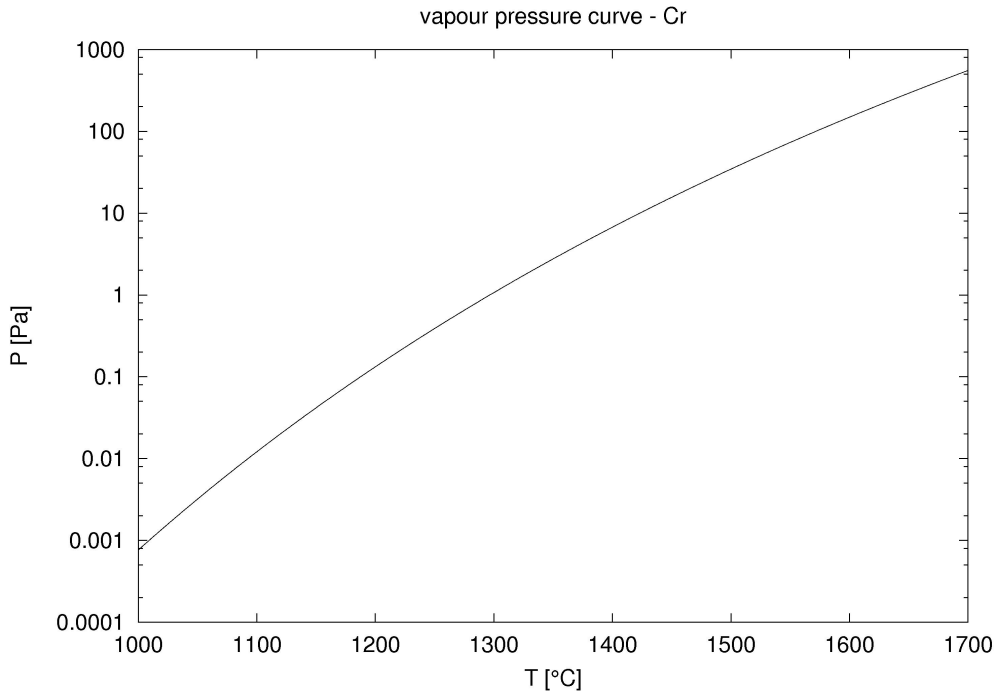

Figure A.1: Vapour pressure curve of Cr [CD:\Scripts\Pressure\vapour_pressure_curve_Cr.m] Data taken from Ref. [35]

The water feedthrough is used for watercooling of a cylinder around the high temperature evaporation source. It is a copper tube with 6 mm outer and 4 mm inner diameter.

A.3 Dimensioning of the Equipment

To get a rough estimation of the required heating power the vapour pressure used for the pickup process described in Ref. [27] was compared to the vapour pressure of chromium. In Ref. [27] the temperature for the optimum single atom pickup of potassium was measured to be 115°C and of rubidium 85°C. This corresponds to a vapour pressure inside the pickup cell of about 10^{-2} Pa=10^{-4} mbar [35] for a pickup cell length of 32 mm. This is one order of magnitude higher than the vapour pressure Toennies and Vilesov suggested in Ref. [50] - (10^{-6} to 10^{-5} mbar = 10^{-4} to 10^{-3} Pa), unfortunately the length of the used pickup cell remains a mystery. Since the pickup process also depends on geometry, as stated in Ref. [49], the different values are no contradiction. In Fig. A.1 the vapour pressure curve of chromium is shown and one can see that a temperature of $\approx$ 1093°C is required to reach a vapour pressure of 10^{-2} Pa.

In contrast to the so far used pickup cells where pressures of about 10^{-2} Pa are sufficient here, with the HT source, higher pressures are needed. The pickup process is better described with a chromium beam crossing the helium-droplet beam. It is described in detail in Sec. 2.3.2. With chromium at a temperature of about 1500°C a vapour pressure of approximately 35 Pa is reached. Based on this temperature I started designing the chromium source.

To get an idea about the required heating power I used a simplified setup for calculations. A chromium cylinder with a 1/2 " = 12.7 mm diameter and a height of 8 mm is mounted on a "M3"-thread rod (3 mm diameter and a length of 77 mm). Fig. A.3 shows a scheme of this arrangement. The chromium is heated from the top. Heatconduction occurs through the chromium, and the connected stainless steel rod to the further end which is cooled to a fixed temperature. Due to the high temperature also radiative losses have to be taken into account.

Ignoring the radiative loss it could be described by a one dimensional heat equation. According to Ref. [15] this would look like Eqn. A.1, with Δ - the laplace operator, T - the temperature field, λ - the heat conductance, and P - the applied heat.

$$\Delta T + \frac{1}{\lambda} P = 0 \tag{A.1}$$

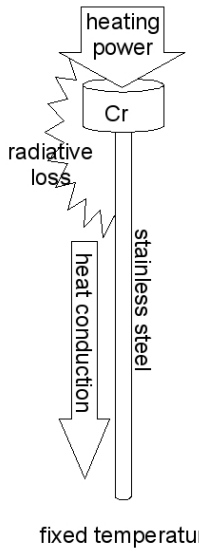

Figure A.2: heating scheme

This Poisson's equation can be solved analytically. Unfortunately the radiative loss was ignored but hence it is proportional to T^4 it definitely can't be neglected at a temperature of about 1500°C. So we add the radiative loss: (Stefan-Boltzmann law [13])

$$\dot{Q} = e_\mathrm{r}\, A_1\, \sigma\, (T_\mathrm{s}^4 - T^4). \tag{A.2}$$

With $\dot{Q}$ equals the radiation power in W. e_r represents the emissivity of the two surfaces (here $e_r = 1$ - the worst case approximation). A_1 is the surface area of my heated parts. For the differential equation A_1 will represented by $dA_1 = b \cdot dx$, with b being the circumference of the two rods. T equals the temperature of the hot area like in the heat conduction equation Eqn. A.1. T_s is the temperature of the surrounding, which, since it is watercooled, has a temperature of $T_\mathrm{s} = 300$ K.

Combining Eqn. A.1 and Eqn. A.2 gives the following:

$$\Delta T + e_\mathrm{r}\, A_1\, \sigma\, (T_\mathrm{s}^4 - T^4) + \frac{1}{\lambda} W = 0. \tag{A.3}$$

This equation cannot be solved analytically, so I used numerical methods for an approximation. I wrote three programs to calculate the temperature distribution of the rods. They can be found in:

[CD:\Scripts\Heating\]

"T_step_heating_Cr_SS.m" calculates the temperature at the cold end when the hot end has a certain temperature and is heated with a given heating power. "T_Cr_hot_end.m" calls "T_step_heating_Cr_SS.m" several times in order to find the temperature on the hot end for a given heating power and a given temperature on the cold end. "temperature_distribution.m" calls "T_Cr_hot_end.m" a few times to calculate the heating power for a given hot and cold end temperature.

In "T_step_heating_Cr_SS.m" the chromium and the stainless steel rods are divided into 100 equally sized parts. Starting with the first part on the hot end the temperature difference and the remaining heat is calculated with equation A.3. This is done for all segments and thus the temperature on the cold end can be calculated.

For a temperature of 1500°C a heating power of $\dot{Q} = (365 \pm 1)$ W is needed. The temperature distribution along the rod is shown in Fig. A.3. The later design differs from the

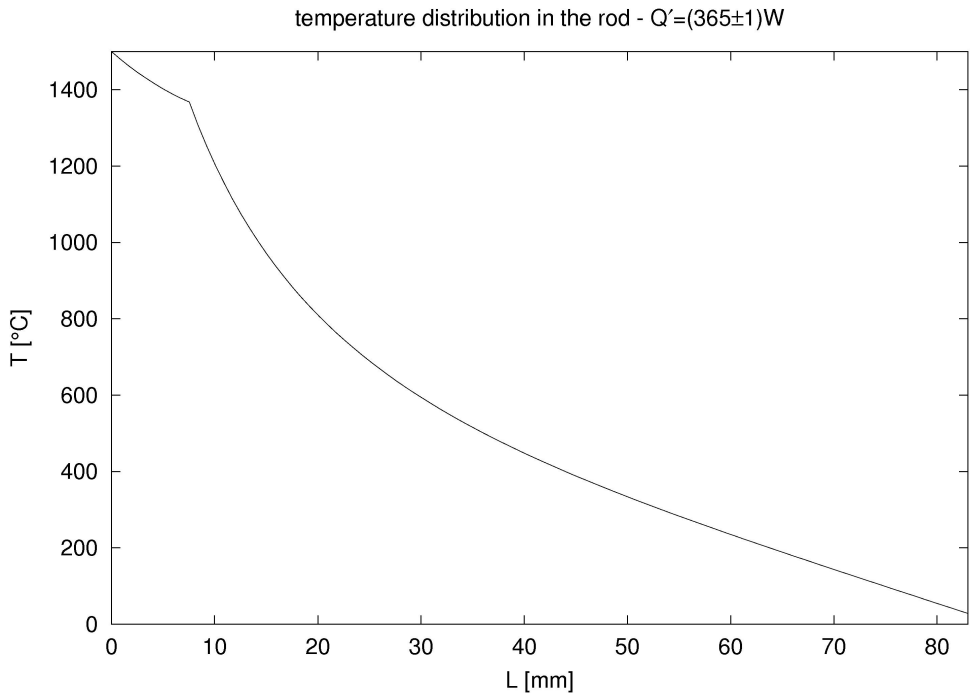

Figure A.3: Temperature distribution of the rod; one can see the buckle at 8 mm, where the Cr cylinder is connected to the stainless steel rod.
[CD:\Scripts\Heating\temperature_distribution.m]

simplified model described above but nevertheless one can estimate the range of the required heating power.

The power supply used for the electron bombardment heating is capable of $U = 1$ kV and $I = 1$ A. So a total of $P = 1000$ W of heating power can be applied.

Since the rest of the apparatus should remain at a lower temperature, it has to be cooled. All heated parts are placed inside a water cooled cylinder. For the dimensioning of the water cooling the temperature of the water used for dissipating a power of $P = 1000$ W was calculated with Eqn. [6]:

$$\Delta Q = cm\Delta T. \tag{A.4}$$

ΔQ, c, m, and ΔT represent the applied heat, the specific heat capacity, the mass, and the temperature difference. In my case I use a heat flux and a mass flux by dividing both sides of the equation by the time t. If you use running water it is more convenient to use the volume per time instead of the mass per time. Applying this to the equation A.4 it changes to:

$$P = c\frac{V}{t}\rho\Delta T \tag{A.5}$$

With P, $\frac{V}{t}$, ρ being the heating power, the water volume flowing through the cooling area per time and the density. If one uses "litre per minute" and a water density of 1 kg/L the equation simplifies further. With normal water pressure (2 bar to 4 bar) it is possible to get up to 12 L/min. Using a tube with 4 mm to 5 mm inner diameter and a length of about 4 m the flow rate is reduced to 2 L/min to 4 L/min. If an even smaller tube with only 3 mm inner

diameter and a length of 2 m is used the value decreases further to 0.5 L/min to 1 L/min. Again taking the worst case scenario (0.5 L/min) and applying $P = 1000$ W increases the water temperature by approximately $\Delta T = \frac{P}{c\rho}\frac{t}{V} = 30°\text{C}$. With this result I decided to use a copper tube with 6 mm outer and 4 mm inner diameter for the water-cooling.

A.4 Prototype Design

In this section the whole prototype setup will be described in detail. Starting from the mechanical parts, also the electric components and the software written to control the prototype will be explained.

A.4.1 Hardware

Since this will be a source to evaporate chromium, I will start with explaining the mounting of this material. Chromium rods with a purity of 99%+ have been bought from "Metallium, Inc." [1]. They are cylindrically shaped with a diameter of 1/2" = 12.7 mm and a height of 1" = 25.4 mm, weighing 32 g each. For further use, the rod is cut into three pieces with a height of approximately 8 mm. This can be found in Fig. B.17 [CD:\Drawings\Prototype\Cr_cylinder.dxf].

Experiments showed that, if a high evaporation rate is needed, directly heating the chromium leads to discharges due to a higher local pressure. So a crucible made of a conducting material with a low vapour pressure is used - like tantalum (Ta). Other materials, such as tungsten or molybdenum, are possible too. A Ta rod with an outer diameter of approximately 16 mm was used and a crucible is formed by removing a cylindrical volume. The drawing can be seen in Fig. B.18 [CD:\Drawings\Prototype\Crucible.dxf]. It should be processed in a way that one of the chromium pieces described above entirely fits into the opening without protruding from the crucible.

Several ways have been tried to hold the crucible. Unfortunately all easy approaches using stainless steel failed due to the high temperature. Finally, Ta sheets holding the crucible in the desired position turned out to be a successful approach. A 0.1 mm thick Ta sheet was cut into a rectangle with 160 mm length and 10 mm to 12 mm width. Another rectangle with 40 mm height and 10 mm to 12 mm width is needed to fixate the crucible. Radiation shields can be applied by using sheets with approximately 130 mm height for the first and 150 mm height for the second layer. They are the same width as the other sheets. The sheets are shown in Fig. B.19 [CD:\Drawings\Prototype\Crucible_fixation_sheets.dxf]. The numbers on the sheet represent the following:

1. outer fixation sheet
2. inner fixation sheet
3. first radiation shield
4. second radiation shield

To build the fixation the following steps should be taken in the described order. The result is shown in Fig. B.20 [CD:\Drawings\Prototype\Crucible_fixation.dxf].

[1] 04.06.2010: http://elementsales.com

The outer fixation sheet is bend around the crucible into an "U" - shaped form. The last 25 mm of the shield are folded inwards with an angle of approximately 90° so that both ends completely overlap.
Then the inner fixation sheet is added. The inner fixation sheet is also "U" - shaped around the crucible and the ends (last 10 mm) are folded 180° outwards. It is inserted with the crucible into the outer fixation sheet and the both sheets are spot welded together. The crucible should be removed before progressing.
Now the radiation shields are added. They should only touch the fixation sheet at their further ends where they are connected to the fixation sheet. They should also be "U" - shaped with the least possible distance to eachother and to the fixation sheet without touching. In the "U" - shaped position they are spot-welded to the fixation sheet.
In the end the two overlapping ends of the fixation sheet are spot-welded to eachother and a hole is drilled there to fit a M3 threaded rod.
This construction has good mechanical stability in two directions. To fasten it in the third axis it is clamped with two metal pieces onto the threaded rod. The metal pieces have to fit into the lower end of the outer fixation sheet. Two stainless steel blocks with 22 mm width, 10 mm depth and approximately 5 mm height are used. A centred hole to fit the M3 threaded rod (3.5 mm) is drilled through the blocks vertically. This is shown in Fig. B.21
[CD:\Drawings\Prototype\Crucible_clamping.dxf].

For further assembly three M3 threaded rods with a length of 120 mm are needed. For each rod a ceramic tube, preferably aluminium oxide, for insulation purposes has to be constructed. The inner diameter must be large enough to fit the threaded rods, the outer diameter must be smaller then 5 mm. Their length is one 60 mm and two 50 mm pieces. At their ends a notch should be cut into the ceramics. Since the ceramic tubes will be used as insulators, the threaded rods are inserted into the tubes and secured on both ends with nuts. The notches described before make sure that the volume inside the tube is not sealed by the nuts. Fig. B.22 shows the dimensions and the assembling
[CD:\Drawings\Prototype\Crucible_and_filament_fixation.dxf].

The above parts are mounted on the water cooled base plate of the cooling cylinder. The water cooled base plate is a massive brass block with a few feedthroughs and mounting points. This part, among others, was drawn using AutoCAD 2005. Two drawings were made, one to show the dimensions and one detail drawing where also related parts can be found. The files are named "base_plate_dimension.dxf" and "bottom_180109.dwg" (AutoCAD 2005) and can be found here: [CD:\Drawings\Prototype\].
In Fig. B.23 the size of the base plate is displayed. The cylinder has a overall height of 20 mm and a step at half the height, reducing the former diameter from 108 mm to 102 mm. Later the cooling cylinder will be placed there and secured with screws. The holes for those screws are drilled radial towards the centre of the baseplate at the holes 5, 6 and 7. This is also shown in Fig. B.23.
For the cooling of the base plate copper tubes are soldered on the bottom, the area with the 108 mm diameter. Here tubes with 6 mm outer and 4 mm inner diameter were used but according to Sec. A.3 tubes with an even smaller inner diameter would be sufficient too. The tubes have to be placed in a way that the holes, required in the baseplate which are described in the following, are not blocked.
Fig. B.24 shows the position and dimension of the needed holes. All the holes should be drilled through the whole base plate although some of them will only be used for screws. This will

improve the capability for the use under vacuum conditions. The holes are numbered and described below.
Holes numbered 5, 6 and 7 are used for positioning the base plate and therefore the whole prototype inside the vacuum chamber. They should fit M4 threaded rods. The baseplate will be secured by nuts on each side of the holes. The tubes for the water cooling must be placed around those holes in a distance, since one has to tighten the nuts.
Number 2 is used as electrical feedthrough and has a diameter of 7 mm.
The crucible fixation and the fixation of the filaments require the holes numbered 1, 3 and 4. The above described ceramic tubes should fit through easily, therefore the hole diameter is about 5.2 mm. On the upper side of the base plate - the area with 102 mm diameter - countersinks should be made on those holes. Their opening angle is 90° and they are 5 mm deep. It is pictured in the lower part of Fig. B.24 - the "M - M cut".
Beside the countersinks the holes 8, 9, 10 and 11 are drilled and a thread is cut into them to fit M3 screws.
Into the countersinks cones are inserted. They are the same size as the countersink but have to be higher for at least 1 mm. They are pictured in Fig. B.25 and the AutoCAD file can be found here: [CD:\Drawings\Prototype\Klemmring.dwg]. Since there are three countersinks, three cones are needed. In the centre, along the cone's axis, a hole is drilled to fit the ceramic tubes. The cones are cut on one side along the cone's axis to get a gap of about 1 mm. When the ceramic tube is inserted and both, the cone and the tube, are put in the holes 1, 3 or 4, the tube is still loose. When a pressure along the axis of the cone is applied to the cone, it will keep the tube in place without damaging the ceramics.
This is done with two fixation plates - one for the crucible fixation placed in hole 1 and one for the filament fixations placed in holes 3 and 4. The drawings are shown in Fig. B.26 and Fig. B.27. They can be found in the same file as the detailed drawing of the base plate:
[CD:\Drawings\Prototype\bottom_180109.dwg]. They are placed on the flat top of the cone and are fastened with M3 screws to the base plate. For the crucible fixation the screws are placed in the holes 10 and 11 and for the filament fixations 8 and 9 are used. The easiest way to mount the crucible and the filament fixation is to take the ceramic tubes and insert them into the base plate. Then the cone is put on the ceramic tube with the pointed side ahead in a way that it fits into the countersink. Then the fixation plates are added and bolted down in a way that the tubes can still be moved. Before tightening those screws the ceramic tubes should be positioned in a way that both of their ends have the maximum possible distance to metalparts on the base plate, but at least 5 mm.

Now the crucible fixation is placed on the upper side of the base plate. A nut is screwed onto a M3 threaded rod and the rod is inserted into the ceramic tube centred on the baseplate (hole number 1). The rod should stick out on the lower side of the baseplate for at least 2 cm and is secured on this side again by a nut. The height of the crucible fixation can now be varied by changing the position of the two nuts on the rod. It must not exceed a total height of 7 cm measured from the top of the baseplate to the centre of the crucible. Caution has to be taken when securing the position since the ceramic will break if one tightens the nuts too much.

The filament fixation is mounted in the same way. The other two threaded rods with 120 mm length are inserted into the ceramic tubes at position 3 and 4. Again they are secured by two nuts one for each side of the rod. They stick approximately 1.5 cm out of the ceramic tubes on the top of the base plate.

With two nuts the filament fixation adapter plate is secured on these two rods. The dimensions of this plate can be found in Fig. B.28
[CD:\Drawings\Prototype\Filament_fixation_adapter_plate.dxf]. For further assembly 4 M3 threaded rods with the length of 40 mm each are needed. One of these is screwed in the third hole of the fixation plate described above. It is secured by a counter nut from the lower side of the plate.

The filament fixation ring drawn in Fig. B.29
[CD:\Drawings\Prototype\Filament_fixation_ring.dxf] is now placed on this threaded rod and secured with two nuts. It should be parallel to the bottom of the crucible and the crucible should be centred when looking through the ring.
This can be achieved by changing the height of both, the ring and the crucible. Nevertheless the overall height of the ring measured from the top of the base plate must not exceed 10.5 cm. If the crucible has a horizontal offset the fixation sheets can be bend carefully. The other 3 M3 threaded rods are now inserted into the holes in the fixation ring and secured by nuts. If they stick out over the inner circle (102 mm diameter) of the baseplate, they either have to be moved or cut to a shorter length. When changing their position a minimum distance of at least 5 mm to the crucible fixation has to be taken into account.

Now the filaments have to be placed on the filament clamping. The filaments used are pin - based (G4) halogen lamps with 20 W. A lower wattage result in a higher efficiency (5 W and 10 W have also been tested), which can be neglected since it is about 90%, but a lower lifetime of the filaments. These light bulbs are usually used for desk lamps and can be bought in several hardware stores. Two different designs can be found. The filament is either parallel or perpendicular to the pins. For my uses the lamps with the perpendicular filaments are necessary.
The bulb of the lamp has to be destroyed but the glass around the pins and the pins itself should remain intact. Also the filament shouldn't be harmed. The best way to achieve this is crushing the bulb in a vice carefully. It is a good idea to put the bulb in a plastic bag first since a lot of quartz splinters are produced. The rest of the bulb has to be removed with pliers carefully.

The filament clamping is drawn in Fig. B.30
[CD:\Drawings\Prototype\Filament_fixation_clamping.dxf]. It is a stainless steel disc with 70 mm diameter and about 5 mm height. A semi circle sector is cut out for one of the two pins of the filaments. The other pins are clamped into small (0.5 mm) slits cut into the other semi circle sector of the filament clamping. The purpose of the larger slits (1 mm) is only to leave the clamps flexible. Before the filaments are attached the contacts for the second pins of the filaments has to be added.
Therefore one needs isolated metal parts. Again M3 threaded rods are cut to the following lengths: one 27 mm and two 15 mm. A hole has to be drilled in the centre along the rotational axis for about 6 mm with 0.8 mm diameter. The pins of the filaments have to fit into it. A drawing can be found in Fig. B.31 [CD:\Drawings\Prototype\Filament_contacts.dxf].
The contacts are kept in place by the filament contact fixation 1 B.32
[CD:\Drawings\Prototype\Filament_contact_fixation1.dxf]. It is a Macor plate with two holes to bolt it down to the filament clamping. It has additionally three holes with M3 threads for the filament contacts described above.

Now the filaments are placed in the following way. The filament contact fixation 1 is mounted on the filament clamping and the filament contacts are inserted into it with the

drilled hole on the side of the filament clamping. The threaded rod with 27 mm length has to be in the middle hole.

The filaments are placed one by one. A screwdriver can be used to pry the small slits open so that the filaments can be inserted easily. One pin goes into the slit and the other pin should fit into the filament contacts. They can be varied in height by screwing the filament contacts in or out. For further adjustments the filaments should be sticked in as deep as possible on the filament clamping. The filament itself should be placed parallel to the filament clamping and the filaments should all be at the same height.

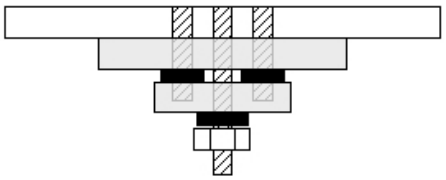

Figure A.4: Contacting the filaments;
hatched parts ... filament contacts
black shaded parts ... crimp eyelets
parts ordered from top to bottom:
filament clamping B.30
filament contact fixation 1 B.32
filament contact fixation 2 B.33
nut

The filament clamping with the attached filaments can now be placed on the filament fixation ring using two nuts for each of the three rods. Now the distance of the filaments to the crucible has to be adjusted in the following way. Using the three fixation points of the filament clamping it is possible to tilt and move the clamping and therefore change the position of the filaments. The overall height must be adjusted by changing the position of the filament ring itself. The easiest way to change a horizontal offset is by bending the crucible fixation sheet. With these degrees of freedom the filaments should be positioned behind the crucible with a distance of about 1.5 mm to 2 mm to the crucible. They must be centred relative to the crucible and all the filaments should have the same distance to it.

For the electric contact of the filaments one wire per filament is needed. Three enamelled copper wires are used for that purpose. During the experiments additionally one wire was used for a Faraday cup and one for a repulsion shield. This gives a total of 5 wires glued with epoxy resin into hole 2 of the base plate. The wires are connected to the filament contacts with crimp eyelets.
To keep them in place another Macor plate is needed, see Fig. B.33 [CD:\Drawings\Prototype\Filament_contact_fixation2.dxf]. First the crimp eyelets for the outer filaments are placed on the threaded rods. Then the Macor plate (filament contact fixation 2) is placed on the rods. In the end the middle filament is connected and secured with a nut. This is displayed with a schematic drawing in Fig. A.4.1.

To prevent heating of the vacuum chamber a cooling cylinder has to be put on the base plate around all the heated parts. The cooling cylinder consists of a copper pipe with 102 mm inner and 108 mm outer diameter. One end is sealed with a top cover made of brass. It is pictured in Fig. B.34 [CD:\Drawings\Prototype\Cooling_cylinder_top.dxf]. The smaller end fits into the cooling cylinder and they are hard-soldered together. On the distant end of the cooling cylinder three holes, 5 mm of diameter each, are drilled. The cooling cylinder will be placed on the base plate and the holes must fit to the holes on the base plate. Then the cylinder can be secured with screws to the base plate.
The cooling cylinder is shown in Fig. B.35 [CD:\Drawings\Prototype\Cooling_cylinder.dxf]. The drawings differ from the actual design since a few holes were drilled additionally into the cooling cylinder. To mount an adsorption plate on the inside of the cooling cylinder two holes are required on the opposite site of the crucible. So before continuing it is crucial to think

about the application.
After making the necessary changes the copper tubes for the water cooling are soldered onto the cooling cylinder and also on the top of the cooling cylinder.
It is a good idea to leave at least 10 cm of the tube ends detached since they will be connected to another tube in the end using Swagelok tube fittings. All the tubes used for water cooling at the prototype setup have 6 mm outer and 4 mm inner diameter.

A.4.2 Electronics

For an electron bombardment heater one needs a power supply for the filaments, a power supply for the target and a controlling unit. The power supply for the filaments is best chosen to supply a power of up to 150% of the filaments power rating, since the filaments can be overcharged for a short time. To stabilise the heating process this power supply must be controllable. A laboratory power supply "EA-PS 3032-10B" from "Elektro - Automatik" is used which can supply up to 10 A at 32 V. This is more than needed for the 20 W at 12 V halogen light bulbs used as filaments. The filaments were tested with up to 34 W (1.9 A at 18 V) which drastically reduces their lifetime to about 10 minutes. At 25 W (1.7 A at 15 V) they can be used for about two hours but for longtime measurements (>6 hours) they were used between 15 W and 20 W (11 V to 13 V). The filaments are wired to the laboratory power supply. A schematic drawing of the wiring can be found in Fig. A.5. The negative contact is connected to the target's power supply negative connector, which is internally connected to grounding my case, via an amperemeter. The positive output with up to 1 kV is connected to the Ta crucible. One might use power supplies with up to 5 kV to increase the heating power. The acceleration voltage (always 1 kV) times the emission current achieved by the filament equals the heating power applied to the target. To control the heating power one can either change the acceleration voltage or, as used here, the emission current by adjusting the filament's power. Adjusting the filament's power is done best by controlling the filament's voltage due to the positive temperature coefficient of the filament's resistance.

Table A.1: Filament's power supply - pin assignment

pin ... sub–D socket's pin number
desc. ... description

pin	desc.
1	nominal voltage value
2	nominal current value
3	reference value
4	digital ground
5	local/extern control (low = extern)
9	actual voltage value
10	actual current value
11	ground (analog)
15	voltage/current control (low = voltage)

The amperemeter mentioned above is used to measure the emission current. The "Keithley 196" multimeter was used for this purpose. it can be read by a computer via GPIB. The measurement of the emission current is part of the control system established in a LabVIEW program, which is discussed in Sec. A.4.3.

The filament's power supply can be controlled by analog signals via a 15 pin sub–D socket. The exact pin assignment can be found in the manual but the used pins are described in Tab. A.1. Pin four is connected to pins five and 15 to set the power supply in extern and voltage controlled mode. In voltage controlled mode the value for the current has to be set

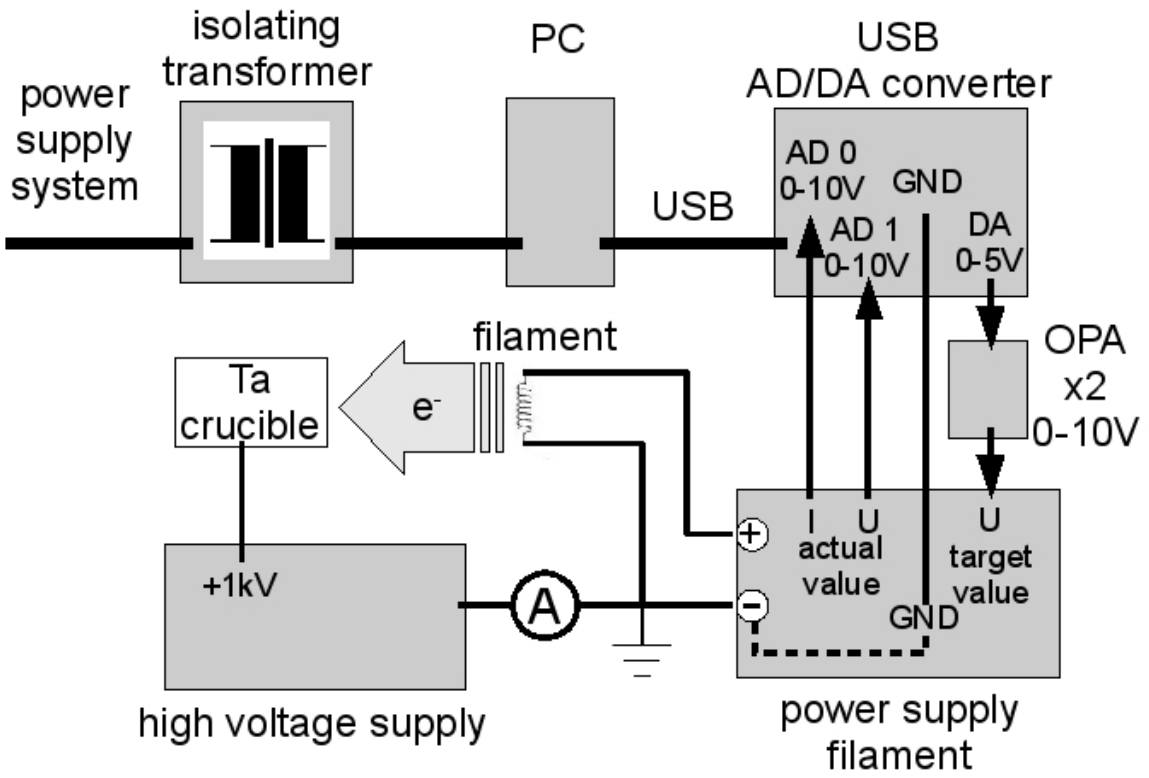

Figure A.5: Schematic drawing of the wiring

to maximum by connecting pins two and three. The pins one, nine, ten, and eleven are lead out of the connector for measuring and controlling with an analog–to–digital (AD) and digital–to–analog (DA) converter. There is no galvanic isolation between the analog interface and the output connectors.

An AD/DA converter form "Quancom" (USBAD8DAC2) is used for controlling and measuring. The pins one, two, and eleven are connected to channels zero, one and ground at the AD section of the AD/DA converter. Since the DA section of the device is only able to deliver a maximum of 5 V a doubler is used. It is an operational amplifier circuit which is connected to the ground and channel zero of the DA section and upscales the input voltage to the doubled value. The two outputs are ground, which is connected to pin eleven, and the doubled signal, which is connected to pin one of the laboratory power supply's interface. Both, the AD/DA converter and the doubler circuit, are powered by plug–in power supplies at 12 V.

The AD/DA converter is also connected to a computer via USB. It is part of the control system mentioned above and also controlled by software.

A.4.3 Software

The heating process was controlled by self–written programs in LabVIEW 8.6. The programs can be found in [CD:\Software\Prototype\]. They depend on sub–vis placed in the subdirectory "necessary VIs".

"Heat.vi" is a PID controller based program to stabilise the heating power by changing the filament voltage. The process is also monitored and the relevant data is written to files. Further details on the file structure can be found within the program. One can enter the voltage of the target's power supply, which is only used to calculate the heating power, the

emission current, the program will stabilise it, the maximum filament voltage, to prevent damaging the filaments, and the thermocouple voltage, to get the temperature of the target. The time, the filament properties, namely the current, the voltage, and the power, and the emission current is displayed. Furthermore the emission current is also displayed in a chart to see the changes over time.
The controlling cycle takes about 2 s, which is quite long and explains the bad stabilisation. It is not clear wether the AD/DA converter or LabVIEW or the combination of both are the cause.

The program "Reset_DA.vi" is used to reinitialise the AD/DA converter if an error occurs.

If discharges occur during the heating process the AD/DA converter might crash. This can be resolved either by the program described above, or by temporary unplugging the power and USB connector of the AD/DA converter.

A.5 Results

A.5.1 Introduction

The prototype's main purpose was to get an idea of the needed heating power for a certain pickup probability of Cr on the He nanodroplet. The pickup probability depends on the number of Cr particles in the interaction region with the He nanodroplet. A rough estimation can be made by comparing the needed vapour pressure per interaction length of potassium and rubidium with the Cr vapour pressure. The vapour pressure depends on the temperature which corresponds to the heating power. The goal was to model the dependencies.

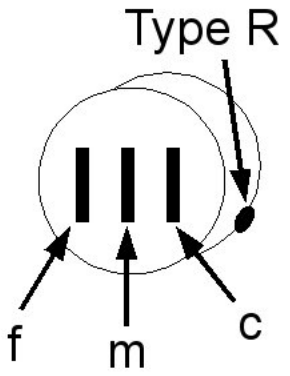

Figure A.6: Filament and thermocouple position

A.5.2 Temperature and Heating Power

The temperature reached with a certain heating power depends on the heat losses. As described in Sec. A.3, due to the high temperature one has to take both the heat conduction and the radiative loss into account. Since the radiative loss is proportional to T^4 it dominates the overall heat loss at temperatures above 600°C or 800°C. Obviously this strongly depends on the setup but could be used as rule of thumb.

Table A.2: Final Temperature

fil ... filament position (f, m, c) see Fig. A.6
d ... filament distance (1 mm or 2 mm)
P ... heating power
T ... temperature reached

fil, d	P [W]	T [°C]
f 1	300	1380
m 1	275	1450
c 1	300	1480
f 2	300	1230
m 2	275	1290

The temperature was measured with a self–built Type R thermocouple. The thermocouple wires were spot–welded to the Ta crucible on the distant side of the filaments. A schematic drawing can be found in Fig. A.6. The filaments are marked relative to their position to the Type R thermocouple with "f" (far), "m" (middle), and "c" (close). The position of the filaments is given by the filament clamping shown in Fig. B.30 with a distance of 5 mm between each filament. The middle filament should be centred relative to the back of the Ta crucible. The distance between the filament and the crucible was varied but showed an optimum at about 1 mm. If the distance is too small discharges will happen because of the higher local pressure due to sputtering of the crucible and evaporation of the filament. The heating power and the temperature is increased by the higher number of electrons hitting the crucible due to the better viewing angle of the filament.

For a given heating power and filament position the temperatures reached are shown in Fig. A.7. The temperatures were monitored up to 300 W of heating power. According to Sec. 2.2.4 a measurement inaccuracy of $\Delta T = \pm 30$°C is assumed. The maximal reached temperatures are shown in Tab. A.2.
One can see that the temperatures reached with 2 mm filament distance is about 10% lower compared to the 1 mm filament distance. In contrast to that one should not pay too much attention to the different temperatures reached at the positions "f", "m", and "c". This can be

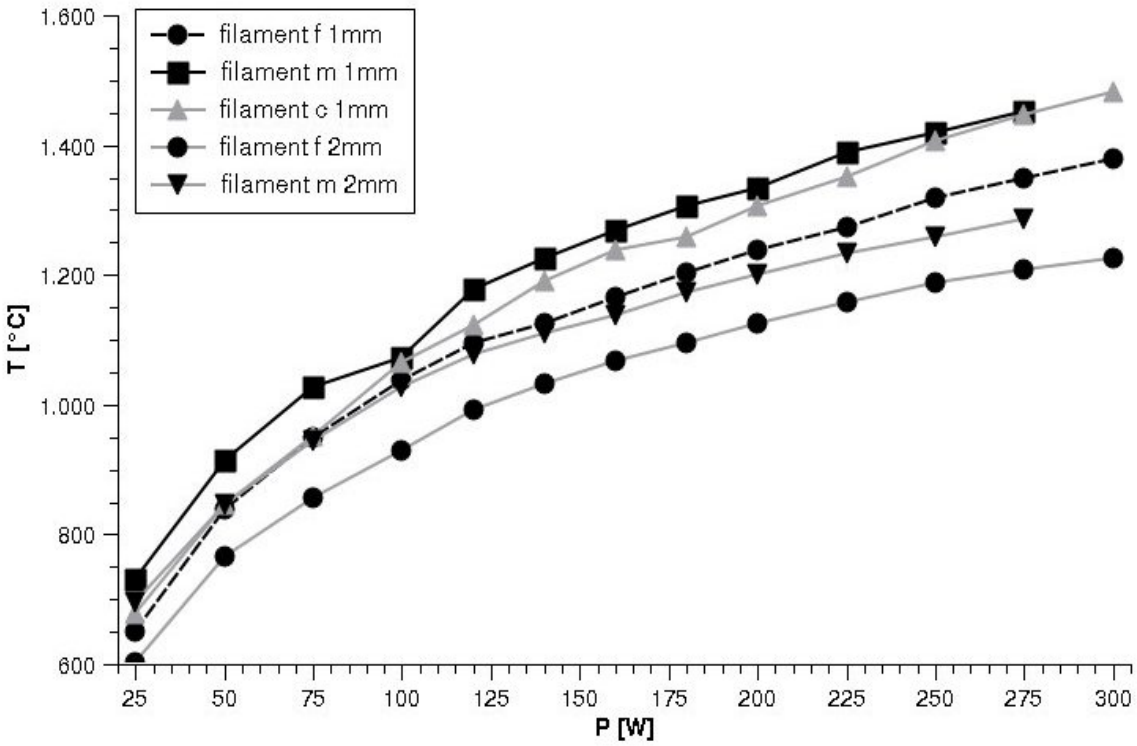

Figure A.7: Temperatures reached under different conditions, [CD:\Analysis\Deposition\Temperature_Prototype.qti]

explained by the temperature distribution of the crucible and the place of the temperature measurement.

A.5.3 Deposition Rate

For a successful pickup of atoms on the He droplet, the droplet beam passes through an interaction area with the gaseous dopant material at a certain pressure. With the constructed HT source one has to think about the pickup process in a different way. A Cr block is heated and the atoms evaporate from the surface. Since the temperature to evaporate Cr is high, the whole surrounding, like the cooling cylinder, will trap the atoms on contact. The pressure defined in an enclosed oven, like the pickup sources used so far [27], may not be a valid picture here. With the atoms "produced" in one spot and directly following line of sight to their trapping point, it has the characteristics of an effusive source. In this section the similarities and differences between the HT source and an effusive source will be revealed and the obtained deposition rates will be shown.

An effusive source can be described as a box with a defined pressure inside. Particles can leave the box through a hole but the number of leaving particles is small compared to the amount inside. The necessary condition for an effusive source is that the leaving particles have no effect on the pressure inside the box. The Cr in the HT source, in contrast to the effusive source, is not enclosed and the particles evaporating from the Cr block will leave the surrounding area of the Cr rapidly. Close to the surface of the Cr block, the vapour pressure may still be defined. The number of particles in the interaction region depend on the evaporation rate which is connected to the vapour pressure.

As mentioned before it is assumed that the Cr atoms will be trapped on any cold surface. So the evaporation rate is proportional to the deposition rate, which can be measured easily.

A Ta sheet is mounted on the inner surface of the cooling cylinder on the opposite site of the crucible's opening. The mass of this adsorption sheet before and after an evaporation process is measured. Knowing the area of the sheet and the distance to the crucible the solid angle can be calculated. Using the Eqn. 1.17 from Sec. 1.5.2 the number of particles leaving an effusive cell at a certain temperature can be calculated. This is done with script "evaporated_mass.m" found in [CD:\Scripts\Deposition\]. It already contains the dimensions of the experiment - the opening area of the crucible ($(1.27 \pm 0.05)\,\mathrm{cm}^2$), the distance to and the area of the adsorption sheet. The adsorption sheet is of rectangular shape with $(6.5 \pm 0.1)\,\mathrm{cm}$ length and $(2.5 \pm 0.1)\,\mathrm{cm}$ width and has two mounting points with a diameter of $(0.60 \pm 0.05)\,\mathrm{mm}$ which shade the adsorption sheet. The shaded area has to be subtracted from the area of the sheet giving an effective area of $(16 \pm 1)\,\mathrm{cm}^2$. It is mounted in a distance of $(4.6 \pm 0.2)\,\mathrm{cm}$ measured perpendicular to the centre of the opening of the crucible. The following assumption is made: a circle with the same surface area as the deposition sheet is used for the calculation of the solid angle.

Table A.3: Adsorbed mass

T ... Temperature measured with Type R thermocouple
P ... heating power
$m_{ht,h}$ ... mass difference of the adsorption sheet per hour
$m_{eff,h}$ ... mass evaporated from an effusive source per hour
Nr ... filenumber [CD:\Measurements\Deposition*.txt]

T [°C]	P [W]	$m_{ht,h}$ [mg/h]	$m_{eff,h}$ [mg/h]	Nr
1300 ± 40	222.8 ± 1.7	15 ± 5	80^{+90}_{-50}	H0102
1301 ± 29	204 ± 10	39 ± 6	70^{+60}_{-40}	H0103
1330 ± 40	199.9 ± 1.9	25.7 ± 3.1	140^{+150}_{-80}	H0116
1370 ± 40	229.8 ± 1.5	78 ± 6	310^{+310}_{-160}	H0111
1450 ± 50	251.8 ± 1.8	110 ± 8	1100^{+1400}_{-700}	H0110
1450 ± 29	274.7 ± 1.5	231 ± 13	1000^{+700}_{-400}	H0113

Six measurements were done using different heating powers, stabilised on the heating power by the self–built LabVIEW program "Heat_091127.vi" found in [CD:\Software\Prototype\]. See Sec. A.4.3 for further information. The mass differences are shown in Tab. A.3, they were measured with a precision scale with an inaccuracy of ±2 mg. The higher inaccuracy found in Tab. A.3 occurs due to calculating the mass difference and scaling it to the adsorbed mass per hour. The measurement runs are shown in Fig. A.8 to Fig. A.13. Starting from the left, one can see the filament's emission current which is directly proportional to the heating power by a factor of 1000. Beneath the residuals of the linear fit for the emission current are given. The diagram in the middle shows the thermocouple voltage with the residuals of the fit underneath. On the top right hand side the temperature dependence on the heating power is shown. This indicates a high inaccuracy in either the temperature measurement or the heating power because the data points look randomly distributed. The calculated fit parameters are shown on the lower right hand side and are partially also given in Tab. A.3. The values in the figures stand for: I_{ec} - emission current, P - heating power, U_{temp} - thermocouple voltage, T - temperature calculated from the thermocouple voltage, m - weighted mass difference, m_{effusive} - mass difference an effusive cell would have produced, t - duration of the measurement, m_{h} - m scaled to one hour measurement time, $m_{\mathrm{effusive,h}}$ - m_{effusive} scaled to one hour measurement time

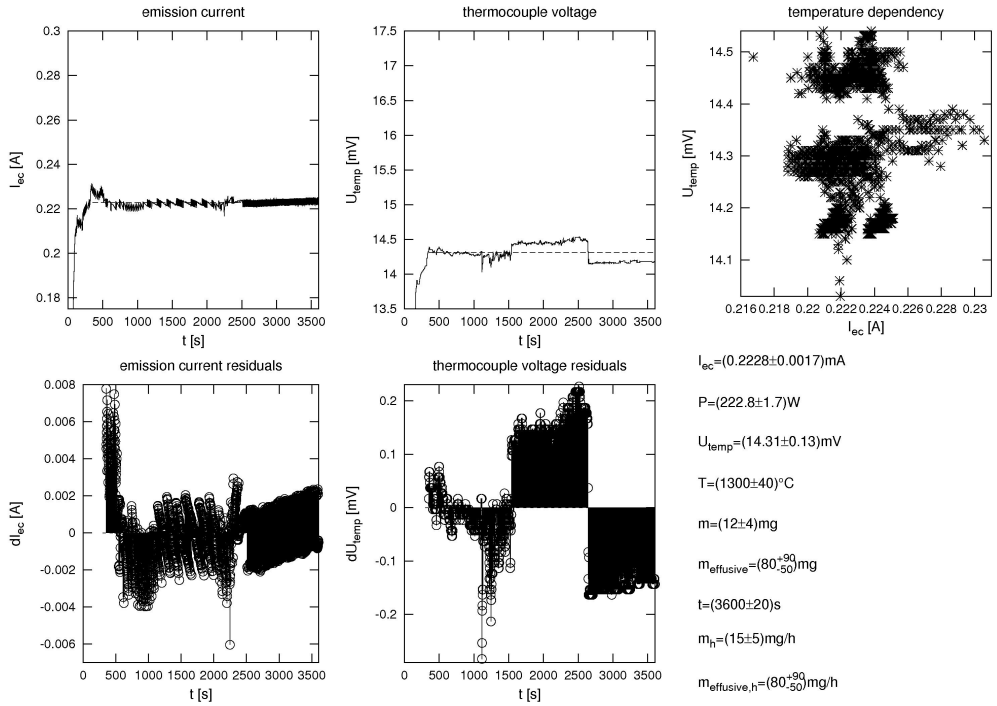

Figure A.8: Adsorption rate at P= 222.8 ± 1.7 W [H0102.txt]

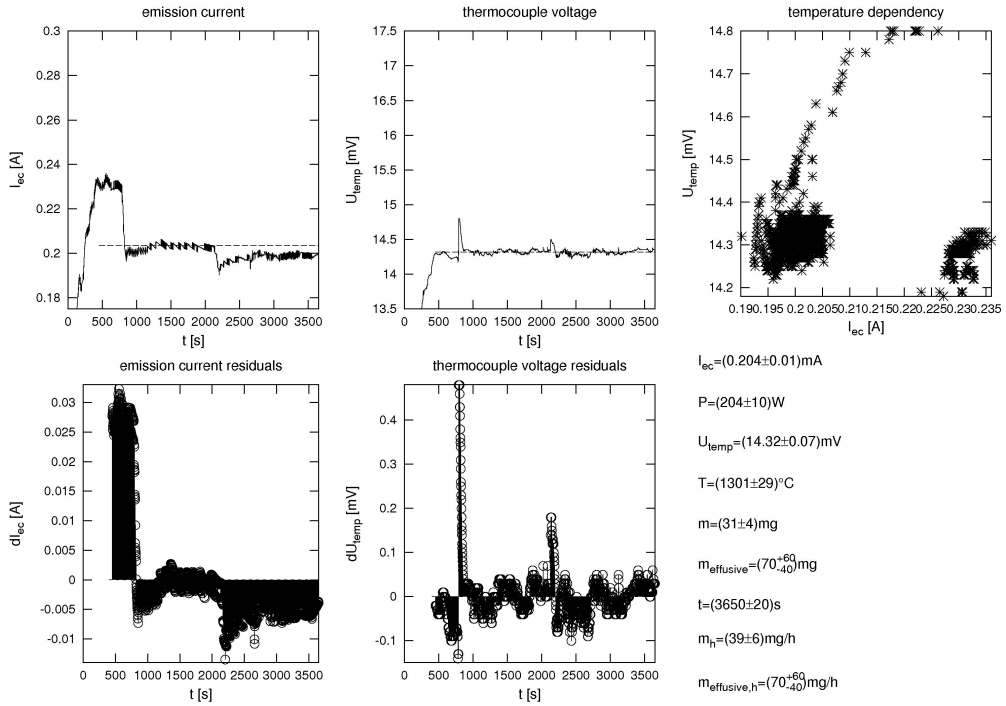

Figure A.9: Adsorption rate at P= 204 ± 10 W [H0103.txt]

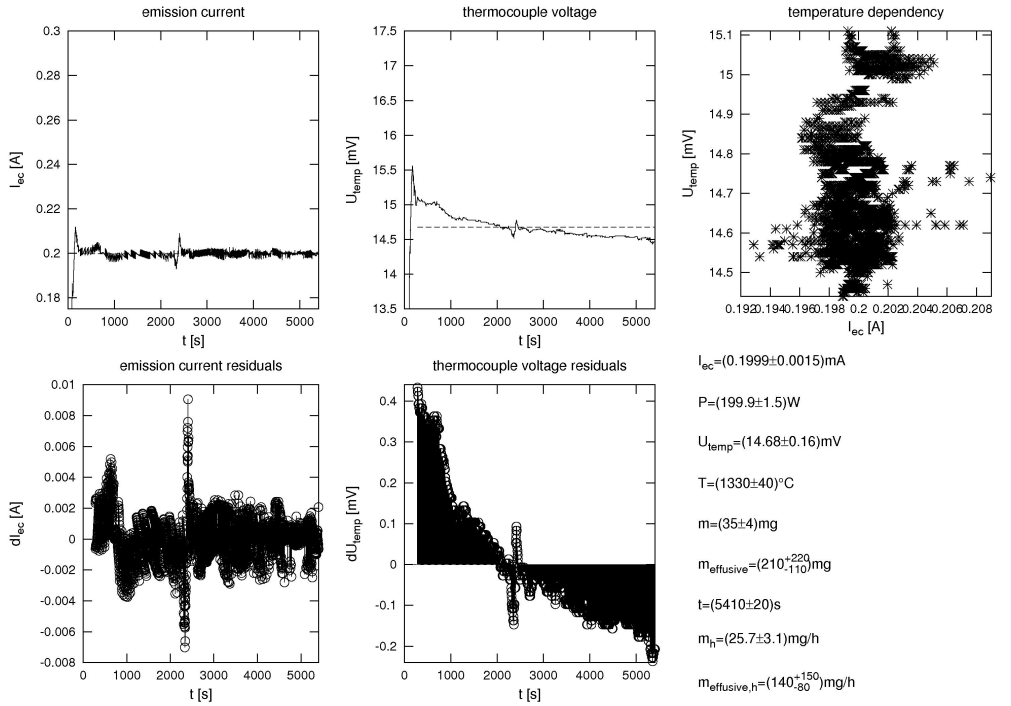

Figure A.10: Adsorption rate at P= 199.9 ± 1.5 W [H0116.txt]

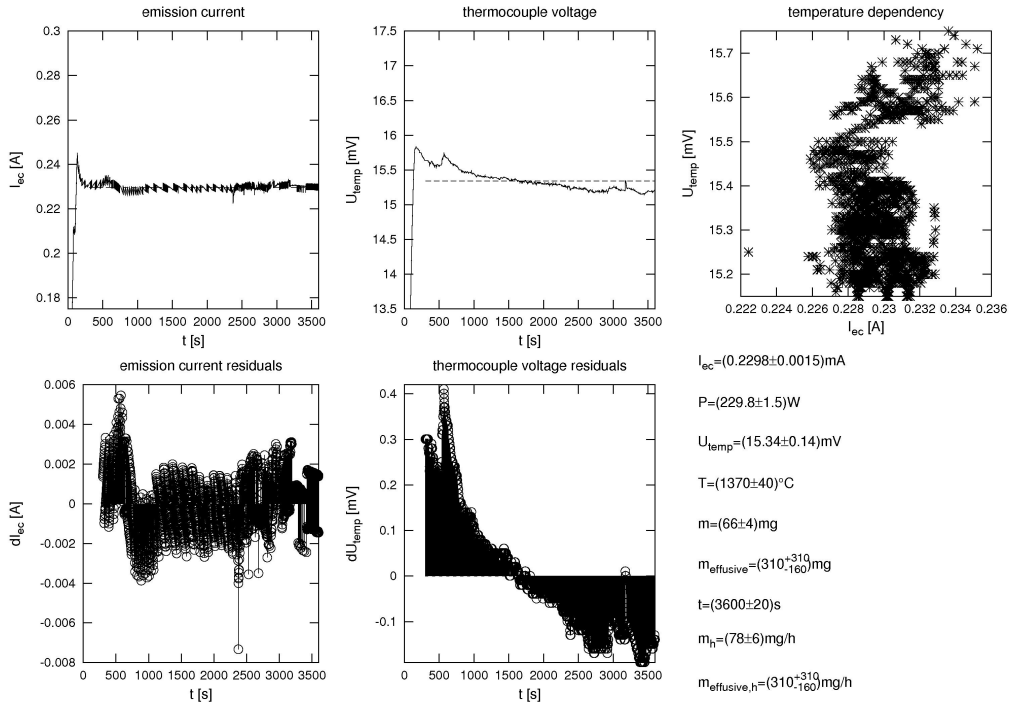

Figure A.11: Adsorption rate at P= 229.8 ± 1.5 W [H0111.txt]

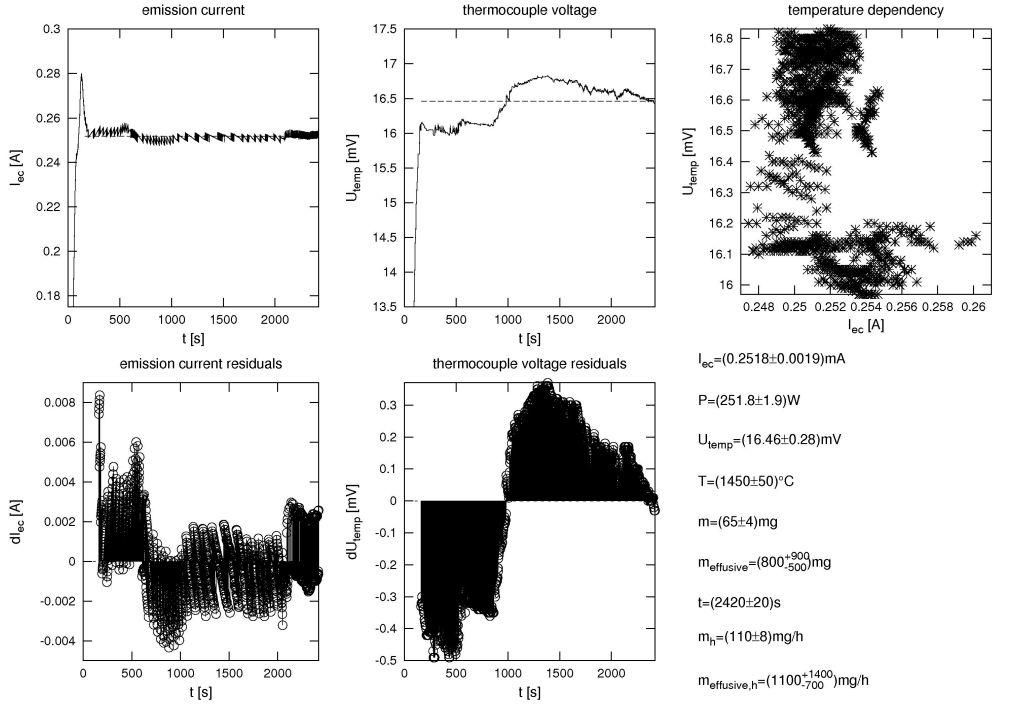

Figure A.12: Adsorption rate at P= 251.8 ± 1.8 W [H0110.txt]

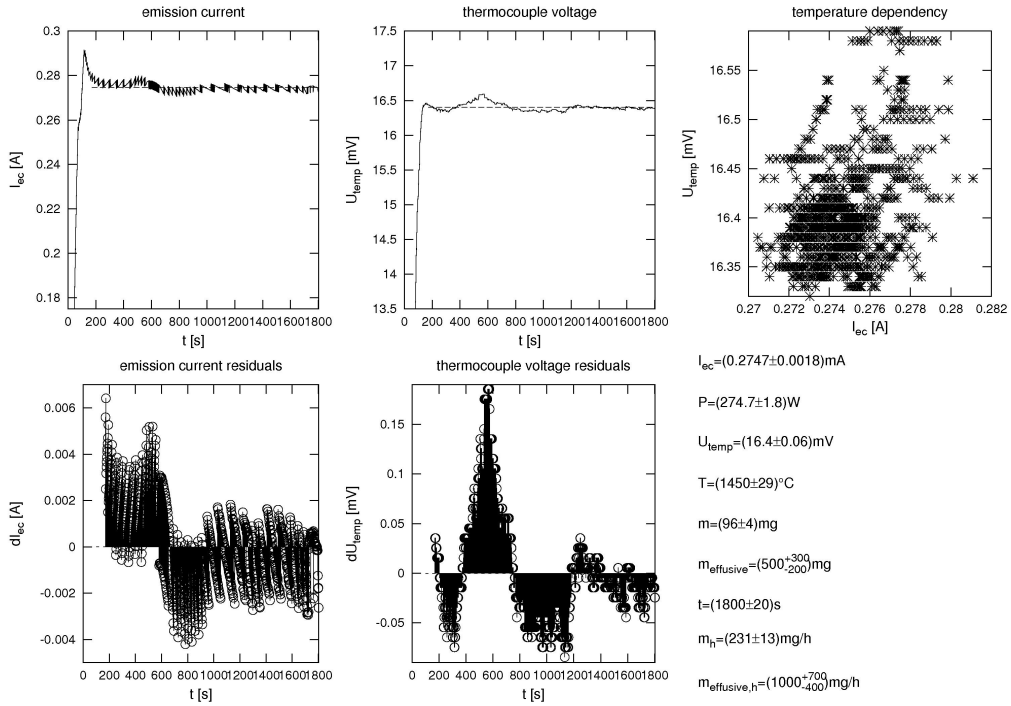

Figure A.13: Adsorption rate at P= 274.7 ± 1.5 W [H0113.txt]

Appendix B

Drawings

Here, drawings for the prototype setup, the high temperature pickup source, and the fixation of the quadrupole mass spectrometer can be found. The drawings were done in QCad (2.0.5.0)[1], a CAD software which should be compatible to AutoCAD. The community edition of this software was released under the terms of GPL and is therefore free for use. The source files can be found on the enclosed CD [CD:\Software\qcad-2.0.5.0-1-community.src.tar.gz]. A windows installer is not included since it is non-free.

All figures are displayed in mm and the drawings are not printed true to scale.

[1] 04.06.2010: http://www.ribbonsoft.com/qcad.html

B.1 Quadrupole Mass Spectrometer

QCad drawings can be found on the enclosed CD [CD:\Drawings\QMS\].

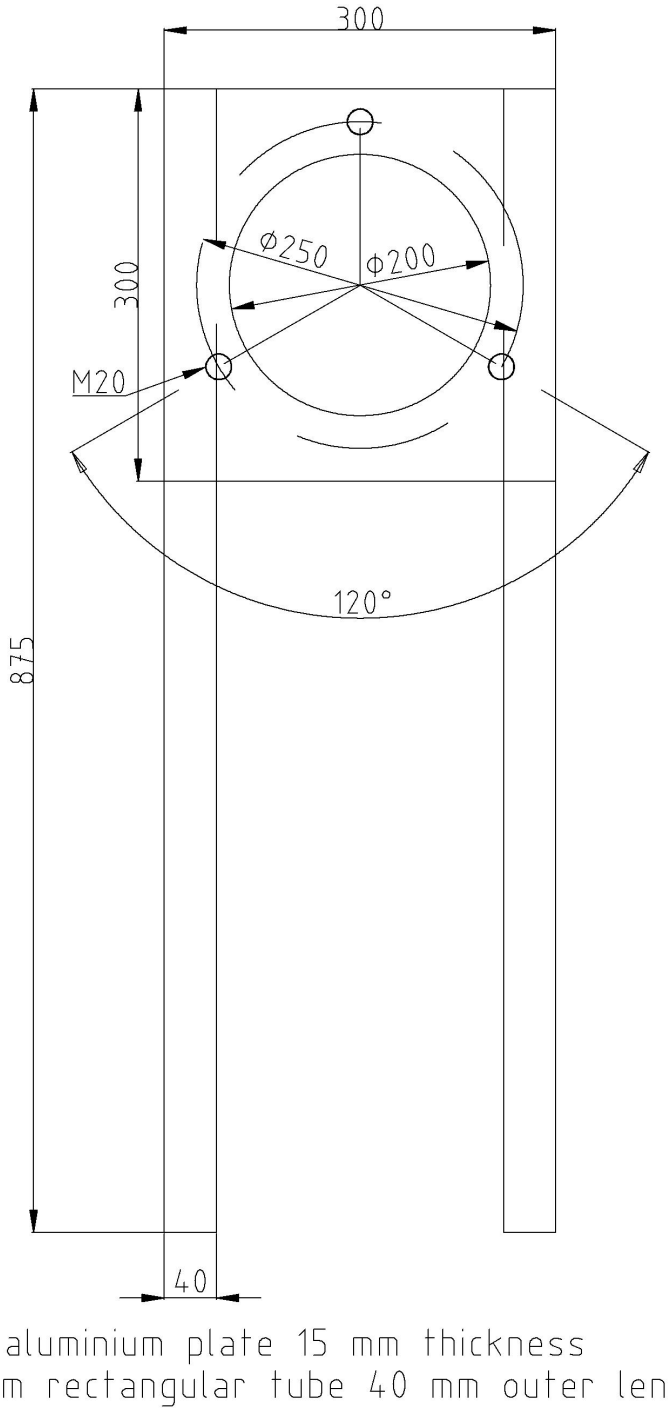

Figure B.1: Fixation of the quadrupole mass spectrometer. Two rectangular aluminium tubes are mounted on the base frame of the apparatus. An aluminium plate (15 mm thick) is used to mount the fixation plate B.2 with three M20 threaded rods of 125 mm length. [CD:\Drawings\QMS \Fixation.dxf]

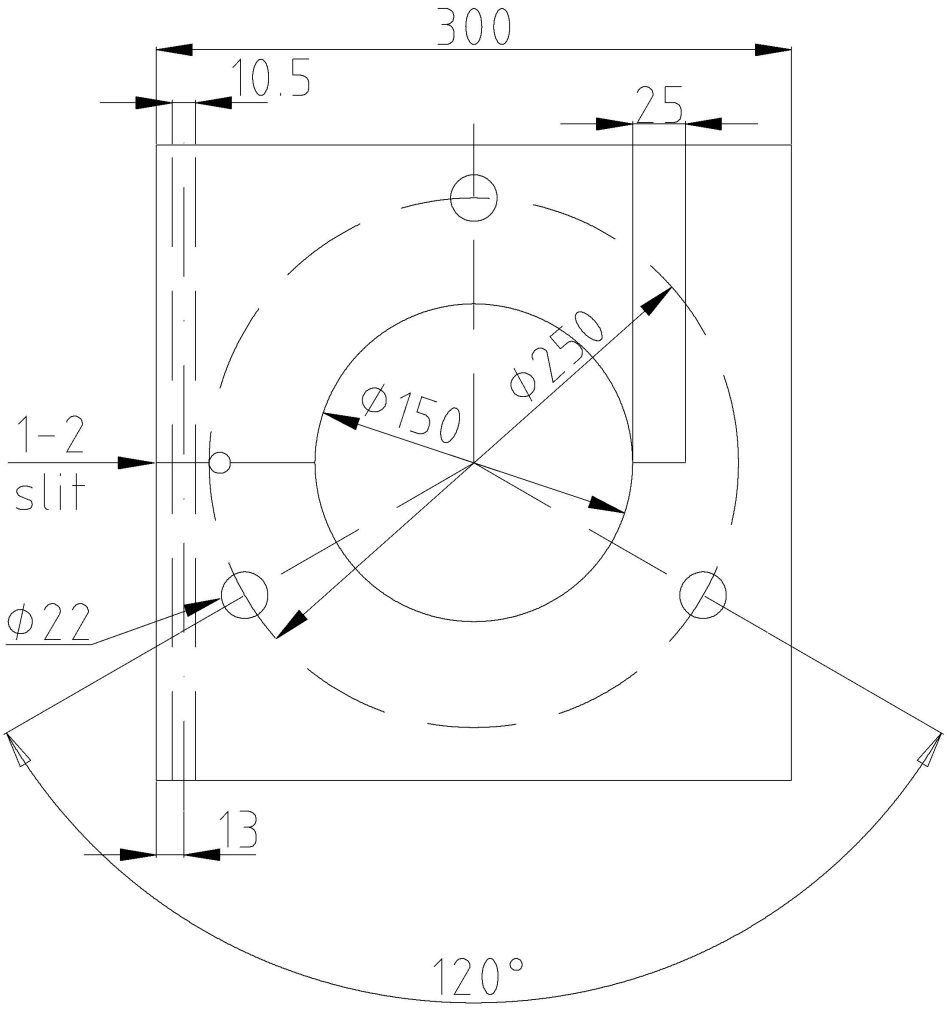

Figure B.2: The QMS chamber is clamped into the 150 mm centred hole by fastening a 340 mm long M10 threaded rod which is put through the 10.5 mm hole drilled alongside through the plate. It is then mounted on the three M20 threaded rods of the fixation B.1. [CD:\Drawings\QMS\Filament_Contacts.dxf]

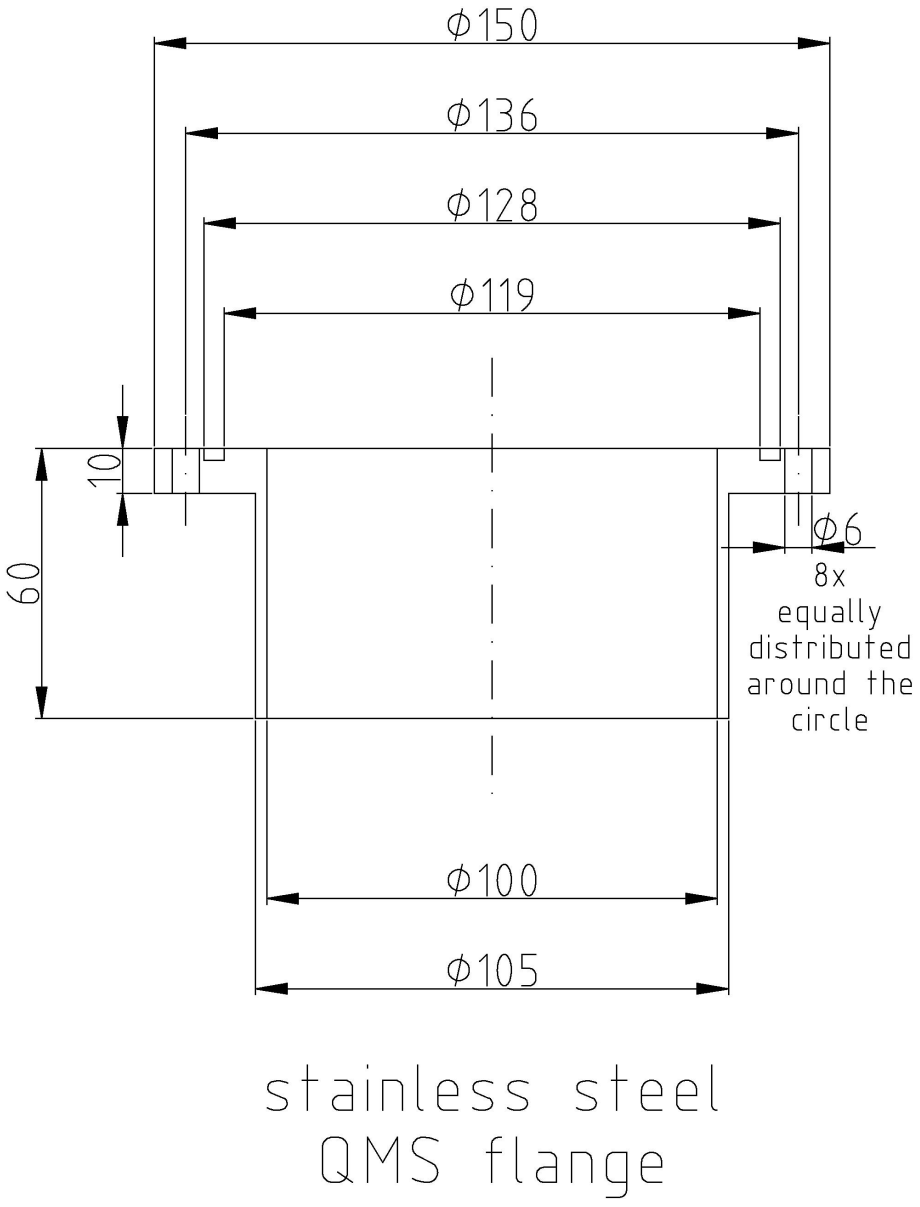

Figure B.3: The flange is welded to a bellow which is connected to the QMS chamber. It can be mounted directly onto the measurement chamber wall. [CD:\Drawings\QMS\Flange.dxf]

B.2 High Temperature Pickup Source

QCad drawings can be found on the enclosed CD [CD:\Drawings\HT_Source\].

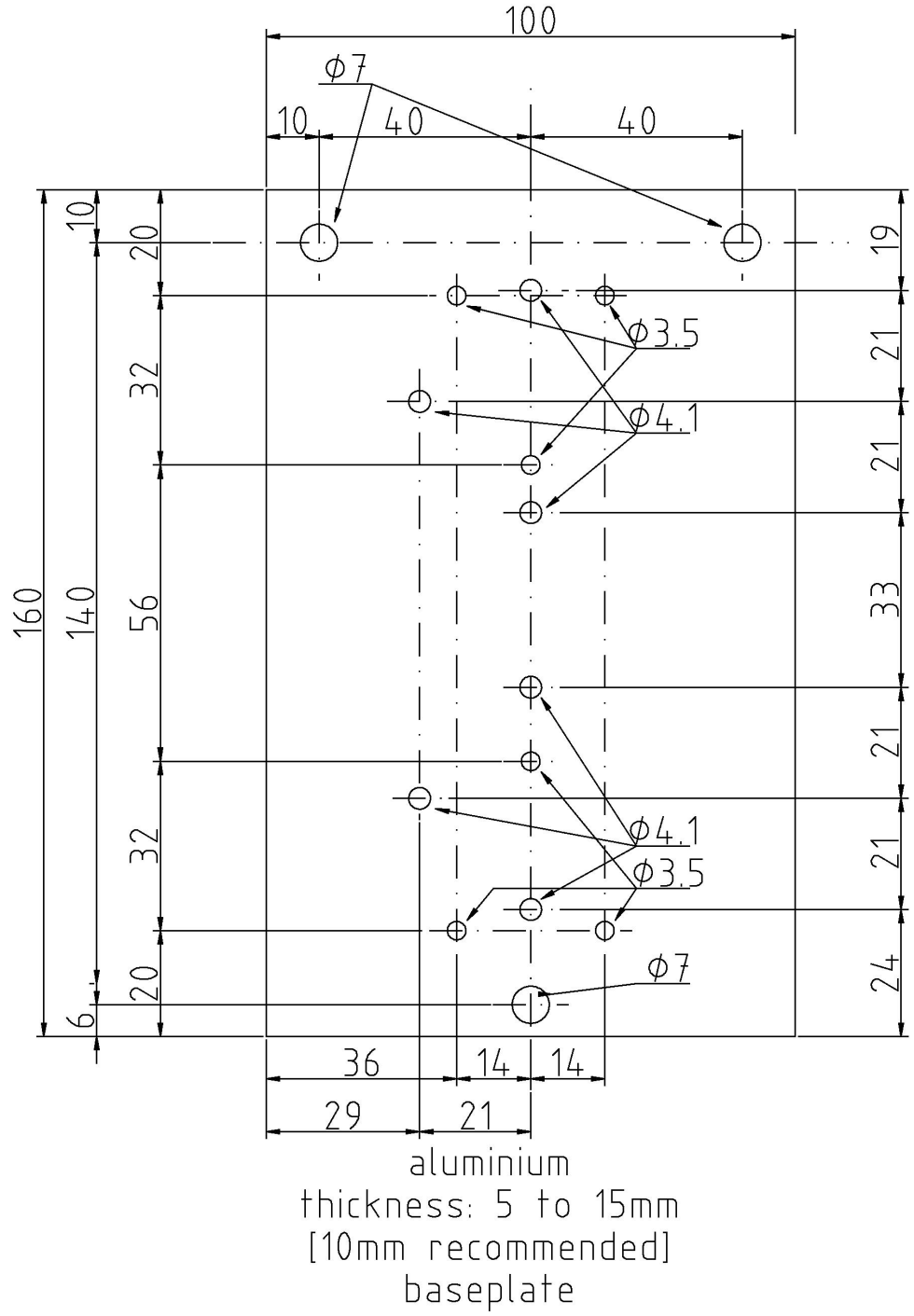

Figure B.4: Baseplate for the pickup chamber, prepared for carrying two different pickup sources, [CD:\Drawings\HT_Source\Baseplate.dxf]

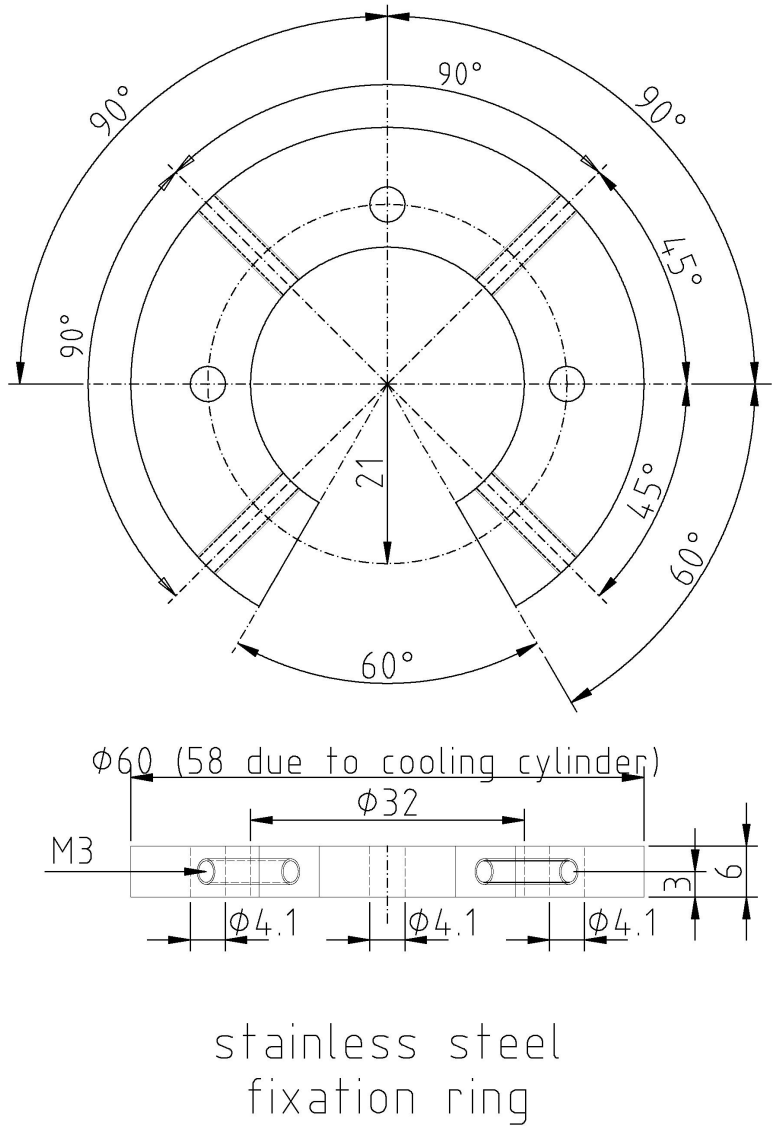

Figure B.5: Fixation ring for the HT source, [CD:\Drawings\HT_Source\Fixation_Ring.dxf]; Layers used: cooling fixation lower SIDETOPdimensioning

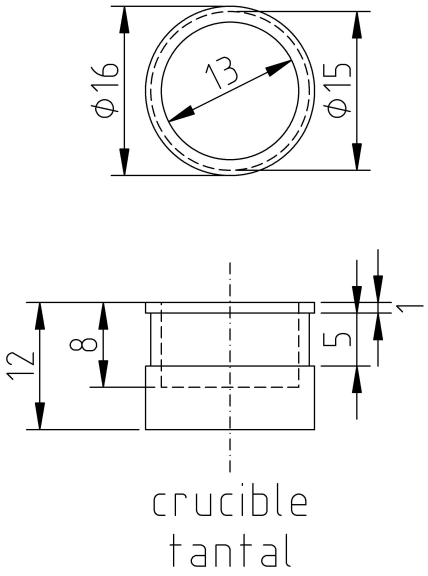

Figure B.6: Tantalum crucible to enclose chromium inside, [CD:\Drawings\HT_Source\Ta_Crucible.dxf]

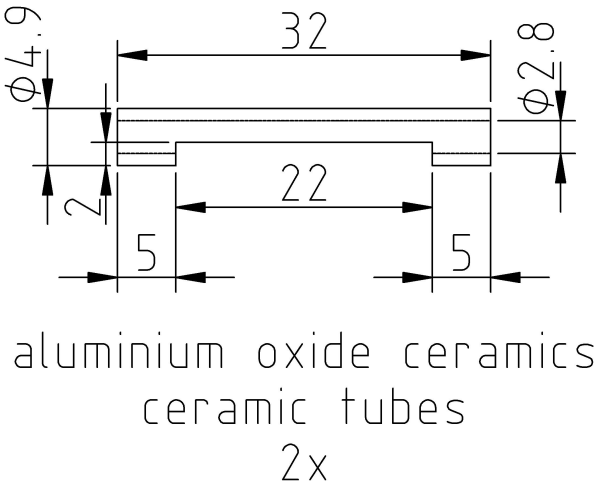

Figure B.7: Ceramic tubes to position the Ta crucible, [CD:\Drawings\HT_Source\Ceramics.dxf]; Layers used: HT fixation tubers ceramics TOPdimensioning

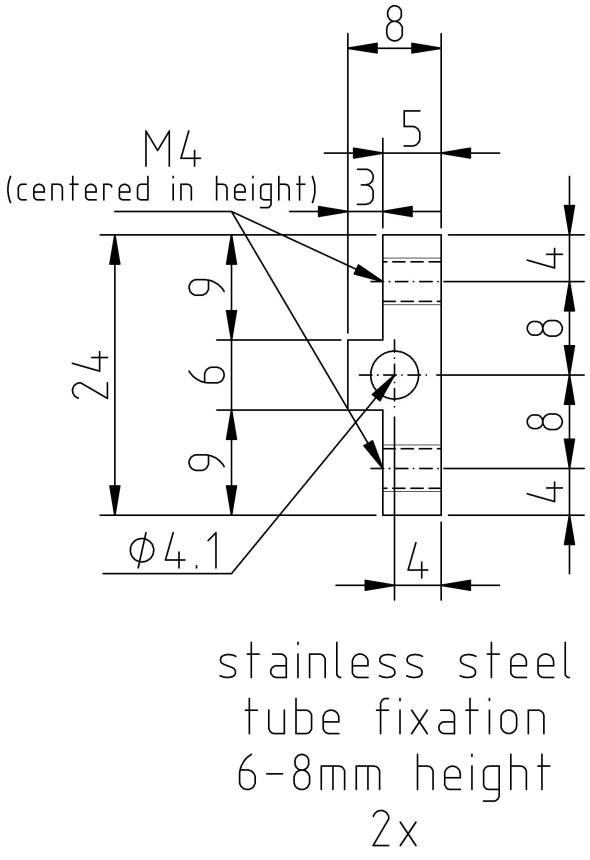

Figure B.8: Tube fixation to position the ceramic tubes, [CD:\Drawings\HT_Source\Tube_Fixation.dxf]; Layers used: HT fixation tubes stainless steel TOPdimensioning

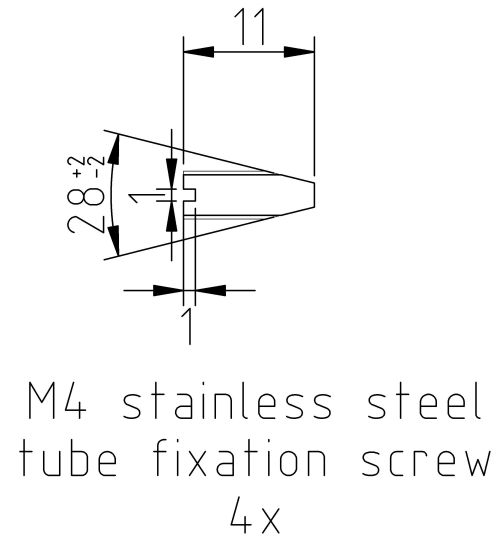

Figure B.9: Screws to align the ceramic tubes which hold the Ta crucible, [CD:\Drawings\HT_Source\Tube_Fixation_Screw.dxf]; Layers used: HT fixation tubes screw TOPdimensioning

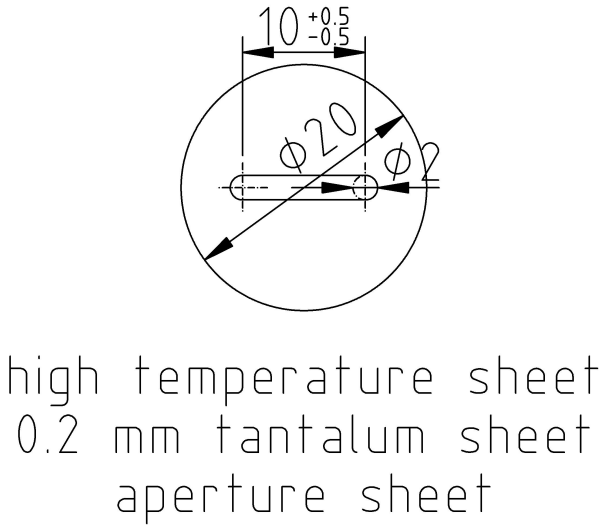

Figure B.10: Aperture sheet to seal the crucible and produce an effusive atomic beam through a slit, [CD:\Drawings\HT_Source\Aperture_Sheet.dxf]; Layers used: slit 1 TOPdimensioning

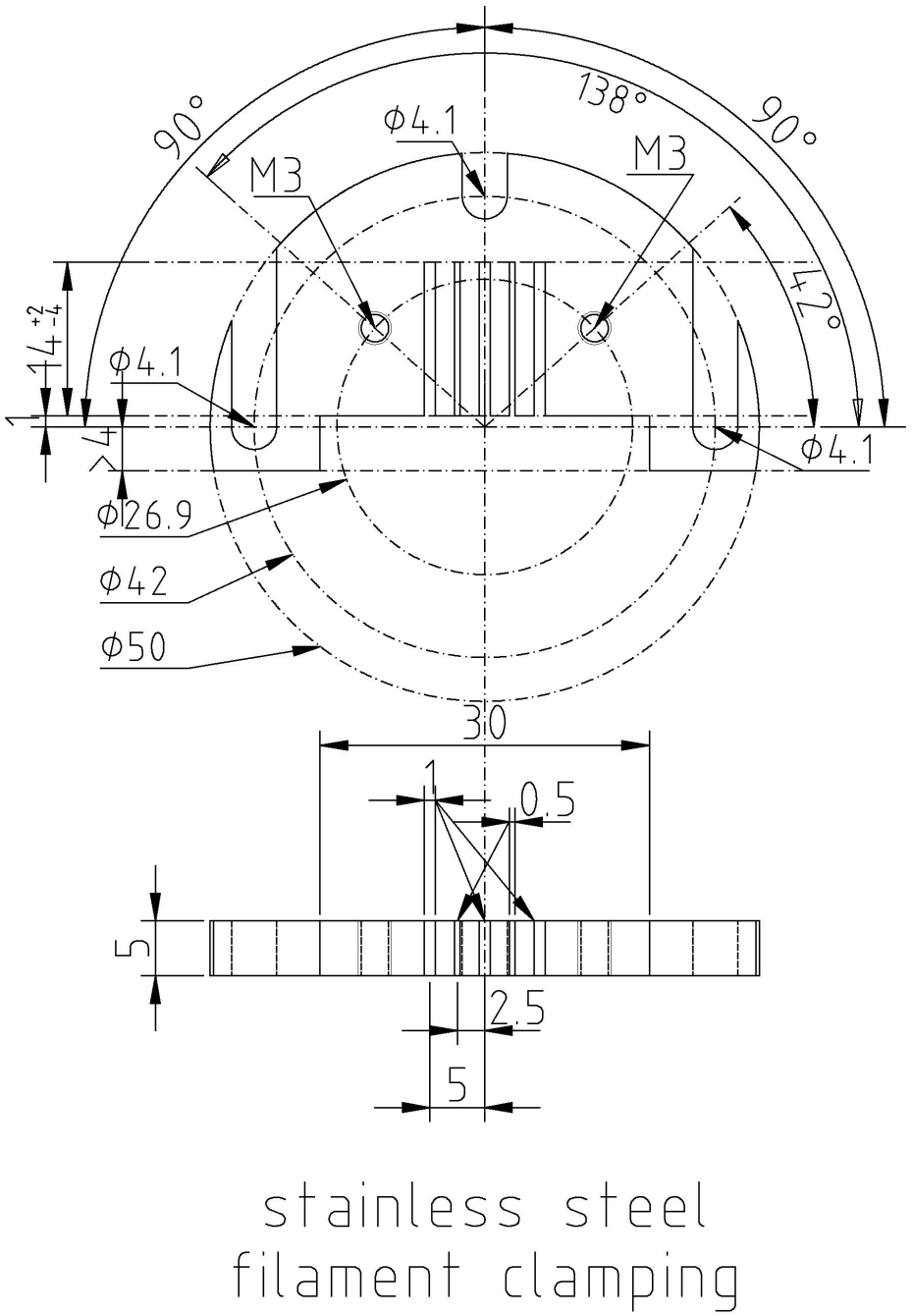

Figure B.11: Filament clamping, ground connector of the filaments, [CD:\Drawings\HT_Source\Filament_Clamping.dxf]; Layers used: filament fixation ground TOPSIDEdimensioning

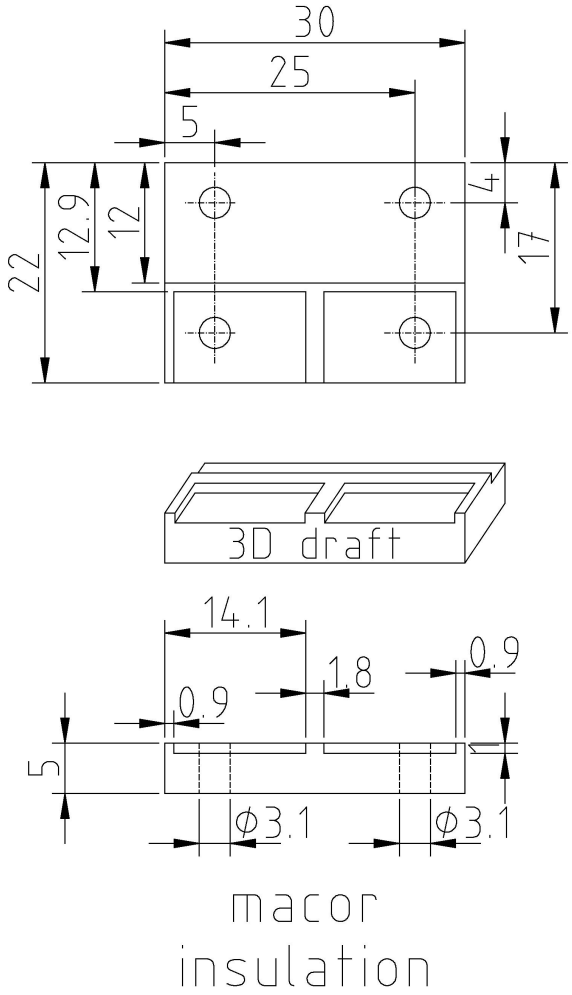

Figure B.12: Filament insulation, used to separate the contacts of the filaments, [CD:\Drawings\HT_Source\Filament_Insulation.dxf]; Layers used: filament fixation insulation TOPSIDEDIAGONALdimensioning

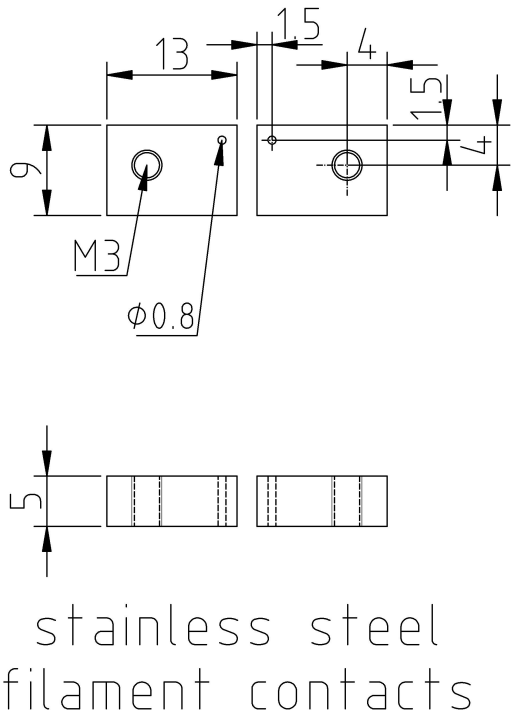

Figure B.13: Filament contacts, second contact to the filaments, the pins fitting into the 0.8 mm holes should be bend slightly for a better contact, [CD:\Drawings\HT_Source\Filament_Contacts.dxf]; Layers used: filament fixation hot TOPSIDEdimensioning

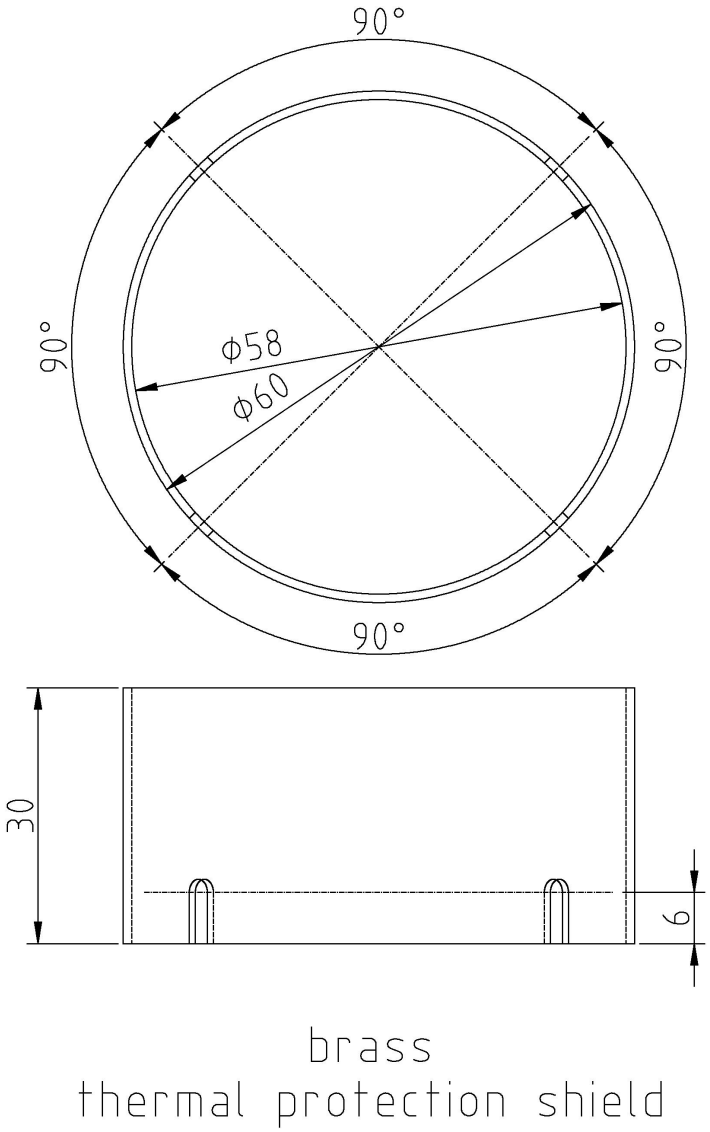

Figure B.14: Thermal protection shield, copper tubes (4 mm outer and 3.75 mm inner diameter) are wound around four to five times and are soldered (better hard soldered) to the cylinder for water cooling, [CD:\Drawings\HT_Source\Thermal_Protection_Shield.dxf]; Layers used: cooling cylinder TOPSIDEdimensioning

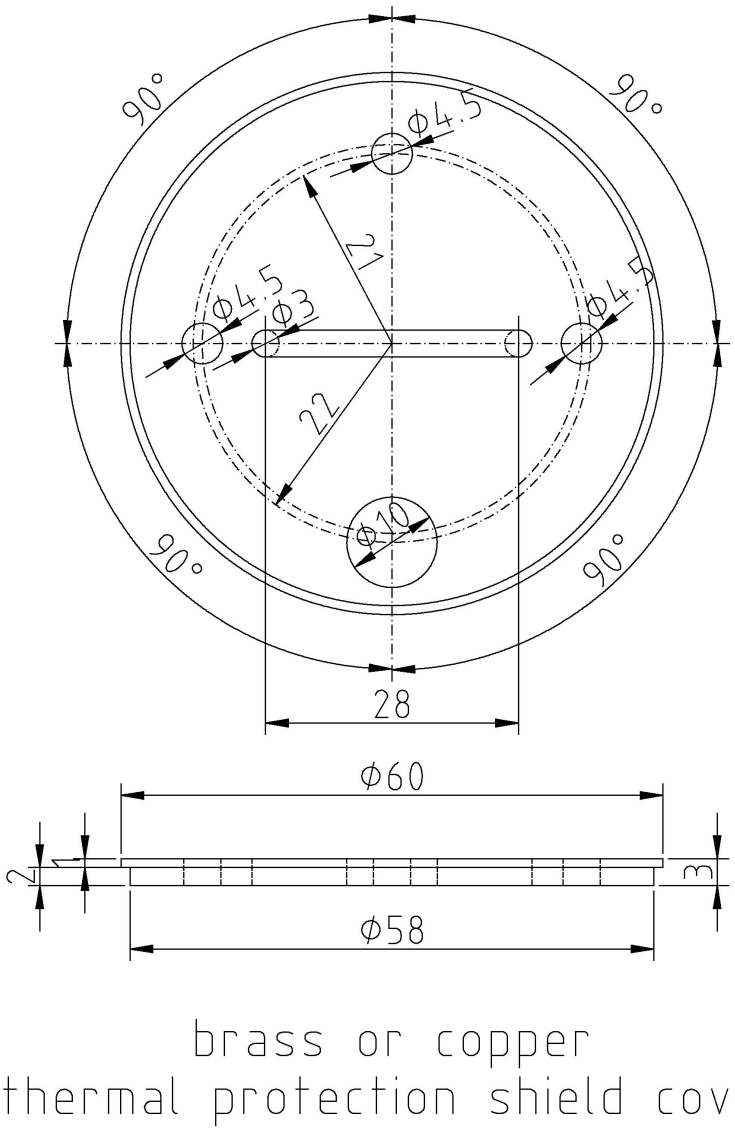

Figure B.15: Thermal protection shield cover: It is inserted with the smaller diameter into the thermal protection shield and then hard soldered to it. It must be aligned in a way that the slits of the thermal protection shield and the holes for the fixation on the M4 rods fit together. [CD:\Drawings\HT_Source\Thermal_Protection_Shield.dxf]; Layers used: cooling upper TOPSIDEdimensioning

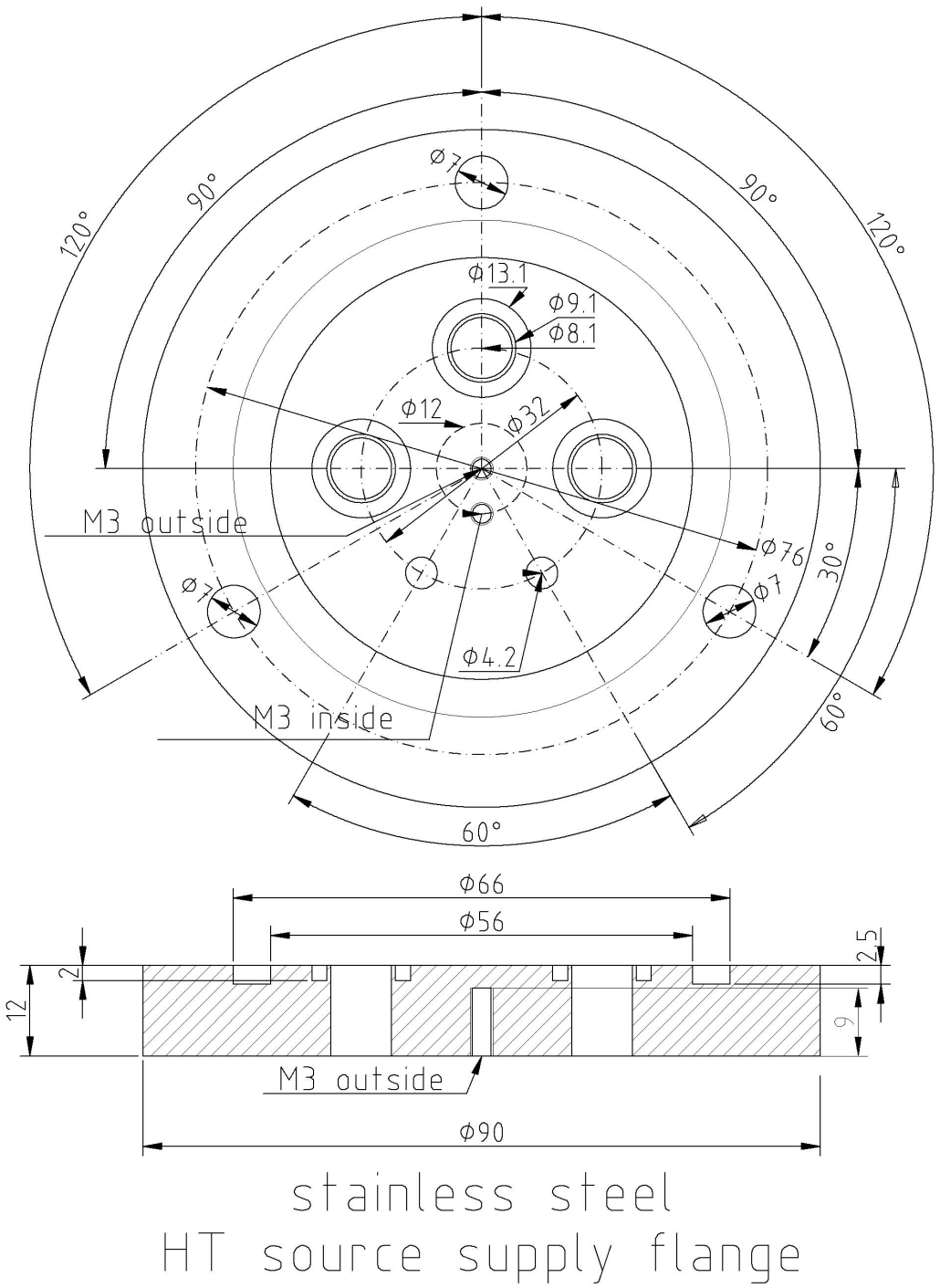

Figure B.16: Flange with feedthroughs: Three electrical feedthroughs (8.1 mm holes), one ground contact (M3 screws inside and outside), and two water feedthroughs (4.2 mm) are required. [CD:\Drawings\HT_Source\Thermal_Protection_Shield.dxf]; Layers used: cooling upper TOPSIDEdimensioning

B.3 Prototype

QCad and AutoCAD drawings can be found on the enclosed CD [CD:\Drawings\Prototype\].

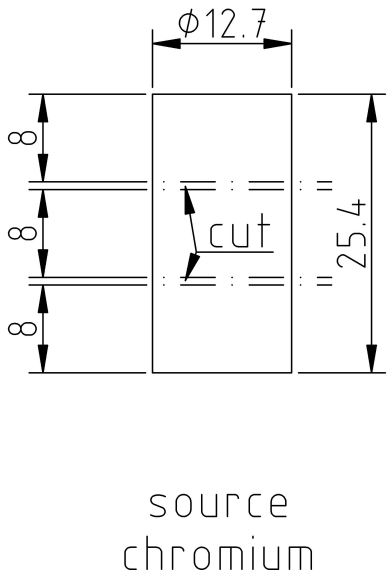

Figure B.17: Chromium cylinder, [CD:\Drawings\Prototype\Cr_cylinder.dxf]

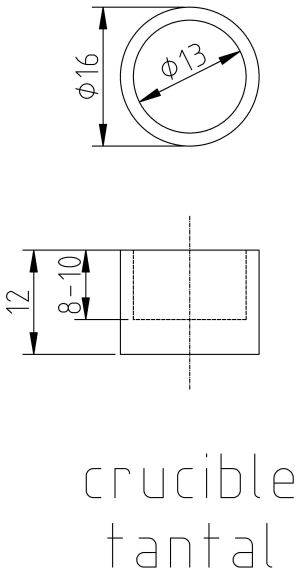

Figure B.18: Tantalum crucible for chromium, [CD:\Drawings\Prototype\Crucible.dxf]

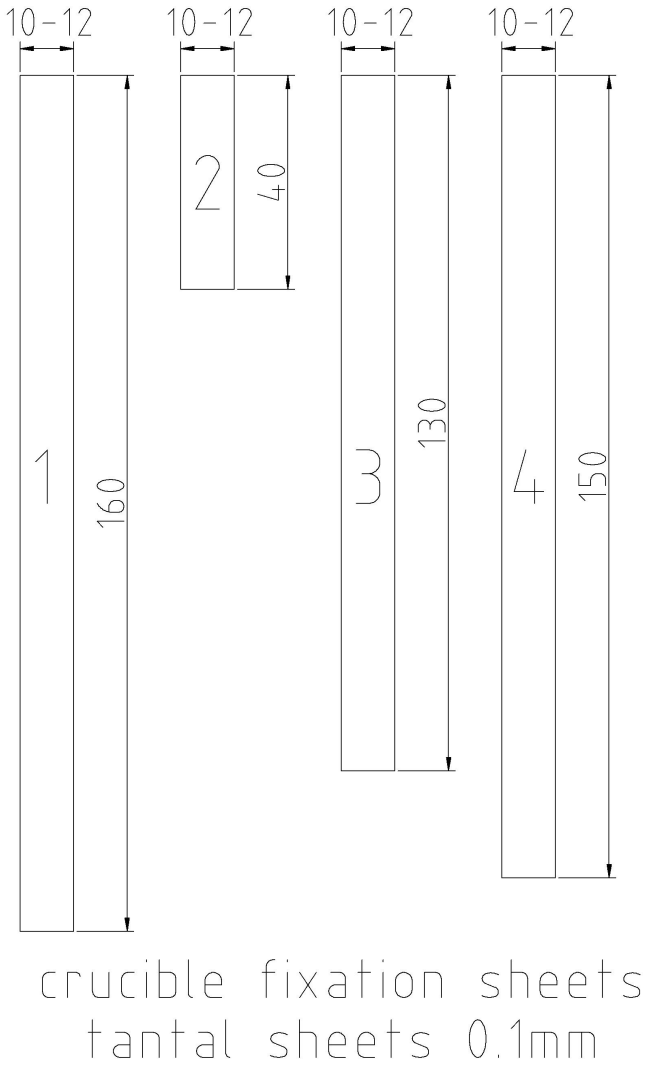

Figure B.19: Dimension of the sheets for the crucible fixation, [CD:\Drawings\Prototype\Crucible_fixation_sheets.dxf]

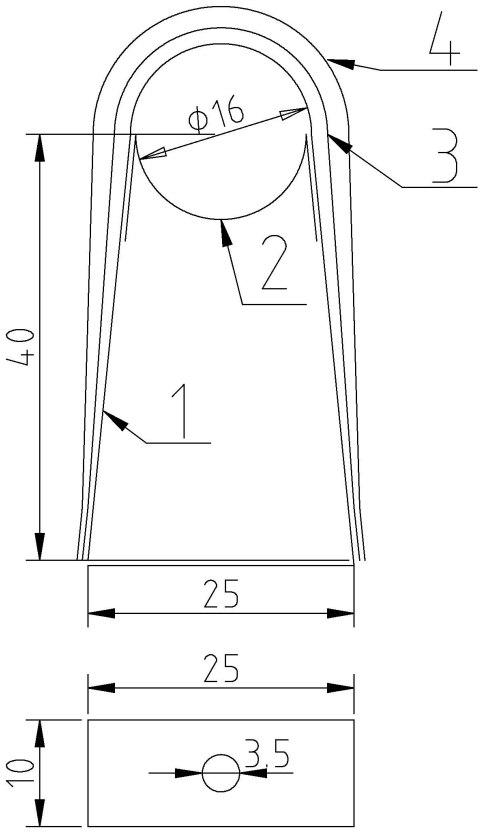

crucible fixation
tantal sheets

Figure B.20: Arranging the sheets for the crucible fixation, [CD:\Drawings\Prototype\Crucible_fixation.dxf]

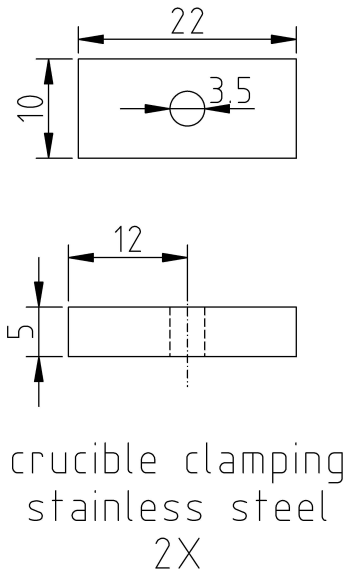

Figure B.21: Pieces to clamp the crucible fixation to the threaded rod, [CD:\Drawings\Prototype\Crucible_clamping.dxf]

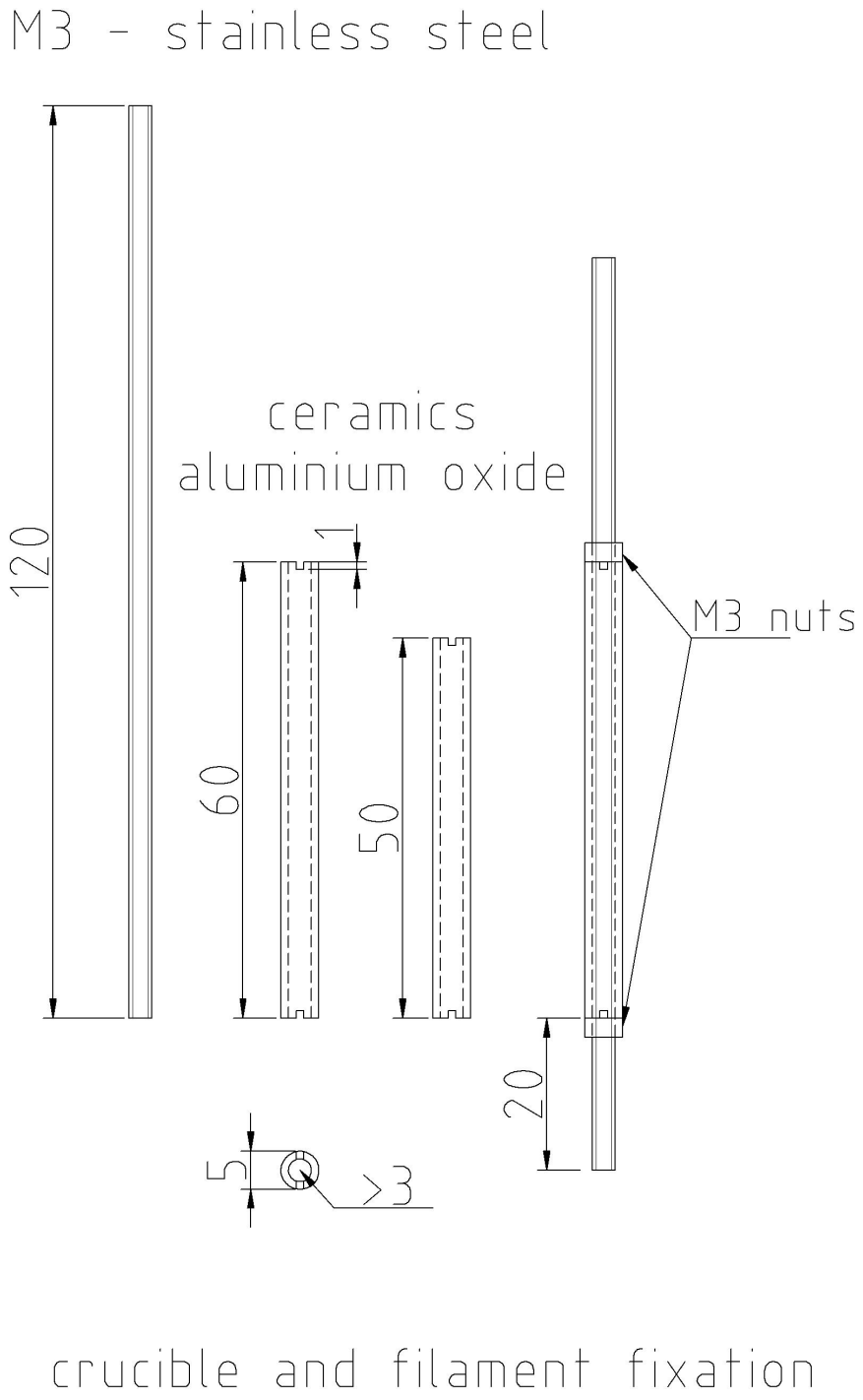

Figure B.22: Threaded rods and insulation ceramics for the mounting of the crucible and filament fixation, [CD:\Drawings\Prototype\Crucible_and_filament_fixation.dxf]

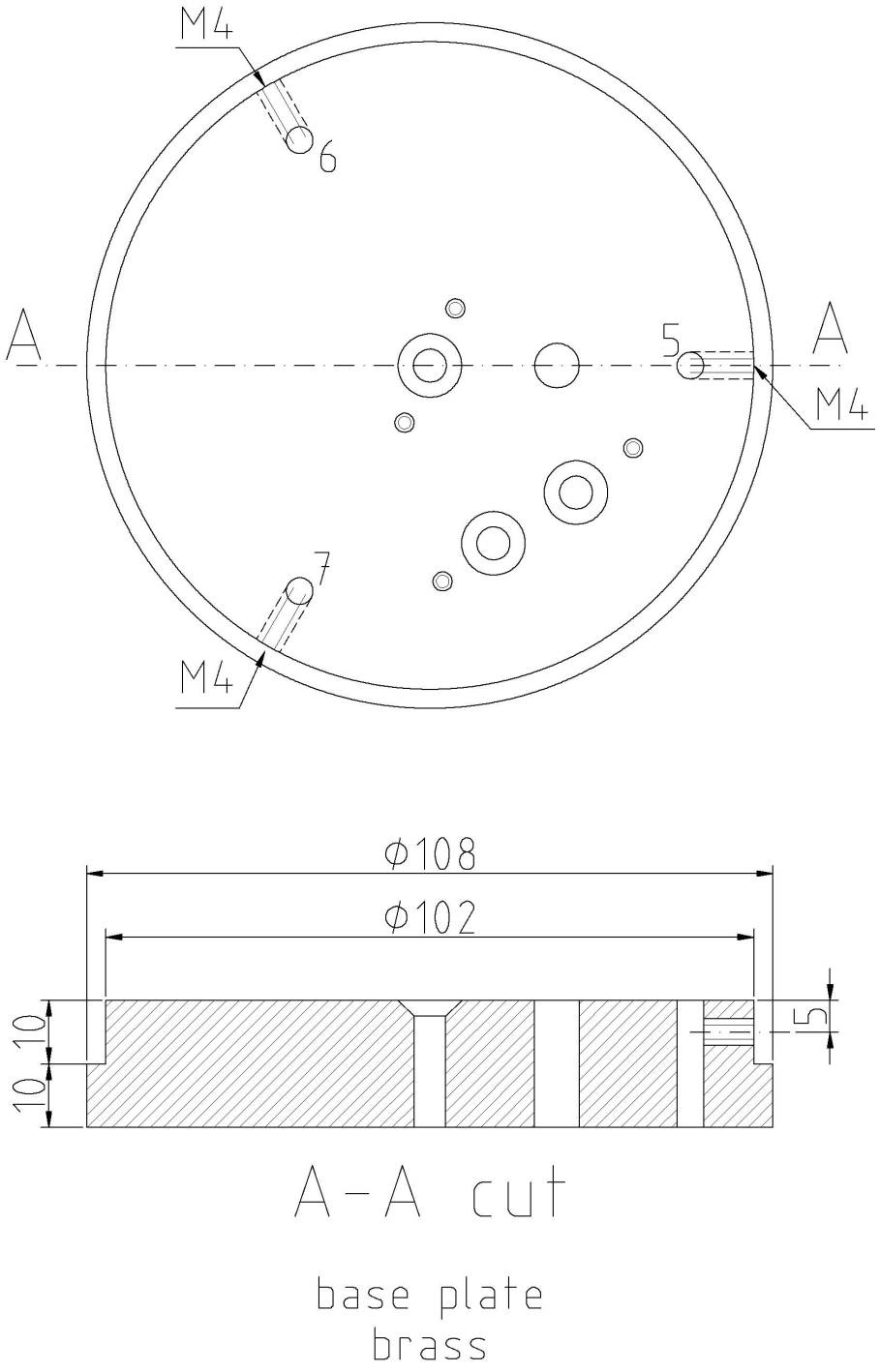

Figure B.23: Dimensions of the base plate, [CD:\Drawings\Prototype\base_plate_dimension.dxf]

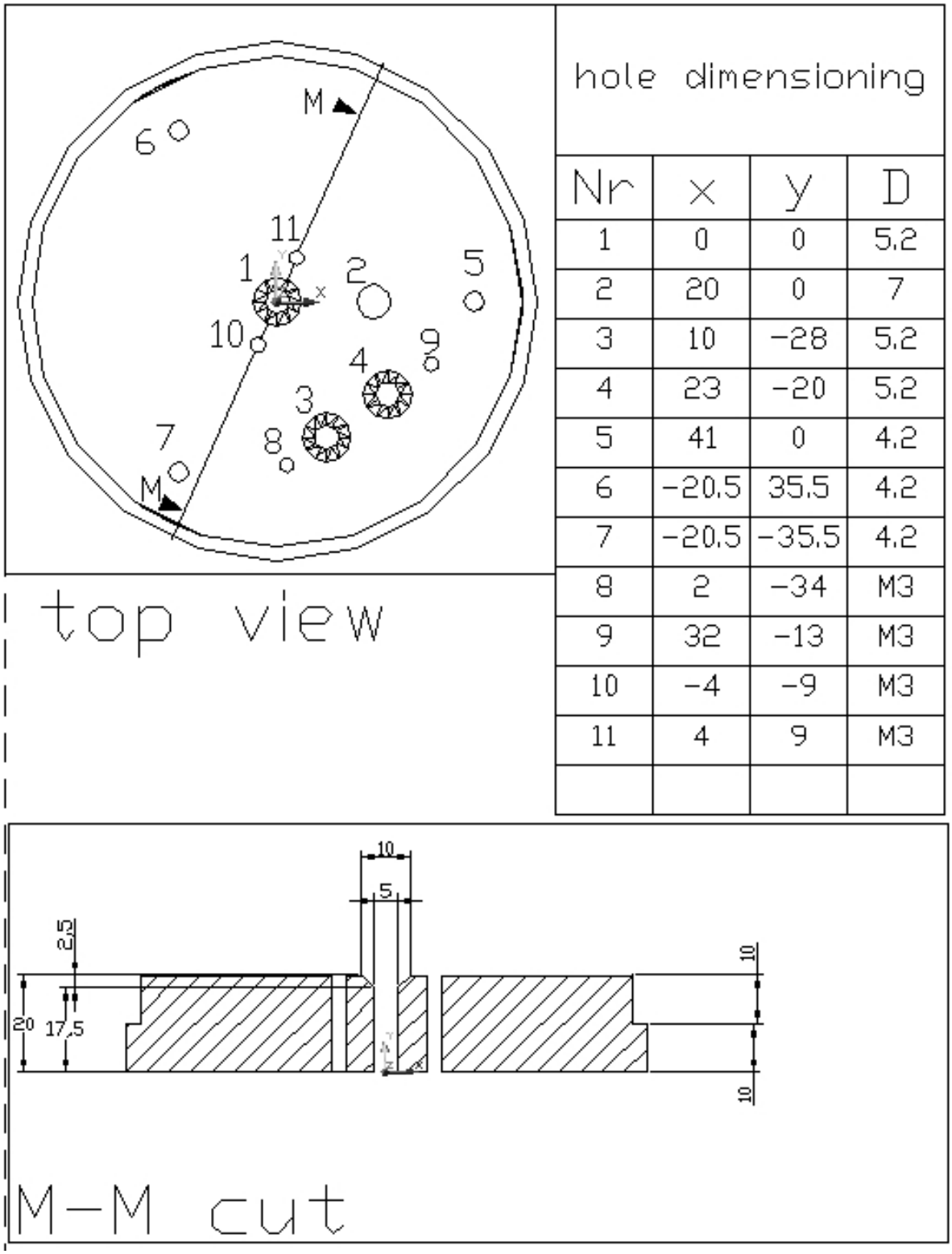

hole dimensioning

Nr	x	y	D
1	0	0	5,2
2	20	0	7
3	10	−28	5,2
4	23	−20	5,2
5	41	0	4,2
6	−20,5	35,5	4,2
7	−20,5	−35,5	4,2
8	2	−34	M3
9	32	−13	M3
10	−4	−9	M3
11	4	9	M3

Figure B.24: Positions and dimensions of holes in the base plate, [CD:\Drawings\Prototype\bottom_180109.dwg]

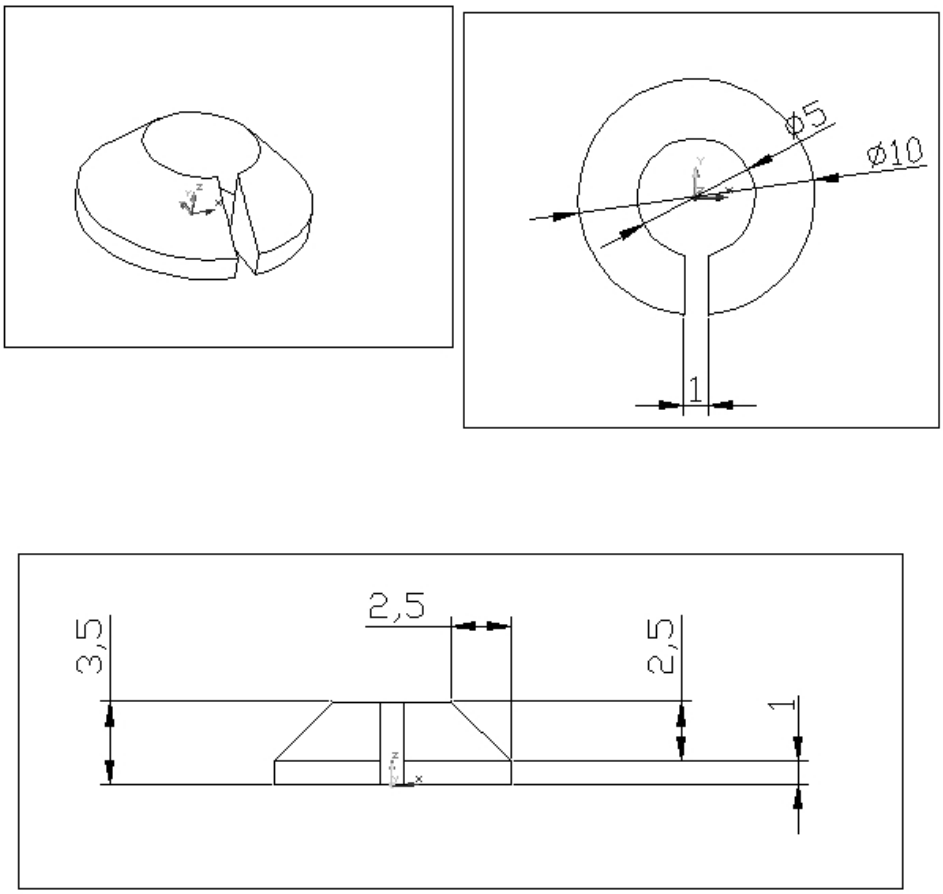

Figure B.25: Plate for fixation the filament fixation on the base plate, [CD:\Drawings\Prototype\bottom_180109.dwg]

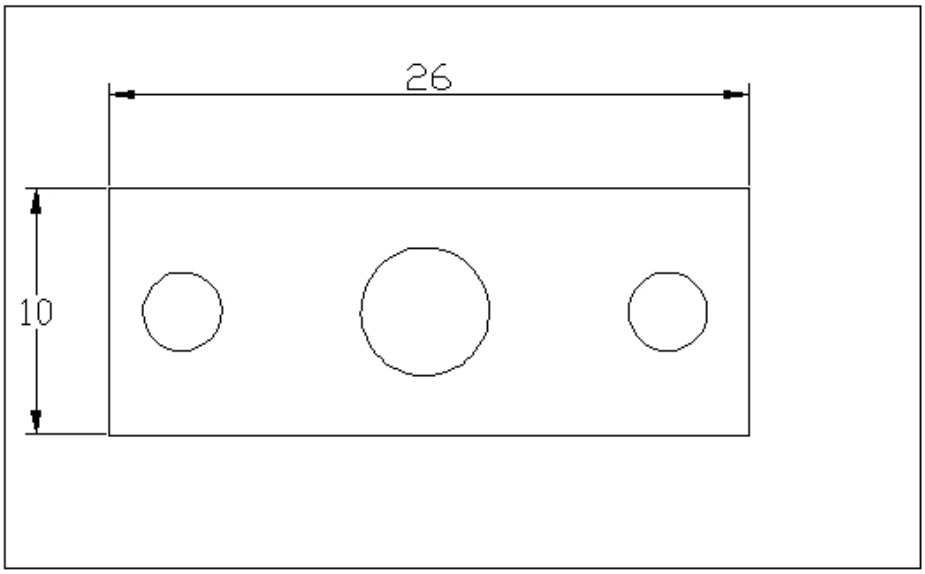

hole dimensions

Nr	X	Y	D
1	3	5	3.2
2	12.8	5	5.2
3	22.7	5	3.2

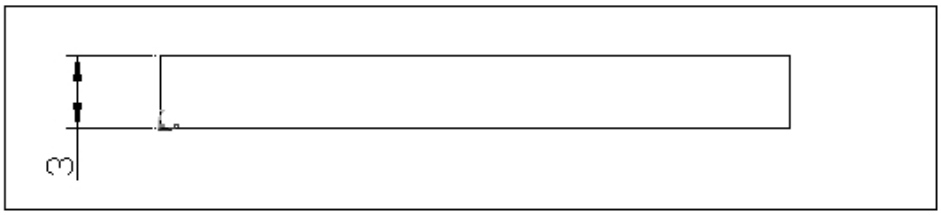

Figure B.26: Plate for fixation the crucible fixation on the base plate, [CD:\Drawings\Prototype\bottom_180109.dwg]

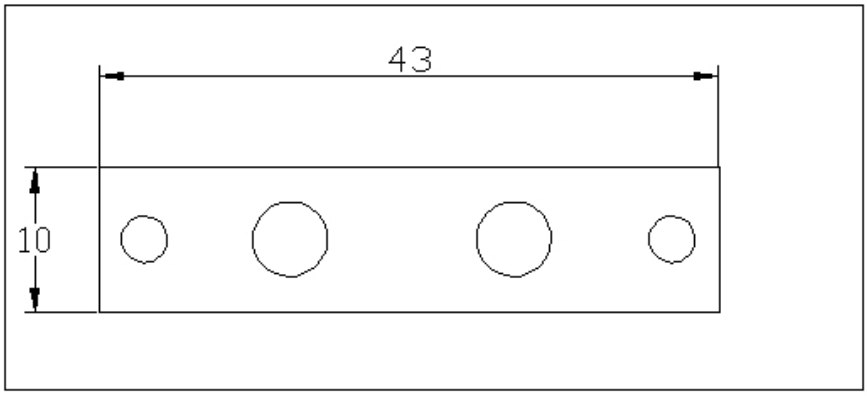

hole dimensions

Nr	X	Y	D
1	3.1	5	3.2
2	13.2	5	5.2
3	28.7	5	5.2
4	40	5	3.2

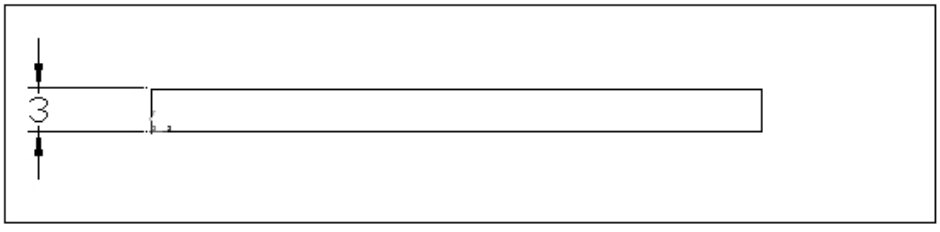

Figure B.27: Plate for fixation the filament fixation on the base plate, [CD:\Drawings\Prototype\bottom_180109.dwg]

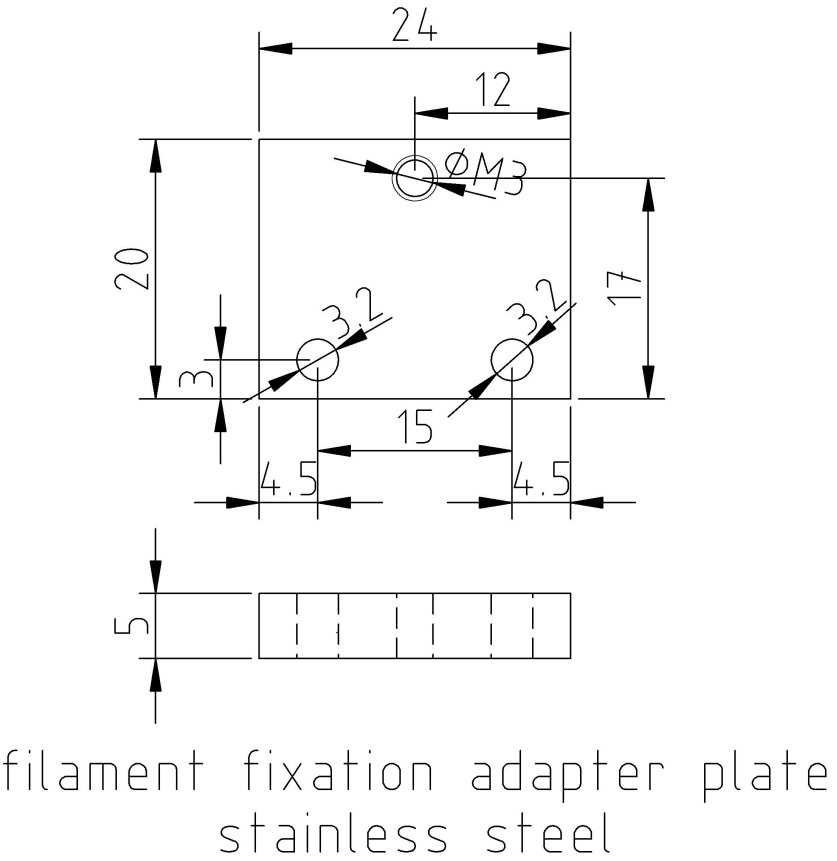

Figure B.28: Fixation plate to mount the filament fixation ring on, [CD:\Drawings\Prototype\Filament_fixation_adapter_plate.dxf]

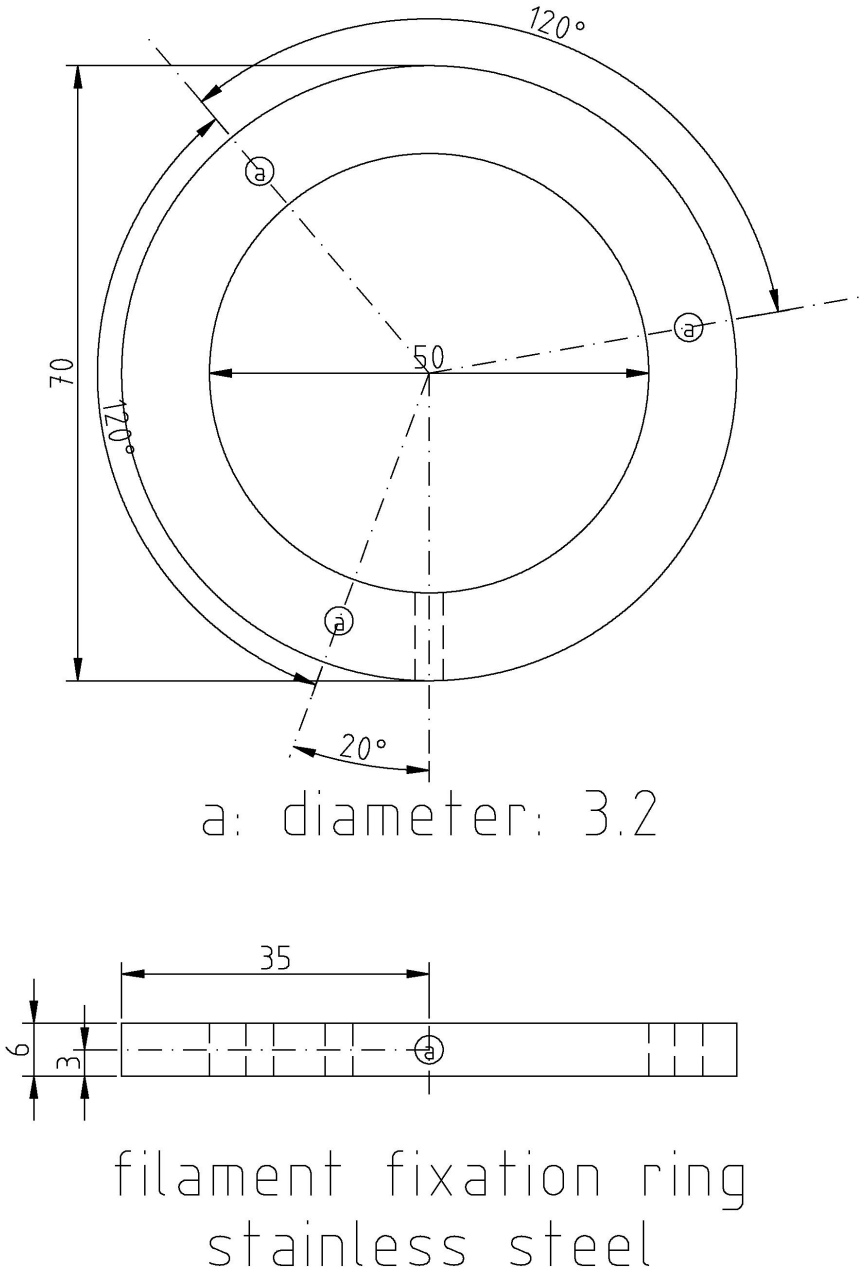

Figure B.29: Fixation ring to mount the filament fixation clamping on, [CD:\Drawings\Prototype\Filament_fixation_ring.dxf]

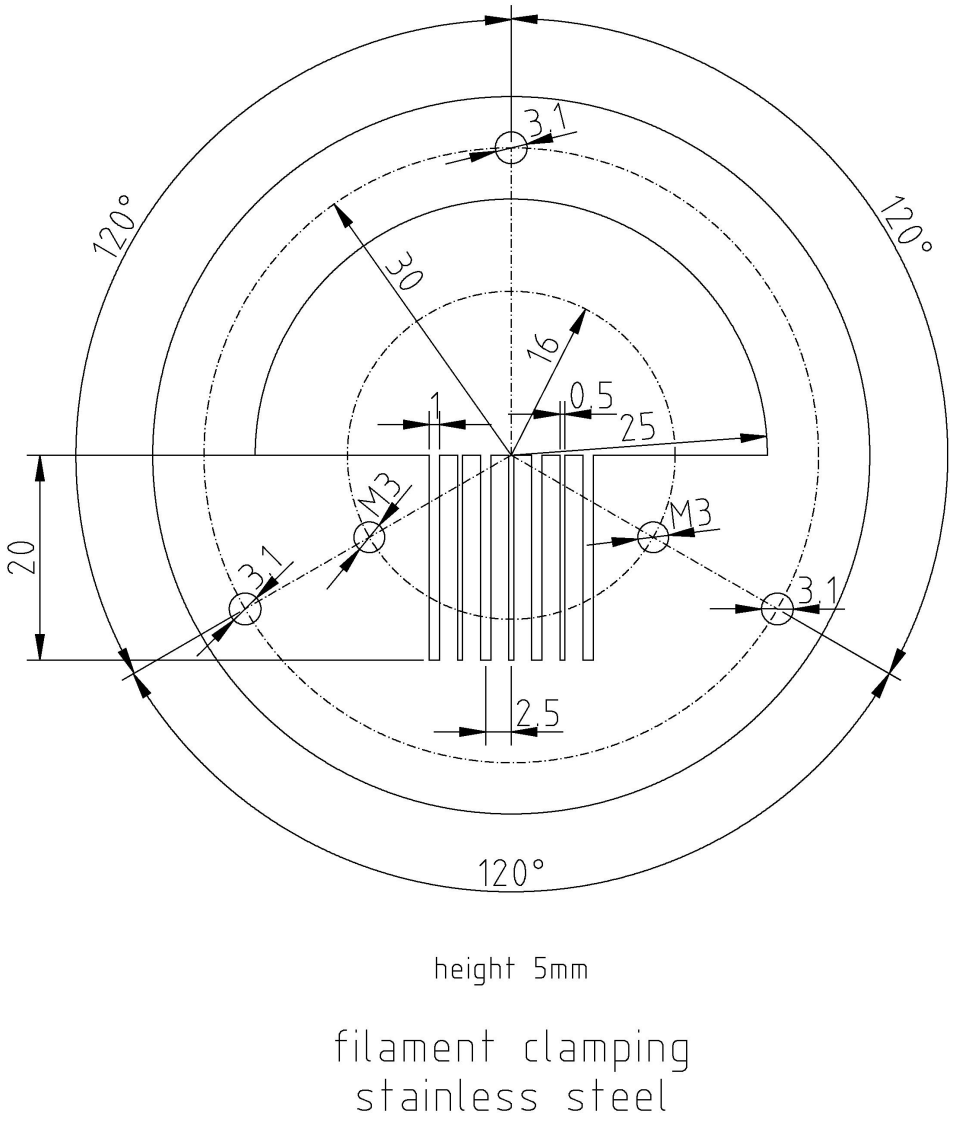

Figure B.30: Filament clamping for placing and securing the filaments (ground), [CD:\Drawings\Prototype\Filament_clamping.dxf]

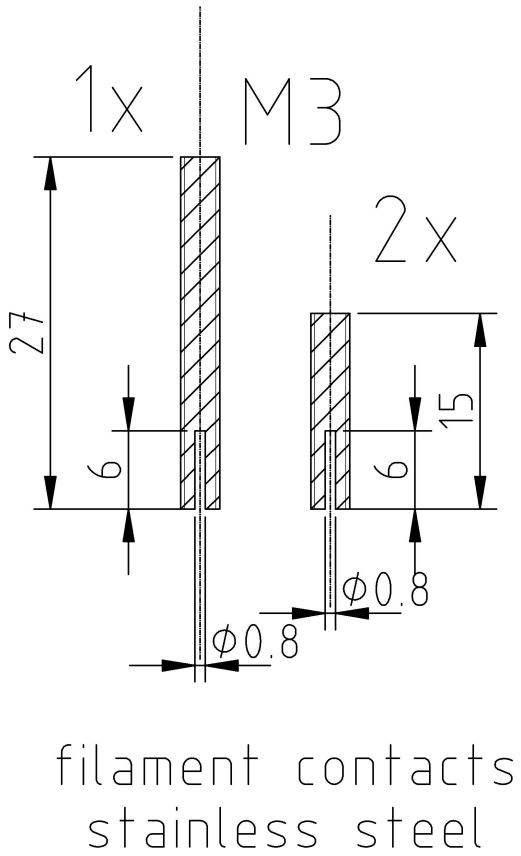

Figure B.31: Filament contacts (hot end), [CD:\Drawings\Prototype\Filament_contacts.dxf]

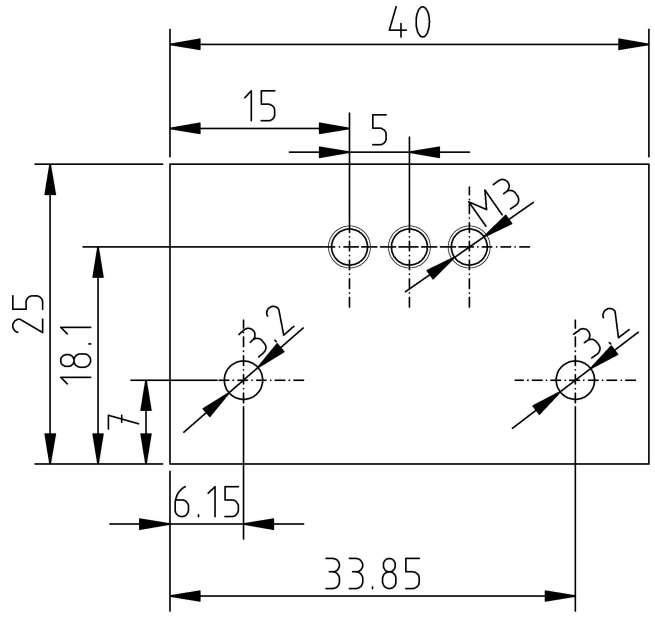

height 5mm

filament contact fixation 1
Macor

Figure B.32: Filament contact fixation 1, [CD:\Drawings\Prototype\Filament_contact_fixation1.dxf]

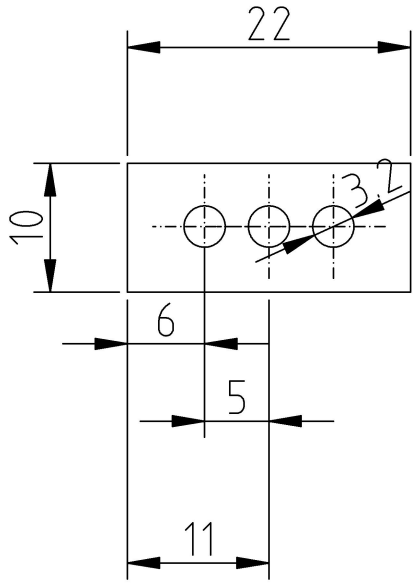

Figure B.33: Filament contact fixation 2, [CD:\Drawings\Prototype\Filament_contact_fixation2.dxf]

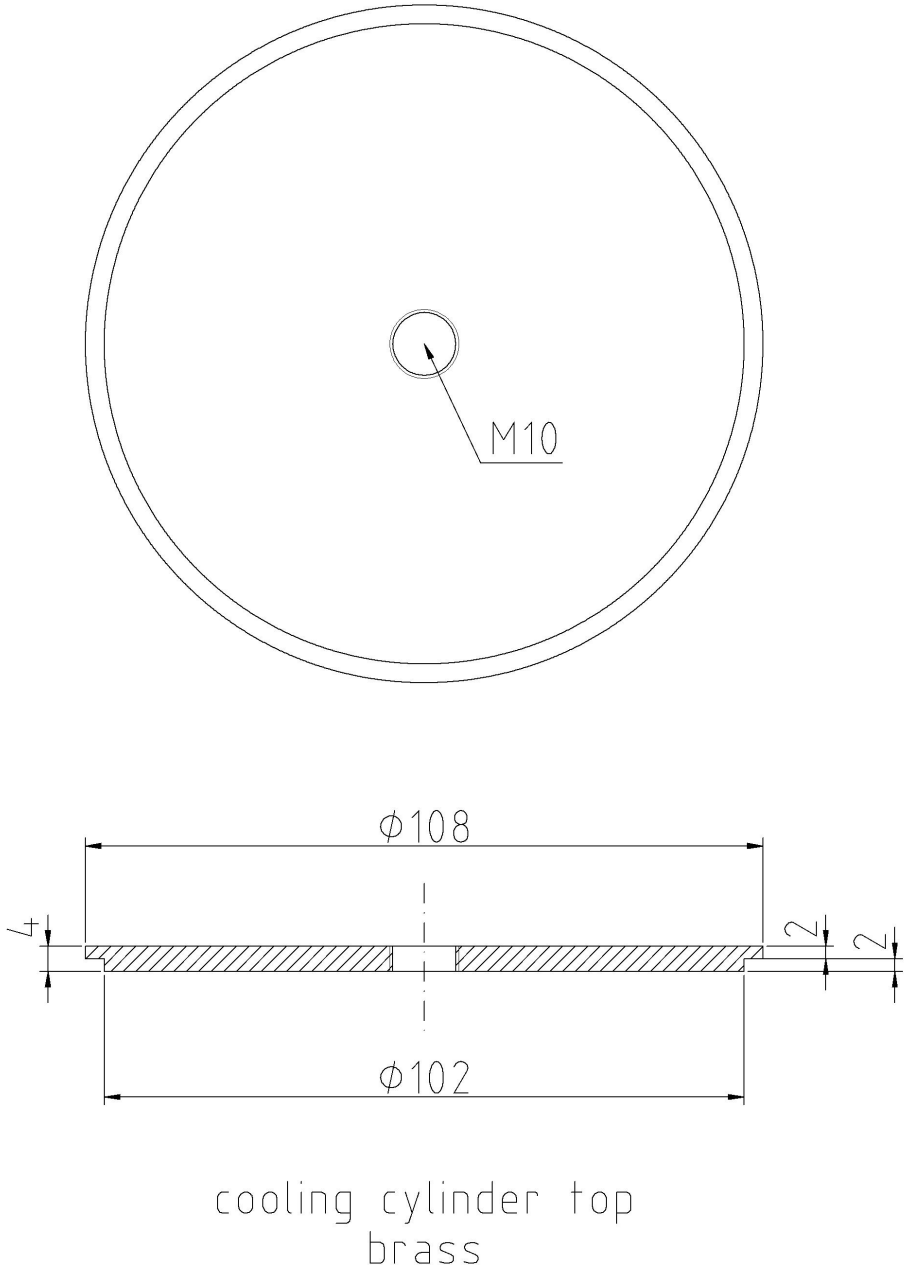

Figure B.34: Cooling cylinder top will be hard - soldered to the cooling cylinder B.35, [CD:\Drawings\Prototype\Cooling_cylinder_top.dxf]

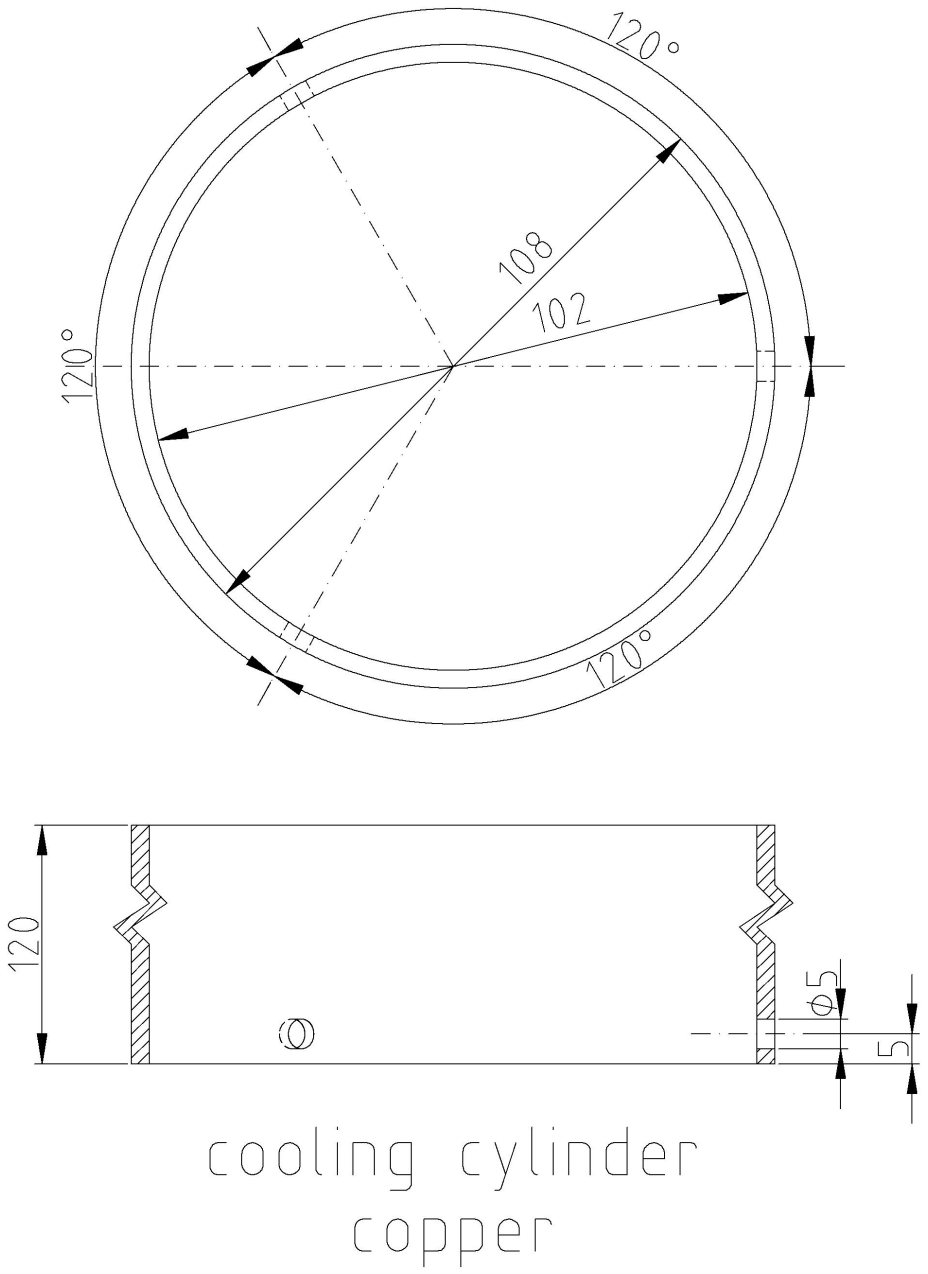

Figure B.35: Cooling cylinder, [CD:\Drawings\Prototype\Cooling_cylinder.dxf]

Bibliography

[1] F. Ancilotto, E. Cheng, M. W. Cole, and F. Toigo. The binding of alkali atoms to the surfaces of liquid-helium and hydrogen. *Zeitschrift für Physik B–Condensed Matter*, 98 (3):323–329, Sept. 1995. 11

[2] F. Ancilotto, G. DeToffol, and F. Toigo. Sodium dimers on the surface of liquid ^{4}He. *Physical Review B*, 52(22):16125–, Dec. 1995. 11

[3] H. Aoki, Y. Asada, T. Hatano, K. Nakamura, K. Ogawa, and Y. Makino. Superconductivity in amorphous Cr films. *Solid State Communications*, 60(9):735–737, Dec. 1986. ISSN 0038-1098. 4

[4] A. Bartelt, J. D. Close, F. Federmann, N. Quaas, and J. P. Toennies. Cold metal clusters: Helium droplets as a Nanoscale cryostat. *Physical Review Letters*, 77(17):3525–, Oct. 1996. 4, 11

[5] E. W. Becker, R. Klingelhofer, and P. Lohse. Strahlen aus Kondensiertem Helium im Hochvakuum. *Zeitschrift für Naturforschung Part A–Astrophysik Physik und Physikalische Chemie*, 16(11):1259, 1961. 6

[6] L. Bergmann, C. Schaefer, T. Dorfmüller, W. T. Hering, and K. Stierstadt. *Lehrbuch der Experimentalphysik, Band 1, Mechanik, Relativität, Wärme.* de Gruyter, 1998. ISBN 3110128705. 1370 pp. 58

[7] L. Bergmann, C. Schaefer, and W. Raith. *Lehrbuch der Experimentalphysik, Band 2, Elektro-Magnetismus.* de Gruyter, 1998. 12

[8] A. Boatwright, J. Jeffs, and A. J. Stace. Ion—molecule reactions and fragmentation patterns in helium nanodroplets. *The Journal of Physical Chemistry A*, 111(31): 7481–7488, Aug. 2007. ISSN 1089-5639. 38

[9] H. Buchenau, E. L. Knuth, J. Northby, J. P. Toennies, and C. Winkler. Mass spectra and time-of-flight distributions of helium cluster beams. *Journal of Chemical Physics*, 92(11): 6875–6889, June 1990. 6, 7, 8

[10] H. Buchenau, J. P. Toennies, and J. A. Northby. Excitation and ionization of ^{4}He clusters by electrons. *Journal of Chemical Physics*, 95(11):8134–8148, Dec. 1991. 7, 9, 47

[11] C. Callegari and W. E. Ernst. Helium droplets as nanocryostats for molecular spectroscopy—from the vacuum ultraviolet to the microwave regime. In F. Merkt and M. Quack, editors, *Handbook of High Resolution Spectroscopy.* Wiley, 2010. 6

[12] P. Claas, S.-O. Mende, and F. Stienkemeier. Characterization of laser ablation as a means for doping helium nanodroplets. *Review of Scientific Instruments*, 74(9):4071–4076, Sept. 2003. 13

[13] H. Frey and R. Haefer. *Tieftemperaturtechnologie*. VDI, 1981. ISBN 3185005038. 57

[14] R. Frochtenicht, M. Kaloudis, M. Koch, and F. Huisken. Vibrational spectroscopy of small water complexes embedded in large liquid helium clusters. *J. Chem. Phys.*, 105 (15):6128–6140, Oct. 1996. 37, 52

[15] G. Gröber, Erk. *Die Grundgesetze der Wärmeübertragung*. Springer-Verlag, 1988. 57

[16] A. Gutberlet, G. Schwaab, O. Birer, M. Masia, A. Kaczmarek, H. Forbert, M. Havenith, and D. Marx. Aggregation-induced dissociation of $HCl(H_2O)_4$ below 1 K: The smallest droplet of acid. *Science*, 324(5934):1545–1548, June 2009. 11

[17] J. Harms, M. Hartmann, J. P. Toennies, A. F. Vilesov, and B. Sartakov. Rotational structure of the IR spectra of single SF_6 molecules in liquid He-3 and He-3 droplets. *Journal of Molecular Spectroscopy*, 185(1):204–206, Sept. 1997. 7

[18] J. Harms, J. P. Toennies, and F. Dalfovo. Density of superfluid helium droplets. *Physical Review B*, 58(6):3341–3350, Aug. 1998. 7, 8, 10, 25

[19] M. Hartmann, R. E. Miller, J. P. Toennies, and A. Vilesov. Rotationally resolved spectroscopy of SF_6 in liquid helium clusters: A molecular probe of cluster temperature. *Physical Review Letters*, 75(8):1566–, Aug. 1995. 7

[20] S. Jaksch, F. F. da Silva, S. Denifl, O. Echt, T. D. Mark, and P. Scheier. Experimental evidence for the existence of an electronically excited state of the proposed dihydrogen radical cation He-H-H-He. *Chemistry-a European Journal*, 15(16):4190–4194, 2009. 40

[21] S. Jaksch, A. Mauracher, A. Bacher, S. Denifl, F. F. da Silva, H. Schobel, O. Echt, T. D. Mark, M. Probst, D. K. Bohme, and P. Scheier. Formation of even-numbered hydrogen cluster cations in ultracold helium droplets. *Journal of Chemical Physics*, 129(22):224306, Dec. 2008. 40

[22] T. Jones, J. Sawler, and D. Venus. Simple, calibrated deposition monitor incorporated into an electron beam evaporator. *Rev. Sci. Instrum.*, 64(7):2008–2012, July 1993. 13

[23] B. T. Jonker. A compact flange-mounted electron beam source. *J. Vac. Sci. Technol. A*, 8(5):3883–3886, Sept. 1990. 13

[24] P. H. Kasai and D. Mcleod. ESR studies of Cu, Ag, and Au atoms isolated in rare-gas matrices. *Journal of Chemical Physics*, 55(4):1566–&, 1971. 4

[25] E. L. Knuth and U. Henne. Average size and size distribution of large droplets produced in a free-jet expansion of a liquid. *Journal of Chemical Physics*, 110(5):2664–2668, Feb. 1999. 7

[26] E. L. Knuth, B. Schilling, and J. P. Toennies. *On Scaling Parameters for Predicting Cluster Sizes in Free Jets*, volume 1 of *Rarefied Gas Dynamics*. Oxford University Press, Oxford, 1995. 270 pp. 7

[27] M. Koch. *Magnetic Resonance Spectroscopy of Single Alkali-Metal Atoms Isolated in Superfluid Helium Nanodroplets.* PhD thesis, Graz University of Technology, 11 2009. 1, 7, 8, 9, 15, 17, 25, 56, 68

[28] M. Koch, G. Auböck, C. Callegari, and W. E. Ernst. Coherent spin manipulation and ESR on superfluid helium nanodroplets. *Physical Review Letters*, 103(3):035302–1–4, July 2009. 1, 15

[29] M. Koch, C. Callegari, and W. E. Ernst. Alkali-metal electron spin density shift induced by a helium nanodroplet. *Molecular Physics*, 108(7-9):1005–1010, 2010. 1, 15

[30] M. Koch, J. Lanzersdorfer, C. Callegari, J. S. Muenter, and W. E. Ernst. Molecular beam magnetic resonance in doped helium nanodroplets. A setup for optically detected ESR/NMR in the presence of unresolved Zeeman splittings. *The Journal of Physical Chemistry A*, 113(47):13347–13356, Nov. 2009. ISSN 1089-5639. 1, 15

[31] J. Lanzersdorfer. Assembly and test of a helium cluster beam apparatus for magnetic field studies of atom and molecule doped helium nanodroplets. Master's thesis, Institute of Experimental Physics, Graz University of Technology, 2008. 15

[32] K. K. Lehmann. Potential of a neutral impurity in a large ^{4}He cluster. *Molecular Physics*, 97(5):645–666, Sept. 1999. 11

[33] M. Lewerenz, B. Schilling, and J. P. Toennies. A new scattering deflection method for determining and selecting the sizes of large liquid clusters of ^{4}He. *Chemical Physics Letters*, 206(1-4):381–387, Apr. 1993. ISSN 0009-2614. 7, 10

[34] M. Lewerenz, B. Schilling, and J. P. Toennies. Successive capture and coagulation of atoms and molecules to small clusters in large liquid helium clusters. *Journal of Chemical Physics*, 102(20):8191–8207, May 1995. 7, 9, 10, 11, 36, 38, 46, 51

[35] D. R. Lide, editor. *CRC Handbook of Chemistry and Physics.* CRC Press, Boca Raton, FL, 77th edition, 1996. ISBN 0849304776. 2, 3, 4, 20, 24, 52, 56

[36] E. Lugovoj, J. P. Toennies, and A. Vilesov. Manipulating and enhancing chemical reactions in helium droplets. *Journal of Chemical Physics*, 112(19):8217–8220, May 2000. 11

[37] R. D. McCarty. Thermodynamic properties of helium 4 from 2 to 1500 K at pressures to 10^8 Pa. *Journal of Physical and Chemical Reference Data*, 2(4):923–1042, 1973. 8

[38] M. Mudrich, B. Forkl, S. Müller, M. Dvorak, O. Bünermann, and F. Stienkemeier. Kilohertz laser ablation for doping helium nanodroplets. *Review of Scientific Instruments*, 78(10):103106–8, Oct. 2007. 13

[39] K. Nauta and R. E. Miller. Stark spectroscopy of polar molecules solvated in liquid helium droplets. *Physical Review Letters*, 82(22):4480–4483, May 1999. 52

[40] V. Nehasil, K. Mašek, O. Moreau, and V. Matolín. Miniature electron bombardment evaporation source: evaporation rate measurement. *Czechoslovak Journal of Physics*, 47 (3):261–268, Mar. 1997. 13

[41] NIST. Its-90 table for type r thermocouple, 5 2010. URL http://srdata.nist.gov/its90/download/type_r.tab. 20, 24

[42] H. Pauly. *Atom, Molecule and Cluster Beams I: Basic Theory, Production and Detection of Thermal Energy Beams.* Springer Series in Atomic, Molecular, Optical, and Plasma Physics. Springer, Berlin, 2000. ISBN I3540669450. 344 pp. 9, 12

[43] P. Plessis and P. Marmet. Electroionization study of acetylene and fragment ions. *International Journal of Mass Spectrometry and Ion Processes*, 70(1):23–44, May 1986. ISSN 0168-1176. 3, 42, 52

[44] A. W. Potts and W. C. Price. Photoelectron spectra and valence shell orbital structures of groups V and VI hydrides. *Proceedings of the Royal Society of London. A. Mathematical and Physical Sciences*, 326(1565):181–197, Jan. 1972. 42, 52

[45] A. Scheidemann, B. Schilling, and J. P. Toennies. Anomalies in the reactions of He^+ with SF_6 embedded in large He-4 clusters. *Journal of Physical Chemistry*, 97(10):2128–2138, Mar. 1993. 9

[46] G. Scoles. *Atomic and Molecular Beam Methods.* Oxford Univ Press, 1988. 6, 9, 12, 13

[47] C.-X. Su, D. A. Hales, and P. Armentrout. The bond energies of Cr_2 and Cr_2^+. *Chemical Physics Letters*, 201(1-4):199–204, Jan. 1993. ISSN 0009-2614. 4, 51

[48] J. P. Toennies and A. F. Vilesov. Novel low-energy vibrational-states of foreign particles in fluid ^{4}He clusters. *Chemical Physics Letters*, 235(5-6):596–603, Mar. 1995. 11

[49] J. P. Toennies and A. F. Vilesov. Spectroscopy of atoms and molecules in liquid helium. *Annual Review of Physical Chemistry*, 49:1–41, 1998. 1, 6, 10, 51, 56

[50] J. P. Toennies and A. F. Vilesov. Superfluid helium droplets: A uniquely cold nanomatrix for molecules and molecular complexes. *Angewandte Chemie-International Edition*, 43 (20):2622–2648, 2004. 1, 6, 7, 36, 56

[51] M. Vala, R. Pyzalski, J. Shakhsemampour, M. Eyring, J. Pyka, T. Tipton, and J. C. Rivoal. Moment analysis for absorption and magnetic circular dichroism bands of atomic P←S transitions: Application to matrix-isolated chromium. *J. Chem. Phys.*, 86(11): 5951–5957, June 1987. 4

[52] M. Vala, K. Zeringue, J. Shakhsemampour, J. C. Rivoal, and R. Pyzalski. Magnetic circular-dichroism studies of matrix-isolated atoms - excited-state spin-orbit-coupling constant reduction of copper in the noble-gases. *Journal of Chemical Physics*, 80(6): 2401–2406, 1984. 5

[53] R. J. Vanzee, C. A. Baumann, and W. Weltner. Electron-spin-resonance of chromium metal atoms and molecules in matrices. *Journal of Chemical Physics*, 82(9):3912–3920, 1985. 4

[54] E. Whittle, D. A. Dows, and G. C. Pimentel. Matrix isolation method for the experimental study of unstable species. *Journal of Chemical Physics*, 22(11):1943, 1954. 6

Danksagung

An dieser Stelle möchte ich all jenen Personen meinen herzlichen Dank aussprechen, die mich bei der Umsetzung meiner Diplomarbeit gefördert haben und die Teil des freundlichen und motivierenden Arbeitsklimas waren.

Univ.-Prof. Mag. Dr.rer.nat. Wolfgang E. Ernst gab mir die Anregung und Möglichkeit bei der Diplomarbeit in das Gebiet der superflüssigen Heliumtröpfchen vorzudringen. Er stand mir mit wissenschaftlichem Rat jederzeit zur Verfügung und unterstützte mich mit persönlichem Einsatz. Obwohl er auf Grund seiner vielfältigen Verpflichtungen belastet war, nahm er sich als Mentor stets meiner Probleme an.

Markus Koch stand mir während meiner ganzen Diplomarbeit immer mit Rat und Tat zur Seite. In vielen Diskussionen konnte ich von seinem Wissen profitieren und dabei auch viele Anregungen für meine Diplomarbeit bekommen. Weiters hat er viel Zeit mit dem Korrekturlesen meiner Arbeit verbracht.

Carlo Callegari ist mir in der ersten Hälfte meiner Tätigkeit als Diplomand auch immer unterstützend und beratend zur Verfügung gestanden, bevor er das Institut nach Italien verlassen hat.

Prof. Laurentius Windholz hat mir Geräte und Material zur Verfügung gestellt. Außerdem bekam ich von ihm viele Anregungen zur Verbesserung meiner Konstruktion.

Auch **Prof. Theo Neger** stellte mir wichtige Geräte zur Verfügung. Nach wie vor ist sein Netzgerät essentieller Bestandteil in meiner Konstruktion.

Matteo Luisi hat mich mit seiner Bakkalaureatsarbeit, die die Charakterisierung des Prototypen abdeckt, unterstützt.

Speziell möchte ich mich auch bei Rupert Maierhofer, Werner Luttenberger und Uwe Seidl bedanken, die Werkstattcrew, die für mich oft auch sehr kurzfristig Bauteile angefertigt hat. Außerdem bekam ich auch hier viele Verbesserungsvorschläge für meine Konstruktion. Ohne die eine oder andere Kritik an meinen Skizzen und Konstruktionszeichnungen hätte ich mich wohl auch nicht so intensiv mit diversen CAD Programmen auseinandergesetzt und dabei so viel dazugelernt.

Josef Friedrich, Reinhard Dämon und Manuel Hafner haben mir viele der elektronischen Schaltungen realisiert und diesbezüglich hilfreiche Tips gegeben.

Abschließend möchte ich mich sehr herzlich bei allen Mitarbeitern und Kollegen des Institutes, insbesondere auch bei den Damen im Sekretariat für das hervorragende Arbeitsklima bedanken.

Nicht unerwähnt lassen möchte ich ein besonderes "Dankeschön" an Mag. Herbert Wallner, meinem Physik Professor am BRG Petersgasse, der mein Interesse an der Physik durch seinen lebendigen Unterricht geweckt und vertieft hat, und mich zur Teilnahme an der Physikolympiade motiviert hat.

Ein besonderer Dank gilt auch meiner Familie, die mir nicht nur das Studium finanziell ermöglicht hat, sondern auch während der gesamten Studiumzeit unterstützend zur Seite gestanden sind.

Möge diese Arbeit für weitere wissenschaftliche Fragestellungen und längerfristig auch für die angewandte Technik hilfreich sein.